Research Square

Preprints are preliminary reports that have not undergone peer review.
They should not be considered conclusive, used to inform clinical practice,
or referenced by the media as validated information.

IRAK4 autophosphorylation functions as a molecular switch to regulate death domain assembly and Myddosome maturation

Marcus Taylor

taylor@mpiib-berlin.mpg.de

Max Planck Institute for Infection Biology https://orcid.org/0000-0002-0904-2122

Niranjan Srikanth

MPI for Infection Biology

Rafael Deliz-Aguirre

MPI for Infection Biology

Deepika Kumari Gola

MPI for Infection Biology

Margaux Bilay

MPI for Infection Biology https://orcid.org/0009-0008-8737-5441

Elke Ziska

MPI for Infection Biology

Ian Kelsall

Medical Research Council Protein Phosphorylation and Ubiquitylation Unit, University of Dundee, U.K.
https://orcid.org/0000-0002-7501-6504

Yogesh Kukathu

University of Dundee https://orcid.org/0000-0002-3274-1642

Article

Keywords:

Posted Date: February 23rd, 2026

DOI: https://doi.org/10.21203/rs.3.rs-8872830/v1

License: This work is licensed under a Creative Commons Attribution 4.0 International License.
Read Full License

Additional Declarations: Yes there is potential Competing Interest. MJT has research projects sponsored by Kymera Therapeutics and is a scientific advisory board member at RheumaGen.

Version of Record: A version of this preprint was published at Nature Communications on October 21st, 2026. See the published version at https://doi.org/10.1038/s41467-026-78773-6.

IRAK4 autophosphorylation functions as a molecular switch to regulate death domain assembly and Myddosome maturation

Niranjan Srikanth[1,2], Rafael Deliz-Aguirre[1,3], Deepika Kumari Gola[1], Margaux Bilay[1], Elke Ziska[1], Ian Kelsall[4], Yogesh Kulathu[4], and Marcus J. Taylor[1]*

1. Max Planck Institute for Infection Biology, Chariteplatz 1, Berlin D-10117 Germany
2. Department of Biology, Chemistry and Pharmacy, Freie Universität Berlin, Berlin 14195, Germany.
3. Humboldt University of Berlin, Unter den Linden 6, Berlin 10117, Germany
4. MRC Protein Phosphorylation and Ubiquitylation Unit, School of Life Sciences, University of Dundee, Dundee DD1 5EH, Scotland, United Kingdom

* Corresponding author: taylor@mpiib-berlin.mpg.de

Abstract:

The organization of signaling proteins into multi-component complexes is essential for innate immune responses and is often achieved through the oligomerization of death domains (DDs). The Myddosome, composed of MyD88 and IRAK family kinases, exemplifies this mechanism. However, how DDs assemble in an ordered and regulated manner to form Myddosomes to control signaling output remains unknown. Here, we show that IRAK4 kinase activity and autophosphorylation are required for IRAK4:IRAK1 heterotypic DD interactions. We discovered that IRAK1 is autoinhibited by its kinase domain, and IRAK4 phosphorylation relieves this inhibition, enabling IRAK1 DD incorporation into Myddosomes. This phosphorylation-dependent switch similarly controls IRAK2/3 incorporation. Thus, IRAK4 autophosphorylation acts as an energy-dependent molecular switch that integrates phosphorylation with protein oligomerization to drive Myddosome maturation and signal transduction. This mechanism demonstrates how enzymatic activity can impose temporal and spatial control over macromolecular assembly to ensure directional and context-dependent inflammatory signaling.

Introduction:

Inflammatory signaling depends on the use of higher-order protein assemblies termed signalosomes[1,2]. Many of these signalosomes are composed of complex mixtures of death domain (DD) oligomers[3]. However these mixtures have a nanoscale order in which DD oligomers are sequentially fused to other oligomers[4]. Therefore dynamic assembly and consequently signaling must require a controlled sequence of homo and heterotypic DD interactions. While structural studies highlight the finescale atomic level features that bind DDs together, how these complexes dynamically assemble in response to signals is less well understood. Given that DD signalosomes activate powerful effector functions like cell death or the release of inflammatory cytokines, assembly must be highly controlled with multiple regulatory steps involved. These regulatory mechanisms are required to ensure a controlled and proportionate response and suppress assembly when cells are in a state of quiescence. Therefore an essential question is how DD signalosome assembly is kinetically and spatially regulated to achieve downstream control.

Signalosomes composed of mixed oligomers of death domains (DDs) are exemplified by the Myddosome, which transduces signals from the IL-1 receptor[5,6]. Myddosome formation begins with the recruitment of MyD88 to the activated receptor, followed by controlled coassembly with IRAK family kinases. The core of this complex is built by the binding and oligomerization of the IRAK4 on a platform of oligomerized MyD88. IRAK4 oligomers then serve as a platform for the binding and oligomerization of either IRAK1, IRAK2, or IRAK3[6,7]. This higher-order complex then engages TRAF6 to propagate downstream signaling[8]. Thus, an essential step in IL-1R signal transduction is controlled DD oligomerization and the co-assembly of IRAK kinases with MyD88 to ensure directed signal transduction. However, it remains unclear how the sequential incorporation of these components is regulated to achieve controlled activation of downstream signaling.

In many cases, DDs are fused to other effector domains. For example, in addition to an N-terminus DD, IRAKs also have a C-terminus kinase domain[9]. This raises the possibility that IRAK kinase domains regulate the ordered assembly of DDs into the Myddosome. Consistent with such a regulatory role, mutations in the IRAK4 kinase domain that inhibit its activity prevent co-immunoprecipitation with IRAK1 in stimulated cells[10]. Therefore, a critical question is how IRAK kinase domains regulate ordered Myddosome assembly. Here, we show that the assembly of heterotypic IRAK4 and IRAK1 DDs is regulated by their kinase domains. IRAK1 most likely exists in an autoinhibitory state where the kinase domain prevents DD co-assembly with the IRAK4 DD. IRAK4 autophosphorylation relieves IRAK1 autoinhibition by facilitating heterodimerization with the IRAK1 kinase domain thereby allowing DD oligomerization. This mechanism of relieving autoinhibition most likely functions with IRAK2 and IRAK3, as inhibition of IRAK4 kinase activity also inhibits their incorporation into Myddosomes. Thus, IRAK4 autophosphorylation functions as an energy-dependent regulatory switch that controls the final stages of DD assembly and Myddosome maturation. Our work highlights how protein oligomerization can be regulated by enzymatic activity to ensure rapid, directed assembly of a signaling complex in response to upstream signals.

Results:

IRAK4 and IRAK1 kinase domains differentially regulate heterotypic DD interactions

Myddosome assembly follows an ordered process initiated by MyD88 oligomerization, which serves as a nucleation point for the sequential recruitment of IRAK4 and IRAK1 [11]. The kinase activity of IRAK4 is important for propagating downstream signaling responses [12–14], and co-immunoprecipitation studies have revealed that Myddosome formation is not exclusively governed by DD interactions [10]. These findings implicate the kinase domain and catalytic activity of IRAK4 as critical regulators of complex assembly and maturation. Structural studies of Myddosomes have solely examined DD assemblies[5–7] in the absence of the IRAK4/1 kinase domains or activity. Here, to delineate the structural mechanisms that modulate DD oligomerization and signaling, we used AlphaFold3 (AF3)[15] to generate a structural model of the mouse Myddosome that includes the IRAK4/1 kinase domains (Fig. 1A). The predicted complex revealed not only a mixed oligomer of DDs, but also an interaction interface between the IRAK4 and IRAK1 kinase domains (Fig. 1A). This predicted structural model suggests that IRAK kinase domain interactions and possibly activity could regulate the controlled assembly and maturation of the Myddosome.

Based on our structural model and previous analysis[10], we expected that the IRAK4/1 kinase domains would be essential for Myddosome assembly and maturation. To delineate the exact role and timing of kinase domain activity in Myddosome assembly, we analyzed the dynamics of MyD88:IRAK4 and IRAK4:IRAK1 heterotypic interactions in live cells. By reconstituting knockout cell lines with IRAK4/1 truncations lacking the kinase domain and tagged with fluorescent proteins (referred to as IRAK4ΔKD and IRAK1-ΔKD), we used an established two-colour high-resolution microscopy assay[11] to analyze the discrete stages of Myddosome assembly.

This experimental approach allowed us to directly assay the co-assembly and stability of these two heterotypic DD interactions, in the presence or absence of the IRAK4 kinase domain, with single-complex resolution.

Examining the first DD interaction in Myddosome assembly, we found that co-assembly of MyD88:IRAK4 was not impacted by the loss of the IRAK4 kinase domain. Both full length and IRAK4-delta kinase domain co-assembled with MyD88, and these assemblies had similar kinetics, size and lifetime distributions (Fig. 1B-D, and S1A). However, signalling was only restored with full-length IRAK4 (Fig. S1B). This is consistent with the IRAK4 kinase domain being critical for signal transduction. Therefore the initial steps of signal transduction and Myddosome formation are solely regulated by DD assembly. We conclude that the heterotypic interactions between the MyD88 and IRAK4 DDs are sufficient to form a stable complex and do not require the IRAK4 kinase domain. However, DD heterotypic assembly alone is insufficient to transduce signaling.

One possible explanation for the lack of signal transduction with the IRAK4-ΔKD could be a failure to recruit IRAK1[10]. Therefore, we next examined the heterotypic DD interactions between IRAK4 and IRAK1. We created EL4 cells with a triple knock out of MyD88, IRAK4 and IRAK1 Myddsome components (referred to as 3xKO cells, Fig. S1C) and reconstituted them with IRAK4-WT-GFP or IRAK4-ΔKD and IRAK1-mScarlet. We found that the IRAK4 consisting solely of the DD (IRAK4-ΔKD) was unable to recruit and incorporate IRAK1 into nascent Myddosome complexes (Fig. 1E-G, Movie S1). The expression of IRAK4-ΔKD was associated with a greater than 6-fold reduction of stable IRAK1 co-assembly (5.36% and 0.80% for IRAK4 WT and IRAK4-ΔKD, respectively; stable colocalization was defined as an association greater than 30s; Fig. 1G). We conclude that the IRAK4 kinase domain is required to recruit IRAK1, thereby leading to Myddosome maturation and downstream signal transduction.

Based on these results and our structural model (Fig 1A, E-G), we hypothesized that the interaction between the kinase domains of IRAK4 and IRAK1 stabilizes the heterotypic DD interaction between these proteins. Therefore, IRAK1 lacking the kinase domain (IRAK1-ΔKD) would be expected to phenocopy the expression of IRAK4-ΔKD. Surprisingly, we observed stable incorporation of IRAK1-ΔKD into assembling Myddosomes (Fig. 1H-J, Fig. S1D, Movie S2). Thus, while the interaction between the IRAK4:IRAK1 DDs is intrinsically stable, the IRAK1 kinase domain possibly auto-inhibits its DD and prevents its incorporation. This would suggest that the interaction with the IRAK4 kinase domain is required to release IRAK1 autoinhibition and allow stable assembly into Myddosomes and downstream signaling.

IRAK4 kinase domain regulates the incorporation of IRAK2/3 into Myddosomes

To determine whether the role of the IRAK4 kinase domain is to relieve autoinhibition in other IRAK family members, we further examined IRAK2 and IRAK3. Similar to IRAK1, IRAK2 and IRAK3 can also co-assemble with MyD88. IRAK2 activates equivalent downstream inflammatory signaling reactions to IRAK1[16], suggesting functional redundancy. In contrast, IRAK3 is proposed to be a negative regulator of signal transduction [17]. Unlike IRAK1, IRAK2 and IRAK3 are putative pseudokinases[18,19]. Given these biochemical differences, Myddosomes composed of IRAK1, IRAK2, or IRAK3 could have different assembly mechanisms. If the IRAK4 kinase domain acts as a universal regulatory switch activating IRAK DD assembly, it would be expected to control the incorporation of IRAK2 or IRAK3 into Myddosomes. We generated a structural model of the mouse Myddosome composed of either IRAK2 or IRAK3 using AF3 (Fig. 2A, B). Similar to the model with IRAK1, we found a predicted binding interface between the IRAK4 and IRAK2 or IRAK3 kinase domains. This supports the hypothesis that the IRAK4 kinase domain relieves autoinhibition across IRAK paralogs.

From this structural model, we hypothesized that the IRAK4 kinase domain regulates the incorporation of IRAK2 and IRAK3 into forming Myddosome complexes. EL4 cells do not express detectable levels of IRAK2 or IRAK3 (Fig. S2A), allowing us to reconstitute EL4-3xKO cells with combinations of full-length and truncated versions of IRAK4, IRAK2, or IRAK3. We found that IRAK2 and IRAK3 are incorporated into Myddosomes with similar kinetics to those of IRAK1 when co-expressed with wild-type IRAK4 (Fig. S2B, C). However, when co-expressed with IRAK4-ΔKD, we observed more transient recruitment and reduced stable incorporation of IRAK2 and IRAK3 into Myddosomes (Fig. 2C-H, Movie S3). Although the defect was less severe than with IRAK1, IRAK4-ΔKD showed reduced stable association with IRAK2/3 puncta compared to WT IRAK4 (Fig. 2E, H). Additionally, deletion of the IRAK4 kinase domain produced smaller IRAK2/3 oligomers (Fig. S2D, E), indicating failed Myddosome maturation. This suggests that the IRAK4 kinase domain regulates the heterotypic assembly of DDs across all IRAK paralogs by possibly relieving intra-molecular inhibition.

If IRAK2/3 are autoinhibited to prevent DD assembly, the removal of the kinase domain would be expected to restore stable heterotypic assembly with the IRAK4 DD. Reconstitution of 3xKO cells with full-length IRAK4 and the IRAK2/3-ΔKD, led to stable heterotypic assembly (Fig. 2I-N, Fig. S2F-G, Movie S4). This suggests that the kinase domain of IRAK4 regulates the controlled assembly of heterotypic DDs by relieving internal inhibition of IRAK2/3 exerted by their kinase domains. We conclude that the IRAK4 kinase domain is a regulator of heterotypic DD assembly and controls the final stages of Myddosome maturation by relieving an intramolecular inhibition present within the IRAK1/2/3 paralogs.

IRAK4 kinase activity is required to stably incorporate IRAK1/2/3 into Myddosomes

Our results show that the IRAK4 kinase domain is required for the stable incorporation of IRAK1/2/3 into Myddosomes. Based on the structural model (Fig. 1A, 2A-B) and biochemical studies [14,19], we predicted that the interaction between the IRAK4 and IRAK1/2/3 kinase domains is regulated by the IRAK4 kinase activity. In vitro, only the phosphorylated IRAK4 domain can heterodimerize with IRAK paralog kinase domains[14,19]. IRAK4 kinase domain autophosphorylates, and this occurs downstream of DD co-assembly with MyD88, which triggers homodimerization and autophosphorylation of serine/threonine residues in its kinase domain[20,21] . Consistent with this molecular sequence of Myddosome assembly, IRAK4 that lacks a DD or has a patient-associated mutation within the DD that inhibits oligomerization[22,23] could not co-assemble with MyD88 or undergo autophosphorylation in response to IL-1 (Fig. S3), highlighting the sequential nature of this process. If IRAK4 kinase activity and autophosphorylation are involved in relieving autoinhibition of IRAK paralogs, IRAK4 kinase-inactive mutants should phenocopy the expression of IRAK4-ΔKD and disrupt IRAK1 incorporation (Fig. 1E to G). To test this hypothesis, we assayed a kinase-inactive version of IRAK4 (IRAK4-K213A/K214A) that has previously been shown to be unable to trigger the incorporation of IRAK1 into Myddosomes[10]. This mutation could not restore IL-1 signaling responses in IRAK4 KO cells (Fig. S1B), consistent with previous studies on IRAK4 kinase requirements[10]. Importantly, IRAK4-K213A/K214A did not disrupt MyD88 oligomerization or MyD88:IRAK4 co-assembly, confirming that the initial steps of Myddosome formation are solely regulated by DD assembly (Fig. S4A-C). Therefore, IRAK4 kinase activity functions as a regulatory checkpoint that specifically regulates signaling events downstream of MyD88:IRAK4 co-assembly and multimerization.

To determine whether IRAK4 kinase activity and autophosphorylation relieves IRAK1 autoinhibition and permits IRAK4:IRAK1 DD coassembly, we directly imaged co-assembly of IRAK1 with WT and kinase-inactive IRAK4. We found that IRAK4-K213A/K214A was unable to recruit and incorporate IRAK1 into nascent Myddosome complexes (Fig. 3A to C, Movie S5). Similar to IRAK4-ΔKD, this kinase-inactive mutant had a 3-fold reduction in stable colocalization with IRAK1 (Fig. 3C). Thus IRAK4 kinase activity and autophosphorylation controls an essential regulatory switch that ensures IRAK1 incorporation and DD oligomerization into nascent Myddosomes. This is consistent with IRAK4 autophosphorylation functioning as a switch which overrides IRAK1 autoinhibition.

To determine whether IRAK4 autophosphorylation functions as a universal regulatory switch in Myddosome maturation, regardless of the final composition, we tested IRAK2/3 incorporation. We found that IRAK4-K213A/K214A only recruited IRAK2 transiently compared to WT, and very few IRAK4-K213A/K214A assemblies formed stable complexes with IRAK2 (Fig. 3D to F). In comparison, IRAK3 had a similar lifetime distribution of co-assembly between the full-length and kinase-dead versions of IRAK4 (Fig. 3G to H). However, there was a 4 fold reduction in the frequency of IRAK3 assemblies that were stably associated with IRAK4 (Fig. 3I). We conclude

that IRAK4 kinase activity and autophosphorylation regulate IRAK1/2/3 incorporation and DD oligomerization in Myddosomes. Therefore, IRAK4 autophosphorylation is a regulatory switch that controls the final assembly stage of Myddosome assembly, regardless of the final composition.

If IRAK4 autophosphorylation functions as a regulatory switch acting on IRAK1/2/3, then IRAK4 kinase inhibitors would be expected to phenocopy kinase-inactive IRAK4 expression and block IRAK1/2/3 recruitment. This effect would also be titratable, such that higher concentrations of the inhibitor would produce more pronounced inhibition of IRAK1/2/3 recruitment and colocalization with Myddosomes. We confirmed that a specific IRAK4 inhibitor[24] blocked autophosphorylation, had no effect on MyD88:IRAK4 coassembly, inhibited downstream signaling, and, like IRAK4-K213/214A[10], inhibited IRAK1 co-immunoprecipitation with MyD88 (Fig. S4D to G). Consistent with our observations in kinase-inactive mutants, the inhibitor also had a pronounced and titratable effect on IRAK1 stability and incorporation into Myddosomes (Fig. 3J). We found similar effects on IRAK2 and IRAK3 (Fig. 3K to M). Therefore, we conclude that IRAK4 autophosphorylation functions as a regulatory switch to control Myddosome maturation, possibly by relieving IRAK1/2/3 autoinhibition and thereby allowing the DDs to co-assemble and oligomerize.

IRAK4 autophosphorylation and heterodimerization of IRAK1:IRAK4 kinase domains are discrete steps in Myddosome assembly

To understand how IRAK4 autophosphorylation serves as a molecular switch in Myddosome assembly, we examined the precise temporal relationship between IRAK4 phosphorylation and Myddosome maturation. Consistent with IRAK4 phosphorylation regulating heterotypic DD assembly, phosphorylated IRAK4 (pIRAK) levels increase during the first 60 minutes post IL-1 stimulation (Fig. S5A,B), indicating that Myddosome assembly and IRAK4 phosphorylation occur contemporaneously. To understand this dynamic process at the level of single complexes, we exploited the asynchronous assembly of Myddosomes in individual cells (Fig. S5C,D) and chemical fixation as a way to observe various assembly intermediates and reconstruct the timeline of assembly and IRAK1 incorporation. Chemical fixation of IL-1-stimulated cells expressing fluorescently tagged Myddosome components and stained with pIRAK4-specific antibodies revealed MyD88 puncta with IRAK4-mScarlet both with and without pIRAK4 (Fig. 4A), whereas MyD88-GFP/IRAK1-mScarlet cells showed puncta containing MyD88 alone, MyD88 with pIRAK4, or MyD88 with both pIRAK4 and IRAK1 (Fig. 4B). Critically, over 80% of MyD88 puncta containing IRAK1 also contained pIRAK4. The relative proportions of these assembly states (Fig. 4A, B) enabled us to reconstruct the Myddosome assembly sequence: MyD88 oligomerization initiates the process, followed by DD-dependent recruitment and oligomerization of unphosphorylated IRAK4, which leads to kinase-domain homodimerization and trans-autophosphorylation, homodimer disassembly, and finally heterodimerization of the phosphorylated IRAK4 kinase domain with the IRAK1 kinase domain, overcoming IRAK1's self-inhibition. This reconstructed timeline of assembly is consistent with the integral role of IRAK4 kinase activity in Myddosome signaling. Furthermore, the timeline suggests that the

discrete step of IRAK4 autophosphorylation is a molecular switch that must be activated to trigger stable IRAK1 incorporation.

A key prediction of our sequential model of Myddosome assembly is that heterodimerization of the IRAK4 and IRAK kinase domains precedes DD oligomerization. Therefore, we would expect the IRAK kinase domain alone to be recruited to nascent Myddosomes independently of the DD, in a manner dependent on IRAK4 autophosphorylation. To test this, we expressed IRAK1 and IRAK2 truncation mutants containing only the kinase domain (IRAK1/2-ΔDD) fused to mScarlet in MyD88-GFP/IRAK1 KO cells and assayed recruitment to Myddosomes using single-molecule microscopy. MyD88 puncta recruited IRAK1/2-ΔDD (Fig. 4C and F, Movie S6). These recruitment events were typically single molecule, transient, and dependent on IRAK4 kinase activity, as their frequency was reduced in the presence of an IRAK4 kinase inhibitor (Fig. 4D, E, G and H). In conclusion, these data show that the kinase domains of IRAK1/2 are sufficient for recruitment to assembling Myddosomes and that this interaction requires IRAK4 kinase activity. Taken together, these findings demonstrate that IRAK4 kinase activity regulates DD assembly by enforcing a sequential order of interactions. In this way, IRAK4 autophosphorylation acts as a switch that directs the timely incorporation of IRAKs and ensures that Myddosome maturation proceeds in a controlled and directional manner.

A IRAK4 phosphomimetic mutant restores IRAK1 heterodimerization and Myddosome incorporation independent of kinase activity

To understand the biochemical nature of this IRAK4 autophosphorylation-mediated switch further, we examined how IRAK4 autophosphorylation contributes to heterodimerization with the IRAK1 kinase domain. The AF3 structural model of the human IRAK4 and IRAK1 kinase domain heterodimer predicts that the phosphorylated residues of IRAK4, in a region referred to as the activation loop[14,20,25,26], are situated at the dimer interface, suggesting a role in regulating this interaction (Fig. 5A). In vitro, we confirmed that only the phosphorylated human IRAK4 kinase domain heterodimerizes with the IRAK1 kinase domain and consequently requires kinase activity (Fig. 5B), which is consistent with previous biochemical analysis[14,19,27]. We reasoned that if a kinase-inactive IRAK4 were combined with rational mutation of the IRAK4 activation loop to mimic the negative charge of phosphorylation, this would induce equivalent conformational changes and an electrostatic environment that could restore heterodimerization with IRAK1, independent of IRAK4 kinase activity. We mutated the threonine/serine residues within this activation loop to glutamic acid (referred to as E-loop mutant), and tested whether it could restore heterodimerization with IRAK1 in vitro by native PAGE (Fig. 5B). We found that this mutation could even partially restore heterodimerization when combined with a kinase-inactive mutant. We then tested whether this triple mutation restored IRAK1 recruitment and assembly in cells and found that it restored IRAK1 recruitment to an IRAK4 kinase-inactive mutant (Fig. 5C-E, Movie S7). Mutating the activation loop to alanine (A-loop) in a kinase-active IRAK4 also reduced IRAK1 oligomerization and incorporation into Myddosomes (Fig. S6C through F). As these mutations were analyzed in human alleles of IRAK4 and IRAK1, we tested the equivalent activation loop mutations in mouse alleles and found that E-loop phosphomimetic mutations could restore IRAK1 recruitment to a kinase-inactive IRAK4 allele (Fig. S6G through L). These data show that autophosphorylation facilitates the confirmation change in IRAK4 that leads to heterodimerization with the IRAK1 kinase domain. Our results thus provide a molecular mechanism that explains how IRAK4 autophosphorylation functions as a molecular switch to control directional DD assembly and Myddosome maturation.

Discussion

Here, we demonstrate that IRAK4 kinase-domain autophosphorylation functions as a molecular switch that controls the final stages of Myddosome maturation in IL-1 signal transduction. Using a combination of high spatial-temporal resolution microscopy and molecular analysis, we reconstructed the timeline of Myddosome assembly (Fig 6). This timeline demonstrates that IRAK4 autophosphorylation is a distinct step that occurs after MyD88:IRAK4 assembly but before the incorporation of IRAK1, 2 and 3 (Fig. 1A, Fig.1 E-G, Fig. 2A-H, Fig. S2D-E, Fig. 3A-I, Fig. 4). This step is critical because it serves to relieve the auto-inhibitory confirmation of IRAK1, 2 and 3, and allows for the DD of these paralogs to co-assemble on the platform of the IRAK4 DD oligomers co-assembled with MyD88. Thus, IRAK4 autophosphorylation is an energy-dependent biochemical switch that controls the DD assembly multimerization and heteromeric assembly. This mechanism explains why IRAK4 kinase-inactive mutants or kinase inhibitors can suppress Myddosome inflammatory signaling[10,12–14,21,28,29]. In summary, our data demonstrate how the assembly of a DD signaling complex is not solely controlled by mass-action oligomerization. Instead, DD assembly can integrate a powerful regulatory switch using an energy-dependent phosphorylation mechanism to control signal transduction.

Intramolecular inhibition is a widespread protein control mechanism that enables precise temporal and spatial activation of biochemical pathways. Typically, this regulation relies on weak internal interactions that maintain a dynamic equilibrium between inhibited and activatable states. For example, actin polymerization by N-WASP is spatially controlled by autoinhibition of the VCA domain, mediated by weak (10–100 μM) interactions with domains that also sense upstream inputs such as phosphoinositides and activated Cdc42[30]. This arrangement suppresses spurious activation while remaining highly responsive to bona fide activating signals. Our data suggest that IRAK1/2/3 employ an analogous principle: weak affinity interactions between their DD and kinase domain create a dynamic autoinhibited state. Phospho-IRAK4 functions as an energy-dependent switch that competes for the IRAK1/2/3 kinase domain, releasing the DD to join the assembling Myddosome platform. Because IRAK4 autophosphorylation only occurs when co-assembled with MyD88[14], this switch is not a simple on–off toggle but a regulatory checkpoint that ensures IRAK activation occurs only in the context of receptor engagement and is spatially restricted to assembling Myddosomes. In doing so, IRAK4 autophosphorylation links upstream receptor inputs to Myddosome maturation, enforcing directionality and proportionate responsiveness in downstream signaling, features that are especially critical for ensuring that IL-1–induced inflammatory outputs remain tightly coupled to receptor activation. In summary, weak and reversible IRAK1/2/3 intramolecular interactions are strong enough to prevent inappropriate activation, yet labile enough to permit rapid and coordinated transitions into active complexes once the correct stimulus is present. In doing so, they set a dynamic threshold that is responsive to the phospho-IRAK4 switch and enforces directionality over DD assembly and downstream signaling.

Beyond IL-1R signaling, multiple inflammatory signaling pathways transduce signals through oligomeric complexes composed of DDs[1,2,4]. Our data shows that multimerization of DDs can be

controlled by other biochemical processes, such as post-translational modification, beyond the specific interactions between these domains. The integration of autophosphorylation and DD oligomerization stages is possibly conserved outside of mammals, as Toll receptor activation triggers autophosphorylation of the Drosophila IRAK homolog Pelle kinase[31]. Similar to IRAKs, we find enzymatically active signaling proteins that contain DDs and assemble into multimeric complexes, for example receptor-interacting protein kinases (RIPK)[32–34]. This suggests a broader prevalence of enzymatic activity controlling protein oligomerization and directionality in signaling cascades. Our insight into the hierarchical interplay between macromolecular assembly and enzymatic activity explains why IRAK4 kinase inhibitors can disrupt controlled Myddosome signal transduction[28,35], which may also point to a possible broader therapeutic strategy of targeting enzymatic activity to disrupt macromolecular assembly and consequently signal transduction.

Acknowledgements:

We thank Vikram Rao and Pfizer for providing an antibody against phospho-IRAK4. We thank the Max Planck Computing and Data Facility for providing cluster computer resources for data analysis. We thank Kathrin Laettig for assistance with ELISA and cell culture. We thank Radhika Patnala and Arne Fabritius for assistance and advice on figure design and scientific illustrations. We thank all Taylor lab members for critical feedback and commenting on the project. We thank Iain Patten for assistance in developing and drafting the manuscript.

This work was supported by the Max Planck Society and the DFG (project number 499533619) awarded to MJT. YK and IK were supported by the UKRI BBSRC (BB/W007401/1) and UKRI MRC grant MC_UU_00038/3 awarded to YK.

Declaration of interests:

MJT has research projects sponsored by Kymera Therapeutics and is a scientific advisory board member at RheumaGen.

Author contributions: M.J. Taylor, N. Srikanth and E. Ziska, purified proteins for labeling membranes. N. Srikanth and R. Deliz-Aguirre wrote and validated custom image analysis scripts. N. Srikanth performed imaging experiments. E. Ziska performed Western Blot verification of cell lines and time course analysis of pIRAK4 production. E. Ziska and D. Gola performed immunoprecipitation and Western Blotting experiments. N. Srikanth and M.J Taylor performed experimental design. N. Srikanth performed data analysis, curation and visualization. Ian Kelsall and Yogesh Kulathu designed and validated the IRAK4 phosphomimetic mutant. Ian Kelsall purified recombinant WT and mutant versions of the IRAK1 and IRAK4 kinase domains and performed native gel electrophoresis. M. Bilay performed data analysis on blinded pIRAK4 immunofluorescence data. The project was conceived and supervised by M.J. Taylor. The manuscript was prepared by N. Srikanth, E. Ziska and M.J. Taylor with input from all authors.

Material and Methods

KEY RESOURCES TABLE

REAGENT or RESOURCE	SOURCE	IDENTIFIER
Antibodies		
Rabbit polyclonal anti-IRAK4	Cell Signaling Technology	Cat# 4363; RRID:AB_2126429
Rabbit monoclonal anti-IRAK1 (D51G7)	Cell Signaling Technology	Cat# 4504; RRID:AB_1904032
Rabbit monoclonal anti-phospho-IRAK4 (Thr(P)-345/Ser(P)-346)	Pfizer (Vikram Rao)	
Camelid sdAb FluoTag®-X4 anti-GFP-Atto488	NanoTag Biotechnologies GmbH	Cat# N0304-At488;
goat anti-rabbit conjugated to Alexa Fluor 647	Invitrogen	Cat# A21246
goat anti-human conjugated to Alexa Fluor 647	Invitrogen	Cat# A21445
Nano-secondary AF568	Chromotek	Cat# srbAF568-1
Rabbit monoclonal anti-β-actin	Cell Signaling Technology	Cat# 4970; RRID:AB_2223172
Rabbit polyclonal anti-IRAK2	Cell Signaling Technology	Cat# 4367
Rabbit monoclonal anti-IRAKM [EPR26376]	Abcam	Cat#ab307708
Goat Anti-Rabbit HRP	Jackson Lab	Cat# 111-035-144
Goat Anti-Mouse HRP	Jackson Lab	Cat# 115-035-166
Rabbit Anti-Goat HRP	Jackson Lab	Cat# 305-036-045
Goat polyclonal anti-MyD88	R&D systems	Cat# AF3109 RRID:AB_2146703
Mouse monoclonal anti-RFP	Chromotek	Cat# 6G6
Bacterial and Virus Strains		

BL21 Rosetta	Novagen	Cat# 70954
NEB Stable	NEB	Cat# C3040
TOP10	Thermo	Cat# C404003
DH10EMBacY	Geneva Biotech	
Chemicals, Peptides, and Recombinant Proteins		
IRAK4 kinase inhibitor, PF-06650833	Sigma-Aldrich	Cat# PZ0327-5MG
His10-Halo-Tencon-SpycatcherV2-IL-1β	Deliz-Aguirre et al.[11]	
Puromycin dihydrochloride	Thermo	Cat# A1113803
Blasticidin	InvivoGen	Cat# ant-bl-05
Mouse IL-1β	Peprotech	Cat# 211-11B
JF646-HaloTag ligand	Luke Lavis, HHMI/Promega	Promega (GA1120)
InstantBlue Coomassie Protein Stain	Abcam	Cat#ab119211
4-(2-aminoethyl) benzene sulphonyl fluoride hydrochloride (AEBSF)	Apollo Scientific	Cat#BIMB2003
5-Bromo-4-chloro-3-indolyl-β-D-galactoside (X-Gal)	ForMedium	Cat#XGAL001
Isopropyl β-D-thiogalactoside (IPTG)	ForMedium	Cat#IPTG025
GSH 4B sepharose	GE Healthcare	Cat#17-0756-01
Dithiothreitol	Melford	Cat#D11000
Gentamycin sulphate	Melford	Cat#G0124
PreScission Protease (GST tagged)	MRC PPU Reagents	Cat#GNNYH4
Ni-NTA agarose	Qiagen	Cat#30210
4-(2-Hydroxyethyl) piperazine-1-ethanesulphonic acid (HEPES)	Sigma-Aldrich	Cat#H3375
Ampicillin sodium salt	Sigma-Aldrich	Cat#A9518
Benzamidine	Sigma-Aldrich	Cat#B6506
Imidazole	Sigma-Aldrich	Cat#56749
Kanamycin sulfate	Sigma-Aldrich	Cat#K1377
Magnesium chloride	Sigma-Aldrich	Cat#M1028

Tetracycline hydrochloride	Sigma-Aldrich	Cat#T7660
β-Mercaptoethanol	Sigma-Aldrich	Cat#M3148
Antibiotic / Antimycotic solution (100 x)	Thermo Fisher	Cat#15240062
Novex 10% Tris-Glycine Mini Gels	Thermo Fisher	Cat#XP00105Box
Novex Tris-Glycine Native Running Buffer (10×)	Thermo Fisher	Cat#LC2672
Novex Tris-Glycine Native Sample Buffer (2×)	Thermo Fisher	Cat#LC2673
Pierce Universal Nuclease	Thermo Fisher	Cat#88701
Sf-900 II SFM insect cell medium	Thermo Fisher	Cat#10902096
Glycerol	VWR	Cat#24388.320
Critical Commercial Assays		
MycoAlert® Mycoplasma Detection Kit	Lonza	Cat# LT07-218
QuickExtract DNA Extraction Solution	Lucigen	Cat# 101098
Mouse IL-2 DuoSet ELISA	R&D Systems	DY402
Experimental Models: Cell Lines		
Human: Gesicle producer 293T cell line	Clontech	Cat# 632617
Insect: *Spodoptera frugiperda* Sf21	Invitrogen	Cat#11497013
Mouse: EL4.NOB-1	ECACC	87020408
Mouse: EL4 MyD88-GFP	Deliz-Aguirre et al.[11]	
Mouse: EL4-MyD88-GFP/IRAK1-mScarlet	Deliz-Aguirre et al.[11]	
Mouse: EL4-MyD88-GFP/IRAK4-mScarlet	Deliz-Aguirre et al.[11]	
Mouse: EL4-MyD88-GFP/IRAK1-KO	Deliz-Aguirre et al.[11]	
Mouse: EL4-MyD88-GFP/IRAK4-KO	Deliz-Aguirre et al.[11]	
Mouse: EL4 MyD88/IRAK4/IRAK1-KO (3xKO)	This paper	
Mouse: EL4-MyD88-GFP/IRAK4-KO MmIRAK4-mScarlet	This paper	
Mouse: EL4-MyD88-GFP/IRAK4-KO + MmIRAK4-(K213/214A)-mScarlet	This paper	

Mouse: EL4-MyD88-GFP/IRAK4-KO MmIRAK4-(R12C)-mScarlet	This paper	
Mouse: EL4-MyD88-GFP/IRAK4-KO MmIRAK4-ΔDD-mScarlet	This paper	
Mouse: EL4-MyD88-GFP/IRAK4-KO MmIRAK4-ΔKD-mScarlet	This paper	
Mouse:EL4-MyD88-GFP/IRAK1-KO+ MmIRAK2-mScarlet-i	This paper	
Mouse:EL4-MyD88-GFP/IRAK1-KO+ MmIRAK3-mScarlet-i	This paper	
Mouse: EL4 3xKO + MmMyD88/MmIRAK4-GFP/MmIRAK1-mScarlet	This paper	
Mouse: EL4 3xKO + MmMyD88/MmIRAK4-(K213/214A)-GFP/MmIRAK1-mScarlet	This paper	
Mouse: EL4 3xKO + MmMyD88/MmIRAK4-(K213/214A)-GFP/MmIRAK2-mScarlet	This paper	
Mouse: EL4 3xKO + MmMyD88/MmIRAK4-(K213/214A)-GFP/MmIRAK3-mScarlet	This paper	
Mouse: EL4 3xKO + MmMyD88/MmIRAK4-ΔKD-GFP/MmIRAK1-mScarlet	This paper	
Mouse: EL4 3xKO + MmMyD88/MmIRAK4-ΔKD-GFP/MmIRAK2-mScarlet	This paper	
Mouse: EL4 3xKO + MmMyD88/MmIRAK4-ΔKD-GFP/MmIRAK3-mScarlet	This paper	
Mouse: EL4 3xKO + MmMyD88/MmIRAK4-GFP/MmIRAK1-ΔKD-mScarlet	This paper	
Mouse: EL4 3xKO + MmMyD88/MmIRAK4-GFP/MmIRAK2-ΔKD-mScarlet	This paper	

Mouse: EL4 3xKO + MmMyD88/MmIRAK4-GFP/MmIRAK3-ΔKD-mScarlet	This paper	
Mouse: EL4 3xKO + hMyD88/hIRAK4-GFP/hIRAK1-mScarlet	This paper	
Mouse: EL4 3xKO + MmMyD88/mMIRAK4-GFP/MmIRAK2-mScarlet	This paper	
Mouse: EL4 3xKO + MmMyD88/MmIRAK4-GFP/MmIRAK3-mScarlet	This paper	
Mouse: EL4 3xKO + hMyD88/hIRAK4 (D329A)-GFP/hIRAK1-mScarlet	This paper	
Mouse: EL4 3xKO + hMyD88/hIRAK4 (D329A/E loop mutant)-GFP/hIRAK1-mScarlet	This paper	
Mouse: EL4 3xKO + hMyD88/hIRAK4 (A loop mutant)-GFP/hIRAK1-mScarlet	This paper	
Mouse:EL4-MyD88-GFP/IRAK1-KO+ MmIRAK1-ΔDD-mScarlet-i	This paper	
Mouse:EL4-MyD88-GFP/IRAK1-KO+ MmIRAK2-ΔDD-mScarlet-i	This paper	
Mouse:EL4-MyD88-GFP/IRAK1-KO+ MmIRAK3-ΔDD-mScarlet-i	This paper	
Mouse: EL4 3xKO + MmMyD88/MmIRAK4-GFP/MmIRAK1-mScarlet	This paper	
Mouse: EL4 3xKO + MmMyD88/MmIRAK4 (A loop mutant)-GFP/MmIRAK1-mScarlet	This paper	
Mouse: EL4 3xKO + MmMyD88/MmIRAK4 (D329A)-GFP/MmIRAK1-mScarlet	This paper	
Mouse: EL4 3xKO + MmMyD88/MmIRAK4 (D329A/E loop mutant)-GFP/MmIRAK1-mScarlet	This paper	
Mouse: Hoxb8 B6 WT primary hematopoietic stem cells	Lichtenstein et al.[36]	
Experimental Models: Organisms/strains		
NA	NA	

sgRNA sequences		
MyD88, ENSMUST00000035092	5’-AAGCAGUGUCCCACAAACAA-3’	
IRAK4, ENSMUST00000074936	5’-UCUGGACCAGUAGAUCCACA-3’	
IRAK1, ENSMUST00000114354	5’-AAACAGGGAGUGGAACCUGG-3’	
Recombinant DNA		
pHR-dSV-MmIRAK4-mScarlet-i	Deliz-Aguirre et al. [11]	
pHR-dSV-MmIRAK4-(K213/214A)-mScarlet-i	This paper	
pHR-dSV-MmIRAK4-(R12C)-mScarlet-i	This paper	
pHR-dSV-MmIRAK4-ΔKD-mScarlet-i	This paper	
pHR-dSV-MmIRAK1-mScarlet-i	This paper	
pHR-dSV-MmIRAK4-mEGFP	This paper	
pHR-dSV-MmIRAK4-K213/214A-mEGFP	This paper	
pHR-dSV-MmIRAK4-ΔKD-mEGFP	This paper	
pHR-dSV-MmIRAK1-ΔKD-mScarlet-i	This paper	
pHR-dSV-MmIRAK2-ΔKD-mScarlet-i	This paper	
pHR-dSV-MmIRAK3-ΔKD-mScarlet-i	This paper	
pHR-dSV40-MmMyD88-3xFLAG-IRESpuro	This paper	
pHR-dSV40-MmMyD88-3xFLAG-IREStagBFP	This paper	
pHR-dSV40-MmIRAK2-mScarlet-i	This paper	
pHR-dSV40-MmIRAK3-mScarlet-i	This paper	
pHR-dSV40-MmIRAK4-ΔDD-mScarlet-i	This paper	
pHR-dSV40-MmIRAK1-ΔDD-mScarlet-i	This paper	
pHR-dSV40-MmIRAK2-ΔDD-mScarlet-i	This paper	
pHR-dSV40-hMyD88-3xFLAG-IREStagBFP	This paper	

pHR-dSV40-hIRAK4-mEGFP	This paper	
pHR-dSV40-hIRAK1-mScarlet-i	This paper	
pHR-dSV40-hIRAK4-D329A-mEGFP	This paper	
pHR-dSV40-hIRAK4-D329A-E-loop-mEGFP	This paper	
pHR-dSV40-hIRAK4-A-loop-mEGFP	This paper	
pHR-dSV40-MmIRAK4-D329A-mEGFP	This paper	
pHR-dSV40-MmIRAK4-D329A-E-loop-mEGFP	This paper	
pHR-dSV40-MmIRAK4-A-loop-mEGFP	This paper	
pFastBac-6His-TEV-GST-3C-AVI-IRAK1(187-527; D358A)	MRC PPU Reagents Lange et al.[19]	DU56583
pFastBac-6His-TEV-GST-3C-IRAK4(160-460)	MRC PPU Reagents	DU65498
pFBDM-GST-3C-IRAK4(160-460; T342E/T345E/S346E)	MRC PPU Reagents	DU66477
pFBDM-GST-3C-IRAK4(160-460; T342A/T345A/S346A)	MRC PPU Reagents	DU66476
pFastBac-6His-TEV-GST-3C-IRAK4(160-460; D329A)	MRC PPU Reagents Lange et al.[19]	DU56578
pFastBac-6His-TEV-GST-3C-AVI-IRAK4(160-460; D329A/T342E/T345E/S346E)	MRC PPU Reagents	DU80380
pFastBac-6His-TEV-GST-3C-AVI-IRAK4(160-460; D329A/T342A/T345A/S346A)	MRC PPU Reagents	DU76427
Software and Algorithms		
Fiji	NIH	https://fiji.sc/
R	CRAN	https://cran.r-project.org/
AF3	Abramson et al. 2024[15]	https://alphafoldserver.com/
GraphPad Prism v10.5	GraphPad	https://www.graphpad.com/
ChimeraX	UCSF Resource for Biocomputing,	https://cgl.ucsf.edu/chimerax

	Visualization, and Informatics	
Image Lab	Bio-Rad	www.bio-rad.com/product/image-lab-software
Fiji/Python/R scripts from image analysis	This study	https://github.com/MJ-Taylor-Lab/IRAK4_Autophosphorylaytion_Paper.git

Methods

Cell Culture

EL4.NOB1 WT (ECACC, and referred to as EL4 in the paper) and gene-edited cells were grown in RPMI (Thermo Fisher Scientific) with 10% FBS (Sigma) supplemented with 2 mM L-glutamine. EL4 cultures were maintained at a cell density of 0.1-0.5x 10^6 cells/ml in 5% CO2, 37°C. HEK-293T cells (Clontech) were grown in DMEM (Thermo Fisher Scientific) with 10% FBS supplemented and 2 mM L-glutamine. All cells were determined to be negative for mycoplasma using the MycoAlert detection kit (Lonza).

Generation of CRISPR/Cas9 triple MyD88/IRAK1/IRAK4 knockout Cell Lines

We purchased WT EL4.NOB1 cells that had been electroporated with Cas9 RNPs loaded with sgRNA targeting the MyD88 (gRNA sequence 5'-AAGCAGUGUCCCACAAACAA-3', ENSMUST00000035092) IRAK4 (gRNA sequence 5'-UCUGGACCAGUAGAUCCACA-3', ENSMUST00000074936) and IRAK1 (gRNA sequence 5'-AAACAGGGAGUGGAACCUGG, ENSMUST00000114354) gene locus from the Synthego Corporation (Redwood CA, USA). From this pooled population, we isolated single cell clones by limited dilution on 96 well plates. We screened and identified MyD88/IRAK1/IRAK4 triple knockout single cell clones by western blot analysis (Fig. S1C). Western blot analysis was performed with the following antibodies: rabbit polyclonal anti-IRAK4 (Cell Signaling Technology, #4363), rabbit monoclonal anti-IRAK1 (D51G7, Cell Signaling Technology, #4504), goat polyclonal anti-MyD88 (R&D systems, #AF3109), and Mouse monoclonal anti-β-actin (Cell Signaling Technology, #4970). EL4 MyD88/IRAK4/IRAK1-KO knockout cell lines referred to as EL4-3xKO.

Western blot analysis of IRAK4 phosphorylation

EL4 wt cells were seeded into 6 well plates at a density of 7.5x10^5 cells/well 24 hours before stimulation. On the next day cells were stimulated with 1ng/ml of recombinant mouse IL-1β (Peprotech) in RPMI for several time points between 1-120 min. To prepare cell lysates, the stimulated and unstimulated cells were briefly washed in PBS to remove IL-1, and then resuspended in 2x SDS-PAGE lysis buffer (Thermo 15493939). Lysates were incubated for 5

mins at 95 C before run on NuPAGE Novex 4-12% Bis-Tris Protein Gels (Thermo) . Samples were then analyzed by western blotting. To visualize the pIRAK signal intensity relative to the IRAK4 signal, the blots were developed with Rabbit monoclonal anti-pIRAK4 (Thr(P)-345/Ser(P)-346) (a gift from Vikram Rao, Pfizer [12]), Rabbit polyclonal anti-IRAK4 (Cell Signaling Technology, Cat# 4363) and Mouse monoclonal anti-ß-actin (Cell Signaling Technology, #4970) for normalization. Chemiluminescence detection (Super signal substrate, Pierce #34095) was imaged with the BioRad ChemiDoc MP Imaging System. For each replicate we ran two gels and WB blots loaded with the identical amount of sample, for each replicate one gel was blotted for IRAK4 and the other for pIRAK4 (see Fig. S4C,D). After IRAK4 or pIRAK4 detection, both blots were stripped and then reprobed with anti-actin to normalize the signal intensity of respective IRAK4/pIRAK4 signal between the two gels. We performed analysis of the Western blot band intensity and quantified the production of pIRAK4 in ImageJ/Fiji. The intensity of the IRAK4 and pIRAK4 band was normalized to the actin loading control on each blot for each replicate. The normalized pIRAK4 value was then divided by the normal IRAK4 value to give a relative value of pIRAK4 production at each time point assayed. Data was visualized and plotted in R.

For Western Blot analysis of pIRAK4 levels in IRAK4 kinase inhibitor treated/untreated EL4 cells (Fig. S3D), we incubated EL4 cells with media containing 20 µM of IRAK4 kinase inhibitor (PF-06650833, stock concentration of 10 mM in DMSO) for 4 hours. DMSO at a final concentration of 0.2% v/v was added to the control samples. EL4 cells were then stimulated with 10-100 ng/ml of recombinant mouse IL-1β for 30 mins. We prepared cell lysates as described above, and ran them on NuPAGE Novex 4-12% Bis-Tris Protein Gels (Thermo). After membrane transfer, cell lysates were probed with anti-pIRAK4 and developed by chemiluminescence as described above.

Co-Immunoprecipitation of Myddosomes from EL4 Cell Lysates

24 hours before stimulation, $5x10^6$ EL4 MyD88-GFP cells were seeded in T-75. The next day, the medium was removed and fresh medium, containing 20µM IRAK4 kinase inhibitor or 0.2% DMSO only, was added. The cells were incubated with IRAK4 kinase inhibitor or DMSO at 37°C for 4 hours. The cells were stimulated with 100 ng/ml of recombinant mouse IL-1β for 15 mins. Stimulated and unstimulated cells were then washed in ice cold PBS, spun down and resuspended in lysis buffer (50 mM Tris, 150 mM NaCl, 1% Igepal/ NP40, pH 8.0). Lysis buffer contained phosphatase and protease inhbitiors (PhosSTOP, Roche, Cat# 04906837001 and Protease Inhibitor Mini Tablets, EDTA-free, Pierce, Cat# A32955) at the manufacturer's recommended concentration. Aliquots of the lysates were stored for downstream analysis (input fraction). Lysates were added to GFP beads (Chromotek: GFP-Trap Magnetic Particles, Cat# M-270) pre-equilibrated in Lysis buffer, and incubated overnight with rotation at 4°C. The next day beads were applied to magnetic racks and the supernatant was removed. Next, the beads were washed in the Lysis buffer, and eluted in 50 µl of the SDS sample loading buffer. The beads were vortexed and incubated for 5 mins at 95°C. The eluted and input fractions were then ran on NuPAGE Novex 4-12% Bis-Tris Protein Gels (Thermo) and analyzed by Western Blot using the antibodies and protocols described above (Fig. S4F).

Design of a phosphomimetic IRAK4 allele

The homodimerization of the IRAK4 kinase domain in the unphosphorylated state positions an activation loop region containing threonine and serine residues into the opposing kinase domain's active site[14]. The resulting auto-phosphorylation of these residues induces a conformational change in the kinase domain and drives the dissolution of the homodimer[14]. As only the phosphorylated IRAK4 kinase domain can interact with the IRAK1 kinase domain, it is most likely these residues that contribute to the heterodimerization interface, thereby allowing IRAK4 autophosphorylation to function as a switch that drives heterodimerization, relieves internal inhibition of IRAK1, and allows its DD to incorporate into the Myddosome complex . To mimic the possibly effect of phosphorylation, and lock IRAK4 in a confirmation that mimics the effect of phosphorylation and can interact with IRAK1 kinase domain, we designed a triple mutant where the threonine 343 and 345, serine 346 was exchanged with the negatively charged glutamic acid (T343E/T345E/S346E, referred to as E-loop mutant). This mutation was combined with the D329A mutation that disrupted IRAK4 kinase activity. This mutation was cloned into a lentiviral vector for expression in EL4 cells and the kinase domain into insect cell expression vectors for in vitro analysis (see below). In addition, a triple mutation was also created that mutated these loop residues to alanine (A-loop). These residues were combined with both kinase active and inactive IRAK4 alleles. (Fig. 5, Fig. S6)

Generation of lentiviral constructs

Full details of the Lentiviral plasmid construction are given below. All full length constructs were confirmed by Sanger sequencing.

pHR-dSV-IRAK4-K213/214A-mScarlet-i/mEGFP, pHR-dSV-IRAK4-ΔKD-mScarlet-i/mEGFP

To prepare the pHR-dSV-IRAK4-(K213/214A)-mScarlet-i/mEGFP and pHR-dSV-IRAK4-ΔKD-mScarlet-i/mEGFP constructs, the mouse IRAK4 sequence with two mutations (K213/214A) and the mouse IRAK4 sequence excluding the kinase domain were ordered as gBlocks (IDT). These gBlocks were fused with a PCR fragment of mScarlet-i (amplified by PCR using the forward 5'-tgctacaagagatgtctgctggaggaagtggaggttctggtggtagtgtg-3' and reverse 5'-aggtcgactctagagtcgcggcc-3' primers) or mEGFP (PCR using the forward 5'-tgctacaagagatgtctgctggaggaagtggaggttctggtggtagtgtg-3' and reverse 5'-ggccgcgactctagagtcgacct-3' primers) and Mlu1/Not1 digested pHR-dSV lentiviral plasmid using Gibson assembly [37]. IRAK4 constructs were fused in frame to mScarlet-i or mEGFP via a 3xGGS linker.

pHR-dSV-IRAK4-mEGFP

Full length IRAK4 (BC051676) was amplified by PCR from a previously described [11] pHR-dSV-IRAK4-mScarlet-i construct. mEGFP was amplified using the above-mentioned primers. DNA fragments were assembled with pHR-dSV lentiviral plasmid digested with Mlu1/Not1 using Gibson Assembly.

pHR-dSV-IRAK1-mScarlet-i

Full length Mouse IRAK1 (NCBI Reference Sequence: NP_001171445.1) was ordered as a codon optimized gBlock (IDT). The gBlock encoded a complementary 5' end to pHR-dSV. This DNA fragments was fused to PCR fragment of mScarlet-i (amplified by PCR using the forward 5'-gggggtagcggaggttctggtggtagtgtgagcaaggg-3' and reverse 5'-cctgcaggtcgactctagagtcgcggccgctttacttgtacagctcgtccatgcc-3' primers) and a pHR-dSV lentiviral plasmid digested with Mlu1/Not1 using Gibson Assembly. IRAK1 was fused in frame to mScarlet-i via a 3xGGS linker

pHR-dSV-IRAK1-ΔKD-mScarlet-i

A fragment of Mouse IRAK1 (NCBI Reference Sequence: NP_001171445.1) that consisted solely of the DD and excluded the kinase domain was ordered as a codon optimized gBlock (IDT). The gBlock encoded a complementary 5' end to pHR-dSV. This DNA fragments was fused to PCR fragment of mScarlet-i (amplified by PCR using the forward 5'-gggggtagcggaggttctggtggtagtgtgagcaaggg-3' and reverse 5'-cctgcaggtcgactctagagtcgcggccgctttacttgtacagctcgtccatgcc-3' primers) and a pHR-dSV lentiviral plasmid digested with Mlu1/Not1 using Gibson Assembly. IRAK1-ΔKD was fused in frame to mScarlet-i via a 3xGGS linker

pHR-dSV-IRAK1-ΔDD-mScarlet-i

A fragment of Mouse IRAK1 (NCBI Reference Sequence: NP_001171445.1, amino acids 101-710) that consisted solely of the kinase domain and excluded the DD was ordered as a codon optimized gBlock (IDT). The gBlock encoded a complementary 5' end to pHR-dSV. This DNA fragments was fused to PCR fragment of mScarlet-i (amplified by PCR using the forward 5'-gggggtagcggaggttctggtggtagtgtgagcaaggg-3' and reverse 5'-cctgcaggtcgactctagagtcgcggccgctttacttgtacagctcgtccatgcc-3' primers) and a pHR-dSV lentiviral plasmid digested with Mlu1/Not1 using Gibson Assembly. IRAK1-ΔDD was fused in frame to mScarlet-i via a 3xGGS linker

pHR-dSV-IRAK2-mScarlet-i, pHR-dSV-IRAK3-mScarlet-i

Full length Mouse IRAK2 (NCBI Reference Sequence: NP_751893.3) and full length Mouse IRAK3 (NCBI Reference Sequence: NP_082955.2) were ordered as codon optimized gBlocks (IDT). The gBlock encoded a complementary 5' end to pHR-dSV. This DNA fragment was fused to the pHR-dSV-IRAK1-mScarlet-i lentiviral plasmid digested with Mlu1/BamH1 (to excise the IRAK1 fragment) using Gibson Assembly. IRAK2/3 was fused in frame to mScarlet-i via a 3xGGS linker.

pHR-dSV-IRAK2-ΔKD-mScarlet-i, pHR-dSV-IRAK3-ΔKD-mScarlet-i

A codon optimized fragment of Mouse IRAK2 (NCBI Reference Sequence: NP_751893.3, amino acids 1-110) and Mouse IRAK3 (NCBI Reference Sequence: NP_082955.2, amino acids 1-110) that consisted solely of the DDs and excluded the kinase domains were ordered from Twist Biosciences cloned into a pHR-dSV-mScarlet-i lentiviral plasmid. This fragment was fused in frame to mScarlet-i via a 3xGGS linker.

pHR-dSV-IRAK2-ΔDD-mScarlet-i

A codon optimized fragment of Mouse IRAK2 (NCBI Reference Sequence: NP_751893.3, amino acids 97-622) that consisted solely of the kinase domains and excluded the DDs were ordered from Twist Biosciences cloned into a pHR-dSV-mScarlet-i lentiviral plasmid. This fragment was fused in frame to mScarlet-i via a 3xGGS linker.

pHR-dSV40-MyD88-3xFLAG-IRES-Puro, pHR-dSV40-MyD88-3xFLAG-IRES-TagBFP

Mouse or Human MyD88 fused to 3xFLAG-IRES-Puro or 3xFLAG-IRES-TagBFP was ordered as a codon optimized gBlock (IDT). The gBlock encoded a complementary 5' end to pHR-dSV. This DNA fragment was fused to the pHR-dSV-IRAK1-mScarlet-i lentiviral plasmid digested with Mlu1/Not1 (to excise the IRAK1 mScarlet-i fragment) using Gibson Assembly.

pHR-dSV40-hIRAK4-D329A-E-loop-mEGFP, pHR-dSV40-hIRAK4-A-loop-mEGFP

Based on structural data and biochemical characterization of IRAK4 autophosphorylation [14], we engineered kinase-inactive mutants of IRAK4 that were still capable of interacting with the IRAK1 kinase domain. IRAK4 undergoes autophosphorylation at the serine and threonine-rich region referred to as the activation loop. Analysis of the AF3 model of the fully assembled Myddosome (Fig 1A) indicates that the IRAK4 active loop region is located at the interface between IRAK4 and IRAK1. To replicate the charged environment induced by phosphorylation in this loop, we substituted S342, T344, and T345 with glutamic acid, creating the E-loop mutant, and combined these mutations with the D329A mutation, which inactivates the kinase domain [12]. Furthermore, we developed an additional mutant by altering the serine/threonine residues within this loop region to alanine, termed the A-loop mutant. These mutants were synthesized as gene fragments by IDT and cloned into the pHR-dSV40 vector backbone in frame with mEGFP using Gibson Assembly. Biochemical analysis of the recombinantly produced IRAK4 kinase domain with these mutations confirmed the restoration of heterodimerization with the IRAK1 kinase domain, even in the absence of IRAK4 kinase activity (see below).

Lentiviral Production and Generation of Stable Expressing EL4 Cell Lines

Lentivirus particles were produced in HEK-293T cells by co-transfection of the pHR transfer plasmids with second-generation packaging plasmids pMD2.G and psPAX2 (a gift from Didier Trono, Addgene plasmid # 12259 and # 12260). Virus particles were harvested from the supernatant after 48-72 hrs, filtered, and applied to EL4 cells. After three days, the transduced EL4 cells were resuspended in fresh RPMI medium. After lentiviral transduction, we select positive EL4 cells expressing fluorescent protein fusion of IRAK4/1 using a BD FACS Aria II at the Deutsches Rheuma-Forschungszentrum Berlin Flow Cytometry Core Facility. Specific details of EL4 cell line generation given below.

To engineer EL4 cells expressing IRAK4 alleles, we transduced EL4-MyD88-GFP/IRAK4 KO cells with lentiviruses encoding WT or mutant IRAK4. 1-2 weeks after lentivirus transduction, we used FACS to select cell populations with homogenous expression levels. EL4 WT cells were used as a negative control and the EL4-MyD88-GFP/IRAK4-mScarlet knock-in cell line

was used to create a sorting gate that selected transduced cells with expression levels that were equivalent to endogenously expressed IRAK4.

To engineer EL4 cells expressing IRAK2 or IRAK3 tagged with mScarlet, we transduced EL4-MyD88-GFP/IRAK1 KO cells with lentiviruses encoding WT IRAK2 or IRAK3 fused to mScarlet-i. 1-2 weeks after lentivirus transduction, we used FACS to select cell populations with homogenous expression levels. EL4 WT cells were used as a negative control and the EL4-MyD88-GFP/IRAK1-mScarlet knock-in cell line was used to create a sorting gate that selected transduced cells with expression levels that were equivalent to endogenously expressed IRAK1.

To engineer the EL4-3xKOs expressing MyD88, IRAK4-GFP and IRAK1-mScarlet, we transduced EL4-3xKOs with lentivirus encoding MyD88-FLAG-IRES-Puromycin. After 1 week of selection with media containing 1 µg/ml of puromycin for 1 week, single cells were sorted in 96 well plates. Single cell clones that grew were assayed by western blot for MyD88 expression level that matched the MyD88-GFP/IRAK4-mScarlet EL4 cell line. Based on this analysis we selected a single clone and transduced it with lentiviruses encoding IRAK1/2/3/4-WT/mutants tagged with mEGFP/mScarlet-i. Cells were then FACS sorted to select GFP/mScarlet positive cells after 1-2 weeks post lentiviral transduction.

To engineer further EL4-3xKOs expressing MyD88, IRAK4-GFP and IRAK1-mScarlet, we transduced EL4-3xKOs with lentivirus encoding MyD88-FLAG-IRES-TagBFP, FACS sorted for TagBFP, transduced the BFP positive cell population with lentiviral constructs and FACS sorted to select GFP/mScarlet positive cells after 1-2 weeks post lentiviral transduction

Baculovirus expression of the kinase domain of human IRAK4, and IRAK1

The kinase domains of human IRAK1 (187-527; D358A) and human IRAK4 (160-460), and all corresponding mutants, were expressed in insect cells. Bacmid DNA was generated by transformation of pFastBac vectors into DH10EMBacY E. coli cells (Geneva Biotech) and was subsequently used for baculovirus generation and amplification in Sf21 (Spodoptera frugiperda) insect cells, as described elsewhere[19,38]. Sf21 insect cells (Invitrogen) were cultured at 27°C in Sf-900 II serum-free medium (Thermo Fisher), either as adherent cultures for bacmid transfection and initial virus amplification, or as suspension cultures for larger scale amplification and protein expression.

Expression cultures of baculovirus-infected Sf21 cells (1-2 litres) were grown at 27°C until the percentage of YFP-expressing cells reached >70%. Cells were harvested by centrifugation at 2,500 × g for 30 min at 4°C. The resulting cell pellets were resuspended in ice-cold buffer (50 mM HEPES pH 7.5, 500 mM NaCl, 20% glycerol, 1 mM AEBSF, 1 mM benzamidine, 20 ppm Pierce Universal Nuclease (Thermo Fisher), 5 mM β mercaptoethanol) and lysed by 30 passes in a Dounce homogeniser on ice. Lysates were clarified by centrifugation at 40,000 × g and 4°C for 40 min. Protein kinase domains were purified using a tandem-affinity approach in which they were first purified by an initial pass over Ni-NTA agarose resin, followed by a second purification step on GSH-4B sepharose, as described previously[39]. Protein was eluted from GSH-resin by

cleavage of the 6His-GST-tag with PreScission Protease at 4°C overnight and concentrated using 10 kDa MWCO centrifugal filter units.

Native PAGE co-migration assay

Co-migration of IRAK1 and IRAK4 on Tris-Glycine gels under native conditions can be used to visualise their interaction[19,27]. 3 µg of IRAK1 (187-527; D358A) and 3 µg of IRAK4 (160-460) were incubated together at 30°C for 1 hour with gentle shaking in 10 µl of 35 mM HEPES pH 7.5, 5 mM MgCl2, 2.5 mM DTT. The samples were cooled to room temperature and added to 10 µl Novex (2×) Tris-Glycine Native Sample Buffer (Thermo Fisher). After mixing well, samples were pre-incubated on ice for 1 hour prior to loading on Novex 10% Tris-Glycine gels (Thermo Fisher). Samples were separated by electrophoresis with Novex Tris-Glycine Native Running Buffer (Thermo Fisher) at a constant voltage of 150 V for 1 h 45 min at 4°C. Gels were stained with InstantBlue Protein Stain (Abcam) and images captured using the ChemiDoc MP Imaging System (Bio-Rad).

Assay of IL-2 release in WT and gene-edited EL4 cells

To measure IL-2 release, we used the Mouse IL-2 DuoSet ELISA kit (R&D Systems, DY402-05) using the manufacturer's protocol. The day before IL-1 stimulation, EL4 cells were resuspended into fresh media. In experiments that measured the effect of the IRAK4 kinase inhibitor, this resuspension media contained the inhibitor (or equivalent 0.2% v/v of DMSO-only in untreated samples) at the reported concentration (Fig. S4G). The next day, the cells were counted and resuspended in fresh media. We then seeded cells in 48-well plates with $1x10^6$ cells in 150 µl of media per well. Cells were allowed to settle for 30 min, before being stimulated with recombinant mouse IL-1β (PeproTech) in 50 µl medium per well at a final concentration of 5 ng/mL. For IL-2 ELISA measurements performed with IRAK4 kinase inhibitor treated cells, the concentration of the inhibitor in the media was kept constant throughout the entire duration of the assay. For the unstimulated controls, 50 µl medium was added with/ without the inhibitor. After incubating the cells for 24 h with IL-1, the plates were centrifuged (800x g for 5 minutes), and supernatants were transferred into a new plate. Supernatants were stored at -80°C until IL-2-ELISA analysis. Absorbance readings were acquired on a VersaMax Microplate Reader (Molecular Devices) at 450 nm. IL-2 release was assayed on three independent days in triplicates. The obtained results were expressed as the fold change in IL-2 release between the stimulated and unstimulated samples (Fig. S1B, S4G).

Imaging Chambers and Supported Lipid Bilayers

SLBs were prepared using a previously published method [40]. Phospholipid mixtures consisting of 97.5% mol 1-palmitoyl-2-oleoyl-sn-glycero-3-phosphocholine (POPC), 2% mol 1,2-dioleoyl-sn-glycero-3-[(N-(5-amino-1-carboxypentyl)iminodiacetic acid)succinyl] (ammonium salt) (DGS-NTA) and 0.5% mol 1,2-dioleoyl-sn-glycero-3-phosphoethanolamine-N-[methoxy(polyethylene glycol)-5000] (PE-PEG5000) were mixed in glass round-bottom flasks and dried down with a rotary evaporator. All lipids used were purchased from Avanti Polar Lipids. Dried lipids were placed under vacuum for 2 hrs to remove trace chloroform and resuspended in PBS. Small unilamellar vesicles were produced by several

freeze-thaw cycles in conjunction with sonication. Once the suspension had cleared, the lipids were spun in a benchtop ultracentrifuge at 35,000xg for 45 min and kept at 4°C for up to five days.

Supported lipid bilayers (SLB) were formed in 96-well glass bottom plates (SWISSCI). 96-well plates were cleaned for 30 min with a 5% Hellmanex solution containing 10% isopropanol heated to 50°C, then incubated with 5% Hellmanex solution for 1 hour at 50°C, followed by extensive washing with pure water. 96-well plates were dried with gas nitrogen and sealed using clear Polyolefin sealing tape (Thermo Scientific) until needed. To prepare SLB on 96-well plates, individual wells were cut out and base etched for 15 min with 5 M KOH and then washed with water and finally PBS.

To form SLBs, SUVs suspension was deposited in each well and allowed to form for 1 hr at 45°C. After 1 hr, wells were washed extensively with PBS. SLBs were incubated for 20 min with HEPES buffered saline (HBS: 20 mM HEPES, 135 mM NaCl, 4 mM KCl, 10 mM glucose, 1 mM CaCl2, 0.5 mM MgCl2) containing with 5 mM NiCl2 to charge the DGS-NTA lipid with nickel. The SLBs were then washed in HBS containing 0.1% BSA to block the surface and minimize non-specific protein adsorption and incubated at room temperature for 30 min. For SLBs set up on 96-well plates the total well volume was 690 µl. Each well was completely filled with HBS containing 0.1% BSA, and 570 µl was removed leaving 120 µl in each well. After blocking, the SLBs were functionalized by incubation for 1 hr with 120 µl His-tagged proteins to get a final concentration of 5 nM. The labeling solution was then washed out with HBS.

Protein Expression, Purification and Labeling for SLB experiments

We functionalized supported membranes with an engineered variant of mouse IL1β (in text referred to as His10-Halo-JF646-IL-1β). This IL-1 variant had been engineered to have a 10x His tag, and could therefore label membranes that contained DGS-NTA lipids. Full details on the design, expression and purification of this construct have been previously reported[11,41]. For microscopy calibration of mScarlet single molecule intensity we used His10-mScarlet-IL-1β. For mEGFP single molecule intensity calibration, mEGFP was expressed and purified as previously described (see references [11] and [41]).

TIRF-Microscopy data acquisition

Dual color imaging of EL4 cells was performed on an inverted microscope (Nikon TiE, Tokyo, Japan) equipped with NIKON fiber launch TIRF illuminator. Illumination was controlled with a laser combiner using the 488, 561 and 640 nm laser lines. Fluorescence emission was collected through filters for GFP (525 ± 25 nm), RFP (595 ± 25 nm) and JF646 (700 ± 75 nm). All images were collected using a Nikon Plan Apo 100x 1.4 NA oil-immersion objective that projected onto a Photometrics 95B Prime sCMOS camera with 2x2 binning and a 1.5x magnifying lens (calculated pixel size of 0.147 µm). Image acquisition was performed using NIS-elements software. All experiments were performed at 37°C. The microscope stage temperature was maintained using an OKO Labs heated microscope enclosure. Imaging frames of live cells was acquired at an interval of 3 s using exposure times of 200-400 ms.

Imaging EL4 cells expressing tagged Myddosome components on IL-1β functionalized SLBs with TIRF-Microscopy

His10-Halo-JF646-IL1β functionalized SLBs were set up as described above and as previously described [11,41]. To quantify the IL-1β density on the SLB before each experiment, wells were prepared that were functionalized with identical labeling protein concentration and time, but with different molar ratios of labelled to unlabelled His10-Halo-IL1β. Before application of cells, SLBs were analysed by TIRF microscopy to check formation, mobility and uniformity. Short time series were collected at wells containing a ratio of labeled to unlabelled His10-Halo-IL1β, (e.g. <1 His10-Halo-JF646-IL1β molecule per μm2) to calculate ligand densities on the SLB based upon direct single molecule counting. All experiments were performed at IL-1 SLB densities of 50 to 80 molecules per μm2.

Before each imaging experiment we acquired calibration images using recombinant mEGFP and mScarlet-i. To image single GFP/mScarlet-i fluorophores, recombinant purified mEGFP and mScarlet-i [41] was diluted in HBS and adsorbed to KOH cleaned glass. Single molecules of GFP or mScarlet-i were imaged using identical microscope acquisition settings to those used for cellular imaging. To image live cells, EL4 cells were pipetted onto supported lipids bilayers functionalized with His10-Halo-JF646-IL1β. EL4 cells expressing complementary GFP- and mScarlet-tagged Myddosome components (e.g., MyD88–GFP together with wild-type or mutant IRAK4–mScarlet or WT or mutant IRAK4-GFP with IRAK1/2/3–mScarlet) were sequentially illuminated with 488 nm (70–100 ms) and 561 nm (100 ms) lasers at 3 s frame intervals.

For pharmacological inhibition experiments, EL4 cells were treated with increasing concentrations of the IRAK4 kinase inhibitor PF06650833 (Sigma) for at least 3 hours prior to imaging (Fig. 3J, K, and L). All treatment conditions contained 0.1% DMSO (v/v). Before imaging, cells were pelleted and resuspended in HBS containing the corresponding inhibitor concentration. The resuspended cells were then added to imaging wells containing HBS supplemented with the same inhibitor concentration, thereby maintaining the dose response conditions throughout microscopy acquisition.

Live cell single molecule imaging of IRAK1, IRAK2 and IRAK3 kinase domain recruitment

His10-Halo-JF646–IL1β–functionalized SLBs were prepared on 25 mm round nano-printed coverslips with a chromium grid, as previously described [41]. Gridded coverslips were used to limit the lateral movement of MyD88-GFP puncta. This stabilization allowed the position of partially assembled Myddosomes to be identified and then interrogated using high-frame-rate imaging of the mScarlet channel to detect transient recruitment of the IRAK1/2/3 kinase domain. EL4-MyD88-GFP/IRAK1-KO cells reconstituted with IRAK1/2/3-ΔDD-mScarlet were allowed to settle on the coverslips for 5–10 minutes. Fields of view containing cells with MyD88-GFP puncta (i.e., partially assembled Myddosomes) were selected.

A reference image was acquired in the GFP channel and widefield (for cell boundaries), followed by continuous imaging in the mScarlet channel. For IRAK1/2/3-ΔDD-mScarlet, an exposure time of 200 ms was used. In this modality, 1200 frames were acquired per field. Data

were collected from cells treated with the IRAK4 kinase inhibitor (as described above) or with an equivalent concentration of DMSO.

To analyze IRAK1/2/3 kinase domain recruitment, the MyD88-GFP reference images were used to manually segment cells in the mScarlet channel. The segmented image stacks corresponding to the cell footprints on the bilayer were processed using TrackMate in FIJI to detect and track IRAK1/2/3 kinase domain recruitment events. From the resulting data files, the mean number of recruitment events per cell (Fig. 4D, G, and J) and the lifetime of recruitment events (Fig. 4E, H, and K) were calculated.

Immunofluorescence staining and quantification of phospho-IRAK4

To analyze the colocalization of phospho-IRAK4 with MyD88-GFP and IRAK4-mScarlet or IRAK1-mScarlet (Fig. 4A, B), EL4 cells were stimulated with IL-1β-functionalized SLBs for 30 mins, and then fixed with 4% (wt/vol) PFA containing 0.5% (wt/vol) Triton X-100 for 20 min at room temperature. Staining was then performed with a traditional two-step staining method. After fixation, cells were washed with PBS, then blocked in PBS containing 10% (wt/vol) BSA and 0.1% Triton X-100 at 4° C overnight. The next day, the cells are stained using a 1 step labeling procedure with antibody solution containing anti-pIRAK4 (1:400, Vikram Rao, Pfizer), Nano-Secondary 647 (1:1000, ChromoTek alpaca anti-human IgG/anti-rabbit IgG, recombinant VHH, Alexa Fluor 647 CTK0101, CTK0102 #srbAF647-1) and FluoTag-X4 anti-GFP conjugated to Atto488 (1:500, Nano Tag Biotechnology, #N0304-At488-L) and FluoTag-X4 anti-RFP conjugated to Atto568 (1:500, Nano Tag Biotechnology, #N0404-AF568-L) in PBS containing 10% (wt/vol) BSA and 0.1% Triton X-100 for 1 hr at room temperature. Subsequently, cells were washed with 2 ml 10% (wt/vol) BSA and 0.1% Triton X-100 and finally with 4 ml PBS before imaging with TIRF microscopy.

To score MyD88 puncta negative or positive for phospho-IRAK4 and IRAK4-mScarlet or IRAK1-mScarlet, TIRF microscopy images were manually segmented into individual cells. The phosphoIRAK4 and IRAK4-mScarlet or IRAK1-mScarlet channels were blinded, and then MyD88 puncta manually identified and scored negative or positive for colocalization with puncta in the blinded phospho-IRAK4 channel and IRAK4-mScarlet or IRAK1-mScarlet channel. Manual identification and scoring was performed in FIJI with the multi-point annotation tool. We blinded the IRAK4/1-mScarlet and pIRAK4 staining channels before manual scoring of MyD88-GFP puncta. We performed this manual analysis for over 400 MyD88-GFP puncta identified in both EL4-MyD88-GFP/IRAK4-mScarlet and EL4-MyD88-GFP/IRAK1-mScarlet cells. Unblinded manual scoring of MyD88-GFP puncta was visualized as a bar graph (Fig. 4A and B).

Quantification and Statistical Analysis

All data are expressed as the mean ± the standard deviation (SD) or mean ± the standard error of the mean (SEM), as stated in the figure legends and results. The exact value of n and what n represents (such as the number of experimental replicates, cells or MyD88-puncta) is stated in figure legends and results. Means were compared using Wilcoxon Rank-Sum test, due to the

small n size of replicate making it difficult to determine whether the data is normally distributed. Data analysis scripts used in this study available at GitHub.

Quantification and analysis of Myddosome intensity, lifetime and dynamics

To quantify the dynamics of Myddosome assemblies labelled with fluorescently tagged MyD88 or IRAKs, we created an image analysis pipeline that runs in FIJI, Python and R. Image analysis scripts were parallelized so that they may run on cluster computers at the Max Planck Computing and Data Facility (Garching, Bavaria, Germany). The aim of this image analysis pipeline was to first process the images to remove intensity count that derived from camera noise or background fluorescence (non-specific cytosolic fluorescent signal), identify and segment single cells, and then identify and track the individual fluorescently labeled Myddosome complexes within the live cell data. To process the image stack, we first subtracted a dark frame image (i.e., an image only containing intensity values from current and noise generated by the camera electronics) from each image file. The dark frame image was created by calculating the mean intensity from 5000 images acquired without light exposure to the camera, and with identical acquisition settings to those used for live cell imaging.

From this point, dark frame subtracted images were processed to create two sets of image stacks: one set was used for intensity measurements to quantify the dynamics of Myddosome assembly (referred to as the intensity reference image). The second set was processed using different filters and parameters best suited to detect punctate structures, and this was used to optimally identify and track the Myddosomes (referred to as the tracking images). To generate an images stack for tracking Myddosome puncta, the GFP/mScarlet images were processed with a median filter with a 11-pixel diameter. The resulting median filtered image is subtracted from the original to remove background intensity. We next applied two methods to address stochastic fluctuation associated with the fluorophore blinking or camera read noise, both which can contribute to errors in particle detection and linking detected particles between frames. First, we applied a second median blur of 5-pixel diameter to even out the field. Because median filters are edge-preserving (keeps silhouette), a 5-pixel diameter median blur preserved punctate structures while further removing background noise. We then applied a moving average of 3 frames to further suppress intensity fluctuations. Because we were interested in detecting Myddosomes (i.e., puncta that possibly contain both MyD88 and IRAK4 or IRAK4 and IRAK1/2/3), we reasoned that combining the GFP and mScarlet channels into a single image would further increase the signal to noise ratio, facilitating the detection and tracking of Myddosome fluorescent puncta. Therefore, all GFP and mScarlet image frames were summed. The result was a single time series with high signal to noise and optimized for particle detection and tracking.

The combination of two median blur filtering steps and running average used to create the tracking reference image skewed intensity values. Therefore, to be able to accurately quantify Myddosome intensity and assembly kinetics, we generated an intensity reference image that preserved intensity values. To accomplish this, we estimate cytosolic background using a median blur with a 25-pixel diameter (3.67μm), which is roughly half the diameter of the cell: SLB interfaces observed in the TIRF field. This median blurred image is an estimate of

background intensity from the cytoplasmic fluorescence (that is GFP or mScarlet tagged MyD88 or IRAKs not assembled into Myddosome complexes). This estimated background fluorescent intensity is subtracted from the dark frame removed images and the resulting image is the intensity reference image from which all shown and analyzed intensity values are derived.

Next, individual cells within the time series were identified using a marker-controlled watershed segmentation (algorithm from Open Source Computer Vision, OpenCV) implemented on a maximum projection image of the GFP intensity channel. The segmented cell boundaries were used to break both the tracking image and intensity reference series into small image series of individual cells. We used the FIJI TrackMate plugin to track the MyD88-GFP/IRAK4/1-Scarlet or IRAK4-GFP/IRAK1/2/3-mScarlet puncta within the tracking image for each segmented cell. We tracked MyD88-GFP/IRAK4/1-mScarlet puncta with a maximum linkage distance of 5 pixels, a tracking threshold of 1.5 and a tolerance of 2 gap-closing frames between detected particles. After processing in TrackMate, tracking coordinates generated were imported into R. To fill in missing frames (i.e., gap-closing frames with no detected particles) within tracks, we approximated the location of the missing puncta using the Euclidean distance from the coordinates of the preceding and following detected particle. We extracted the fluorescence intensity of puncta from the intensity reference frames of both the MyD88-GFP image and the IRAK4/1-mScarlet image. The intensity was measured from a 5x5 circular pixel region center of the puncta centroid. To achieve sub-pixel accuracy, we segmented a square matrix of pixels from images. This square was centered on the puncta centroid. To reduce computational time, this segmented area was expanded 11 fold with the original pixel intensity subdividing in the expanded area pixels. The square was then multiplied against a binary circle mask (diameter of 5 pixels that was also expanded by 11 fold). The pixel intensities of the product were summed to give a puncta intensity for both the GFP or mScarlet channel.

To estimate the number of MyD88 and IRAKs within tracked Myddosome assemblies, the fluorescent intensity was divided by the median intensity of single GFP and mScarlet fluorophores. To compute the distribution of single fluorophore intensities, images of single GFP or mScarlet fluorophores adsorbed to glass were processed and analyzed identically to MyD88-GFP, IRAK4-GFP and IRAK4/1/2/3-mScarlet images. We restricted the analysis to MyD88-GFP and IRAK4/1-mScarlet puncta tracked for three or more frames, to focus our analysis to *bona fide* Myddosome assemblies nucleating at the plasma membrane. Puncta were scored positive for IRAK4/1/2/3 recruitment when the normalized fluorescent intensity of at least 1.5x IRAK4/1s for 30 seconds or more (Fig. 1D, G, J, Fig. 2E, H, K, N, Fig. 3C, F, I, J through M, Fig. 5E, Fig. S3C, E , Fig. S4H, and Fig. S5E). IRAK4/1/2/3 dwell time distribution was calculated by summing consecutive frames where the IRAK4/1/2/3 signal intensity was above this fluorescent intensity threshold (Fig. 1C, F, I, Fig. 2D, G, J, M, Fig. 3B, E, H, Fig. 5D, Fig. S3B and Fig. S5D). To calculate the size distribution of IRAK1/2/3 assemblies we plotted the (Fig. S2D through G and Fig. S5F). We restricted this analysis to IRAK4 puncta which recruit IRAK1/2/3 with a size of 0.75x or above. We performed data visualization using ggplot2, a data visualization package for R.

Supplementary Movies

Supplementary Movie 1: IRAK4:IRAK1 co-assembly requires the IRAK4 kinase domain. Split screen showing EL4-3xKO cells reconstituted with MyD88, IRAK4-WT-GFP (Top) or IRAK4-ΔKD-GFP (Bottom) and IRAK1-mScarlet interacting with IL-1-functionalized SLBs. All movies shown acquired using TIRF microscopy. In the merge panels IRAK1-mScarlet images are shown in magenta and IRAK4-GFP in green. Scale bar, 5 μm.

Supplementary Movie 2: IRAK1 kinase domain is dispensable for IRAK4:IRAK1 co assembly. Split screen showing EL4-3xKO cells reconstituted IRAK4-GFP and IRAK1-WT-mScarlet (top row) or IRAK1-ΔKD-mScarlet (bottom row) interacting with IL-1-functionalized SLBs. All movies shown acquired using TIRF microscopy. In the merge panels IRAK1 images are shown in magenta and IRAK4-GFP in green. Scale bar, 5 μm.

Supplementary Movie 3: IRAK4:IRAK2 and IRAK4:IRAK3 co-assembly requires the IRAK4 kinase domain. Split screen showing EL4-3xKO cells expressing IRAK4-ΔKD-GFP and IRAK2-mScarlet (top row) or IRAK3-mScarlet interacting with IL-1-functionalized SLBs. All movies shown acquired using TIRF microscopy. In the merge panels IRAK3 images are shown in magenta and IRAK4-GFP in green. Scale bar, 5 μm.

Supplementary Movie 4: The IRAK2 and IRAK3 kinase domain is dispensable for co-assembly with IRAK4. Split screen showing EL4-3xKO cells expressing IRAK4-WT-GFP and IRAK2-ΔKD-mScarlet (top row) or IRAK3-ΔKD-mScarlet interacting with IL-1-functionalized SLBs. All movies shown acquired using TIRF microscopy. In the merge panels IRAK2/3 images are shown in magenta and IRAK4-GFP in green. Scale bar, 5 μm.

Supplementary Movie 5: IRAK4 kinase activity is required for stable co-assembly with IRAK1. Split screen showing EL4-3xKO cells expressing IRAK4-K213/214A-GFP and IRAK1-mScarlet interacting with IL-1-functionalized SLBs. All movies shown acquired using TIRF microscopy. In the merge panels IRAK1 images are shown in magenta and IRAK4-GFP in green. Scale bar, 5 μm.

Supplementary Movie 6: The kinase domain of IRAK1, independent of the DD, can be recruited to the partially assembled Myddosome. Split screen showing EL4-MyD88-GFP/IRAK1-KO cells expressing IRAK1-ΔDD-mScarlet interacting with IL-1-functionalized SLBs in the presence of DMSO (top row) or an IRAK4 kinase inhibitor (bottom row). All movies shown were acquired using TIRF microscopy. Scale bar, 5 μm.

Supplementary Movie 7: A phosphomimetic mutation can restore stable IRAK1 co-assembly to a kinase inactive IRAK4 mutant. Split screen showing EL4-3xKO cells expressing human alleles of MyD88, IRAK1-mScarlet and IRAK4-WT-GFP (top row), hIRAK4-D329A-GFP (middle row) and hIRAK4-D329A/E-loop-GFP interacting with IL-1-functionalized SLBs. All movies shown acquired using TIRF microscopy. In the merge panels IRAK1 images are shown in magenta and IRAK4 in green. Scale bar, 5 μm.

Figure 1

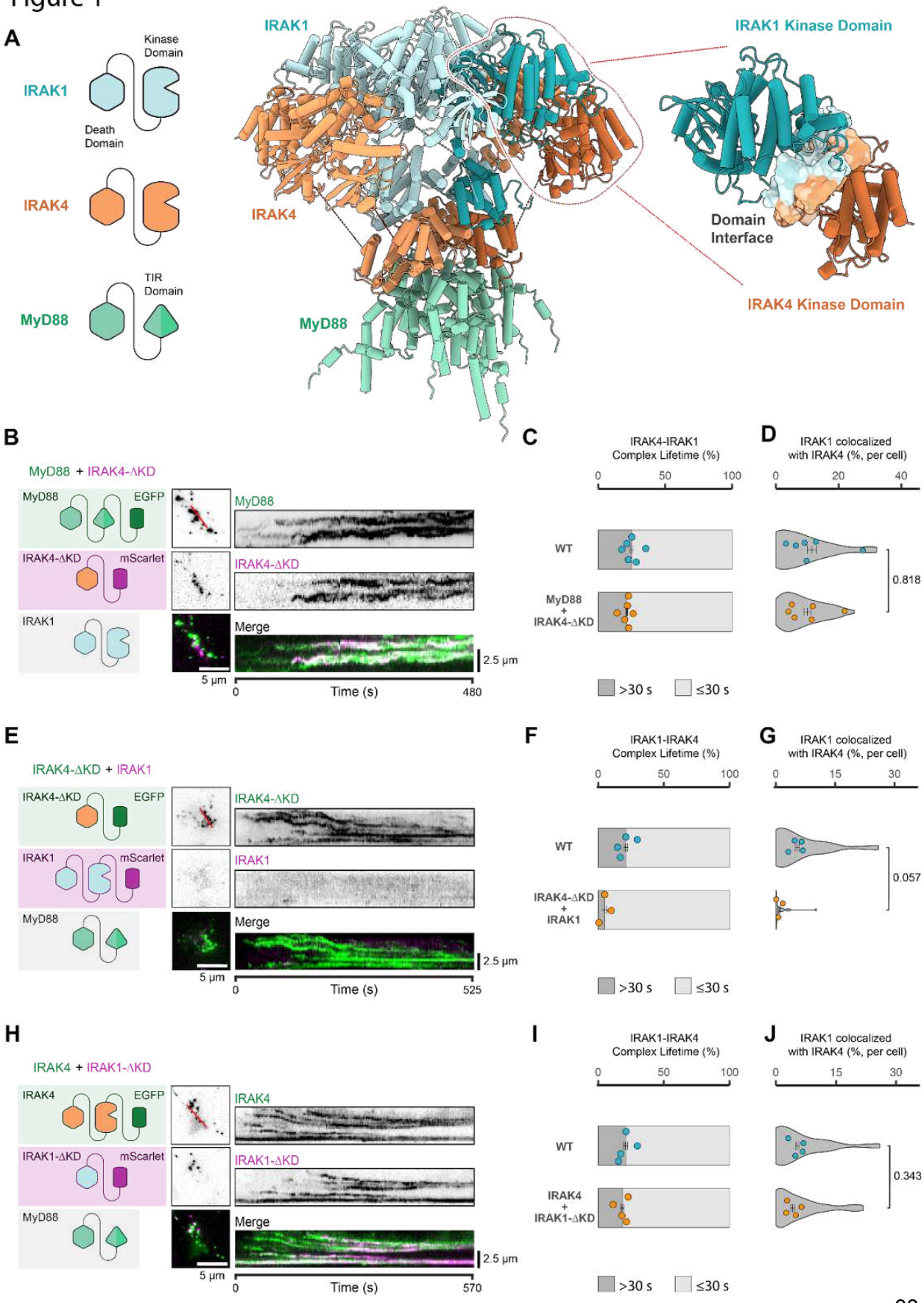

A
Kinase Domain
IRAK1
Death Domain
IRAK4
TIR Domain
MyD88
IRAK1
IRAK4
MyD88
IRAK1 Kinase Domain
Domain Interface
IRAK4 Kinase Domain
B
MyD88 + IRAK4-ΔKD
MyD88
EGFP
IRAK4-ΔKD
mScarlet
IRAK1
MyD88
IRAK4-ΔKD
Merge
2.5 μm
5 μm
0
Time (s)
480
C
IRAK4-IRAK1
Complex Lifetime (%)
0
50
100
WT
MyD88 + IRAK4-ΔKD
>30 s
≤30 s
D
IRAK1 colocalized with IRAK4 (%, per cell)
0
20
40
0.818
E
IRAK4-ΔKD + IRAK1
IRAK4-ΔKD
EGFP
IRAK1
mScarlet
MyD88
IRAK4-ΔKD
IRAK1
Merge
2.5 μm
5 μm
0
Time (s)
525
F
IRAK1-IRAK4
Complex Lifetime (%)
0
50
100
WT
IRAK4-ΔKD + IRAK1
>30 s
≤30 s
G
IRAK1 colocalized with IRAK4 (%, per cell)
0
15
30
0.057
H
IRAK4 + IRAK1-ΔKD
IRAK4
EGFP
IRAK1-ΔKD
mScarlet
MyD88
IRAK4
IRAK1-ΔKD
Merge
2.5 μm
5 μm
0
Time (s)
570
I
IRAK1-IRAK4
Complex Lifetime (%)
0
50
100
WT
IRAK4 + IRAK1-ΔKD
>30 s
≤30 s
J
IRAK1 colocalized with IRAK4 (%, per cell)
0
15
30
0.343

Figure 1. Differential regulation of heterotypic DD interactions in Myddosome assembly by IRAK4 and IRAK1 kinase domains.

(A) AF3-predicted model of the Myddosome complex containing the DDs and kinase domains of IRAK4/1. Unstructured linker regions between the DD and kinase domain were removed and represented as a dashed line. Left, schematic domain organization of MyD88, IRAK4, and IRAK1. Right, AF3-predicted model with detail of the putative IRAK4–IRAK1 kinase domain interface (outlined in dashed red). The IRAK4/1 kinase domain heterodimer interface is highlighted.

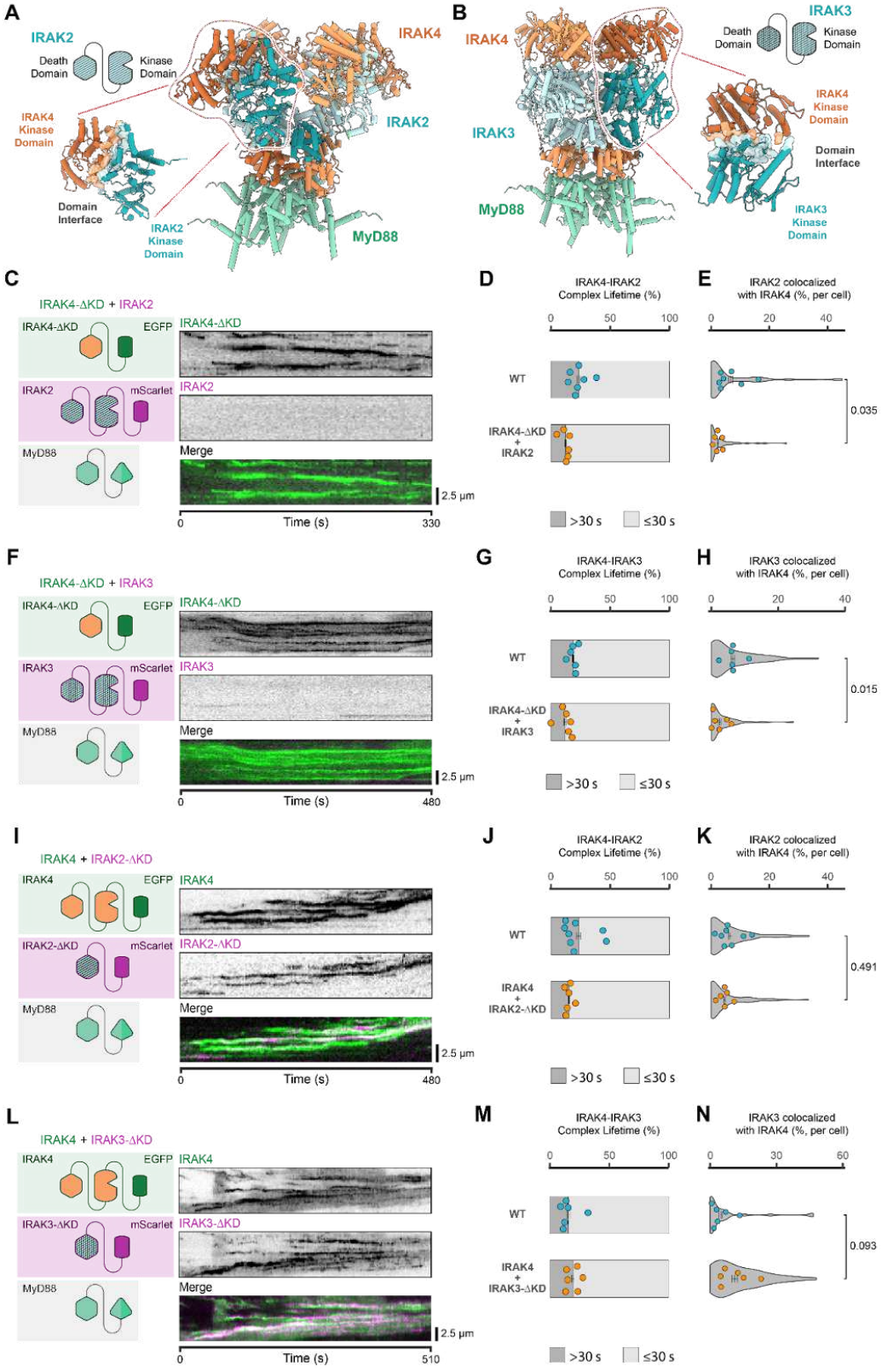
(B-D) Deletion of the IRAK4 kinase domain does not disrupt MyD88–IRAK4 assembly. (B) Representative TIRF image of EL4-MyD88-GFP/IRAK4-KO cells expressing IRAK4-ΔKD-mScarlet, with red line indicating the position used for kymograph generation (left panel). Corresponding kymograph shown on the right. Scale bar, 5 μm and 2.5 μm. (C) Proportion of MyD88–IRAK4 colocalized puncta with lifetimes ≤30 s or >30 s for IRAK4-WT versus IRAK4-ΔKD paired with MyD88-WT. Data points represent replicate means. (D) Percentage of total MyD88 puncta stably colocalized with IRAK4-WT versus IRAK4-ΔKD. Violin plots show single-cell distributions with replicate means superimposed.

(E-G) Deletion of the IRAK4 kinase domain disrupts IRAK4–IRAK1 assembly. (E) Representative TIRF image of EL4-3xKO cells expressing IRAK4-ΔKD-GFP with IRAK1-mScarlet, with red line indicating the position used for kymograph generation (left panel). Corresponding kymograph shown on the right. Scale bar, 5 μm and 2.5 μm. (F) Proportion of IRAK4–IRAK1 colocalized puncta with lifetimes ≤30 s or >30 s for IRAK4-WT versus IRAK4-ΔKD paired with IRAK1-WT. (G) Percentage of total IRAK4 puncta stably colocalized with IRAK1 for IRAK4-WT versus IRAK4-ΔKD.

(H-J) Deletion of the IRAK1 kinase domain does not disrupt IRAK4–IRAK1 assembly. (H) Representative TIRF image of EL4-3xKO cells expressing IRAK4-GFP with IRAK1-ΔKD-mScarlet, with red line indicating the position used for kymograph generation (left panel). Corresponding kymograph shown on the right. Scale bar, 5 μm and 2.5 μm. (I) Proportion of IRAK4–IRAK1 colocalized puncta with lifetimes ≤30 s or >30 s for IRAK4-WT paired with IRAK1-WT versus IRAK1-ΔKD. (J) Percentage of total IRAK4 puncta stably colocalized with IRAK1-WT versus IRAK1-ΔKD. Violin plots show single-cell distributions with replicate means superimposed.

Data from n = 3 to 6 independent replicates for each allelic pairing, with 2–23 cells per replicate. Bars in C, D, F, G, I and J represent mean ± SEM.

Figure 2


A
IRAK2
Death Domain
Kinase Domain
IRAK4
IRAK2
IRAK4 Kinase Domain
Domain Interface
IRAK2 Kinase Domain
MyD88
B
IRAK4
IRAK3
Death Domain
Kinase Domain
IRAK4 Kinase Domain
Domain Interface
IRAK3 Kinase Domain
MyD88
C
IRAK4-ΔKD + IRAK2
IRAK4-ΔKD
EGFP
IRAK2
mScarlet
MyD88
Merge
2.5 μm
0
Time (s)
330
D
IRAK4-IRAK2 Complex Lifetime (%)
0
50
100
WT
IRAK4-ΔKD + IRAK2
>30 s
≤30 s
E
IRAK2 colocalized with IRAK4 (%, per cell)
0
20
40
0.035
F
IRAK4-ΔKD + IRAK3
IRAK4-ΔKD
EGFP
IRAK3
mScarlet
MyD88
Merge
2.5 μm
0
Time (s)
480
G
IRAK4-IRAK3 Complex Lifetime (%)
0
50
100
WT
IRAK4-ΔKD + IRAK3
>30 s
≤30 s
H
IRAK3 colocalized with IRAK4 (%, per cell)
0
20
40
0.015
I
IRAK4 + IRAK2-ΔKD
IRAK4
EGFP
IRAK2-ΔKD
mScarlet
MyD88
Merge
2.5 μm
0
Time (s)
480
J
IRAK4-IRAK2 Complex Lifetime (%)
0
50
100
WT
IRAK4 + IRAK2-ΔKD
>30 s
≤30 s
K
IRAK2 colocalized with IRAK4 (%, per cell)
0
20
40
0.491
L
IRAK4 + IRAK3-ΔKD
IRAK4
EGFP
IRAK3-ΔKD
mScarlet
MyD88
Merge
2.5 μm
0
Time (s)
510
M
IRAK4-IRAK3 Complex Lifetime (%)
0
50
100
WT
IRAK4 + IRAK3-ΔKD
>30 s
≤30 s
N
IRAK3 colocalized with IRAK4 (%, per cell)
0
30
60
0.093

955

Figure 2. The IRAK4 kinase domain regulates IRAK2/3 incorporation into Myddosome complexes.

(A-B) AF3-predicted models of Myddosome complexes containing the DDs and kinase domains of IRAK4 with IRAK2 (A) or IRAK3 (B). Schematic domain organization of MyD88, IRAK4, and IRAK2/3 and AF3-predicted model with detail of the putative interaction interface between IRAK4 and IRAK2/3 kinase domains (outlined in dashed red). The IRAK4/2 and IRAK4/3 kinase domain heterodimer interface is highlighted.

(C-H) Deletion of the IRAK4 kinase domain disrupts IRAK4–IRAK2 (C-E) and IRAK4–IRAK3 (F-H) co-assembly. (C, F) Representative kymographs from TIRF microscopy of EL4-3xKO cells expressing IRAK4-ΔKD-GFP with IRAK2-mScarlet (C) or IRAK3-mScarlet (F) activated on IL-1–functionalized supported lipid bilayers. Scale bars, 2.5 μm. (D, G) Proportion of colocalized IRAK4–IRAK2 (D) or IRAK4–IRAK3 (G) puncta with lifetimes ≤30 s or >30 s for IRAK4-WT versus IRAK4-ΔKD paired with IRAK2/3-WT. Data points represent replicate means. (E, H) Percentage of total IRAK4 puncta stably colocalized with IRAK2 (E) or IRAK3 (H). Violin plots show single-cell distributions with replicate means superimposed.

(I-N) Deletion of the IRAK2 or IRAK3 kinase domain does not disrupt IRAK4–IRAK2 or IRAK4–IRAK3 co-assembly. (I, L) Representative kymographs from TIRF microscopy of EL4-3xKO cells expressing IRAK4-GFP with IRAK2-ΔKD-mScarlet (I) or IRAK3-ΔKD-mScarlet (L). Scale bars, 2.5 μm. (J, M) Proportion of colocalized IRAK4–IRAK2 (J) or IRAK4–IRAK3 (M) puncta with lifetimes ≤30 s or >30 s for IRAK4-WT paired with IRAK2/3-ΔKD. (K, N) Percentage of IRAK4 puncta stably colocalized with IRAK2-WT versus IRAK2-ΔKD (K) or IRAK3-WT versus IRAK3-ΔKD (N). Violin plots show single-cell distributions with replicate means superimposed.

Data represent n = 6-8 independent replicates for each allelic pairing, with 3-25 cells per replicate. Statistical significance was assessed using the Wilcoxon rank-sum test in panels E, H, K, and N. Bars in D, E, G, H, J, K, M and N represent mean ± SEM.

Figure 3

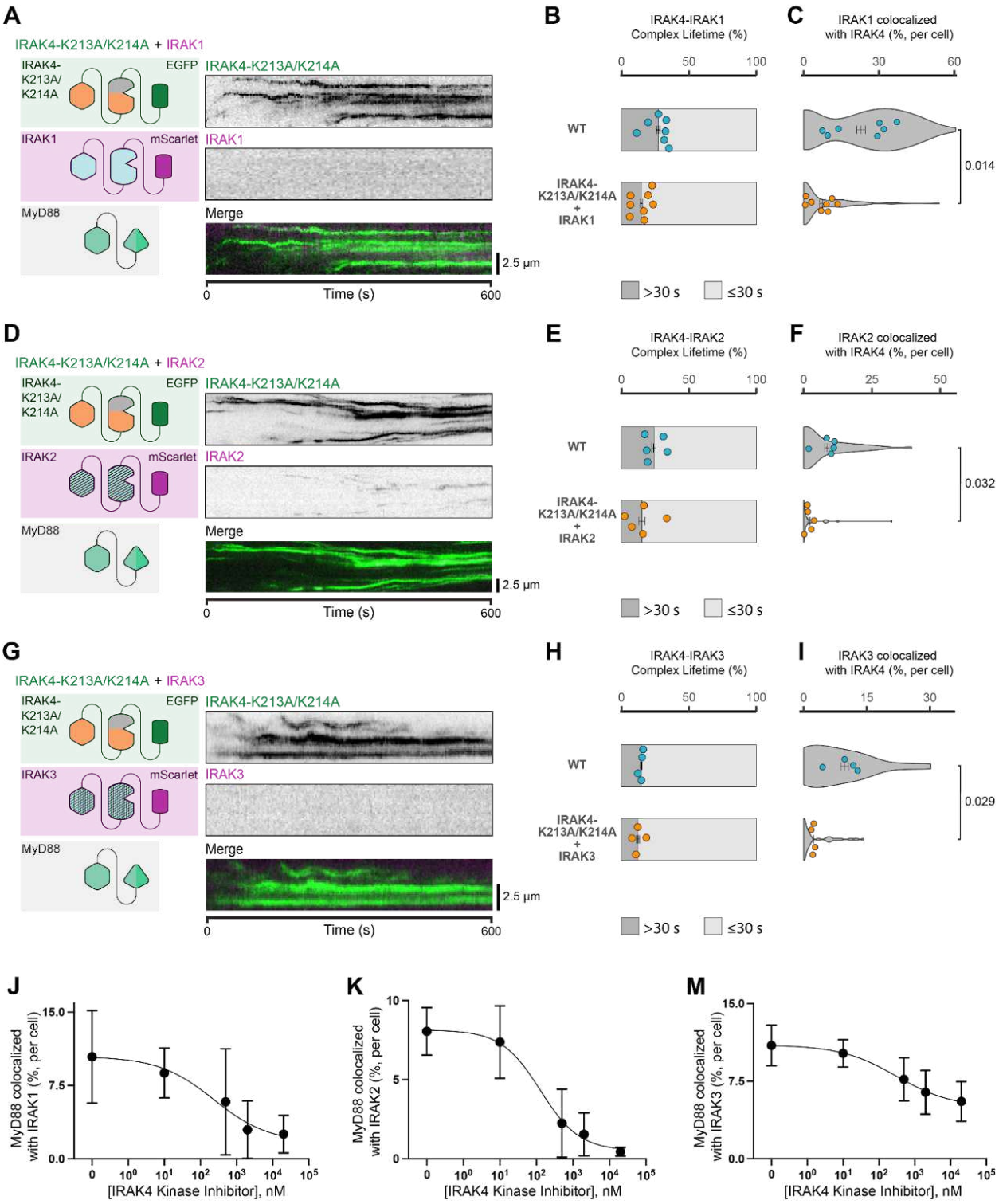


Figure 3. IRAK4 kinase activity is required for stable incorporation of IRAK1/2/3 into Myddosomes.

A kinase-inactive IRAK4 mutant (K213A/K214A) fails to stably incorporate IRAK1 (A-C), IRAK2 (D-F), or IRAK3 (G-I) into Myddosomes.

(A, D, G) Representative kymographs from TIRF microscopy of EL4-3xKO cells expressing IRAK4-(K213A/K214A)-GFP with IRAK1-mScarlet (A), IRAK2-mScarlet (D), or IRAK3-mScarlet (G). Scale bars, 2.5 μm.
(B, E, H) Proportion of colocalized IRAK4–IRAK1 (B), IRAK4–IRAK2 (E), or IRAK4–IRAK3 (H) puncta with lifetimes ≤30 s or >30 s for IRAK4-WT versus IRAK4-(K213A/K214A) paired with IRAK1/2/3-WT. Data points represent replicate means.
(C, F, I) Percentage of total IRAK4 puncta stably colocalized with IRAK1 (C), IRAK2 (F), or IRAK3 (I) for IRAK4-WT versus IRAK4-(K213A/K214A) paired with IRAK1/2/3-WT. Violin plots show single-cell distributions with replicate means superimposed.
(J–M) Stable colocalization of MyD88 puncta with IRAK1 (J), IRAK2 (K), or IRAK3 (M) in cells treated with varying doses of IRAK4 kinase inhibitor.
Data represent n = 5-8 independent replicates for each allelic pairing, with 3-43 cells per replicate. Statistical significance was assessed using the Wilcoxon rank-sum test in panels C, F, I. Bars represent mean ± SEM in panels B, C, E, F, H, and I, and mean ± SD in panels J-M.

Figure 4

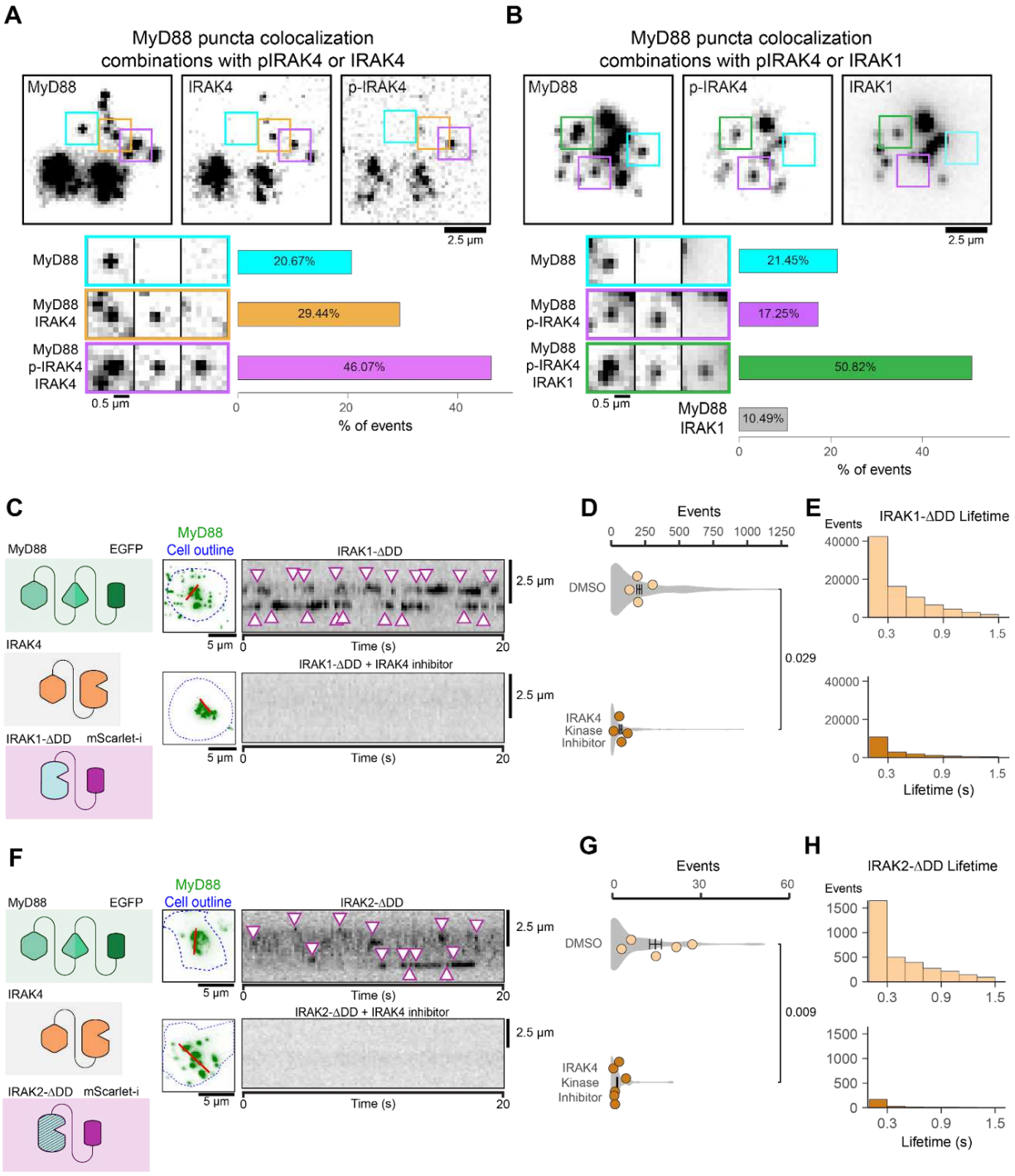


Figure 4. IRAK4 autophosphorylation functions as a regulatory switch for kinase domain–mediated recruitment of IRAK1 and IRAK2.

(A–B) TIRF images of EL4-MyD88-GFP/IRAK4-mScarlet (A) or EL4-MyD88-GFP/IRAK1-mScarlet (B) cells stained for pIRAK4 after activation on IL-1β–functionalized SLBs. Boxes highlight assemblies containing MyD88 alone (cyan), MyD88+IRAK4 (yellow–orange), or MyD88+IRAK4+pIRAK4 (magenta). Bar plots show the

percentage of MyD88 puncta colocalizing with IRAK4 or pIRAK4 (A) and the fraction of pIRAK4 puncta colocalizing with IRAK1 (B). Insets show boxed regions across channels. Data from 445 (A) and 429 (B) puncta. Scale bars, 2.5 μm (overview) and 0.5 μm (insets).

(C–E) Single-molecule TIRF imaging of EL4-MyD88-GFP/IRAK1-KO cells expressing IRAK1-ΔDD-mScarlet. (C) MyD88-GFP reference image and representative kymographs from the IRAK1-ΔDD-mScarlet channel. The red line in the MyD88-GFP image indicates the position used to generate the kymograph in the mScarlet channel. Scale bars, 5 μm and 2.5 μm. (D) Violin plots quantifying recruitment events per cell for DMSO versus IRAK4 inhibitor–treated cells (mean ± SEM; n = 4 experiments, 15-297 cells/condition). (E) Histogram of IRAK1-ΔDD dwell times with or without inhibitor.

(F–H) Equivalent single-molecule TIRF imaging experiments with IRAK2-ΔDD-mScarlet. (F) MyD88-GFP reference image and representative kymographs. Scale bars, 5 μm and 2.5 μm. (G) Recruitment quantified as in (D) (mean ± SEM; n = 5-6 experiments,106-350 cells/condition). (H) Histogram of IRAK2-ΔDD dwell times.

Arrowheads in kymographs (C and F) highlight transient recruitment events of IRAK1/2-ΔDD-mScarlet.

Figure 5

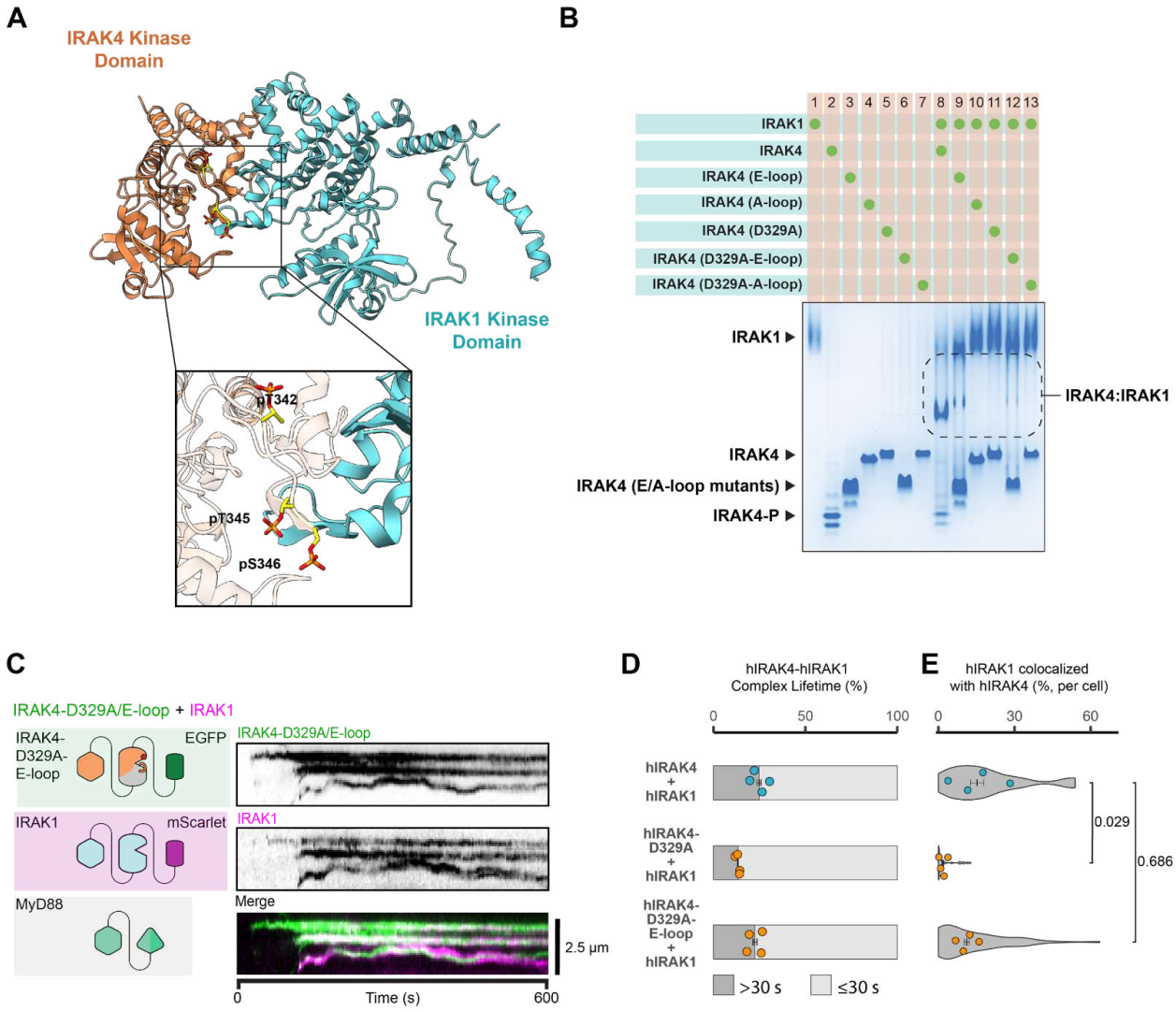


Figure 5. A IRAK4 phosphomimetic mutant restores heterodimerization with the IRAK1 kinase domain and Myddosome maturation.

A) A structural model of the human IRAK4:IRAK1 kinase domain heterodimer was generated with AF3. This model predicts that the phosphorylated serine and threonine residues of IRAK4 within the activation loop are at the heterodimer interface.

B) Native PAGE co-migration analysis of the phosphorylated, unphosphorylated, kinase inactive (D329A) and activation loop mutants (A-loop or phosphomimetic E-loop) of the human IRAK4 kinase domains with the kinase domains of human IRAK1 was performed. The gel was stained with Coomassie Blue. Inputs are indicated above the numbered lanes, and the migration position of co-complexes of IRAK4 kinase domain allelic variants with the IRAK1 kinase domain is highlighted with a dotted line.

C) Representative kymograph from TIRF microscopy of EL4-3xKO cells expressing IRAK4-(D329A/E-loop)-GFP with IRAK1-mScarlet. Scale bars, 2.5 µm.

D) Proportion of colocalized IRAK4–IRAK1 puncta with lifetimes ≤30 s or >30 s for human IRAK4-WT versus IRAK4-(D329A) or IRAK4-(D329A/E-loop) paired with IRAK1-WT. Data points represent replicate means.
E) Percentage of total IRAK4 puncta stably colocalized with human IRAK4-WT versus IRAK4-(D329A) or IRAK4-(D329A/E-loop) paired with IRAK1-WT. Violin plots show single-cell distributions with replicate means superimposed.
Data represent n = 4 independent replicates for each allelic pairing, with 1-29 cells per replicate. Bars in D-E represent mean ± SEM. Statistical significance was assessed using the Wilcoxon rank-sum test in panel E.

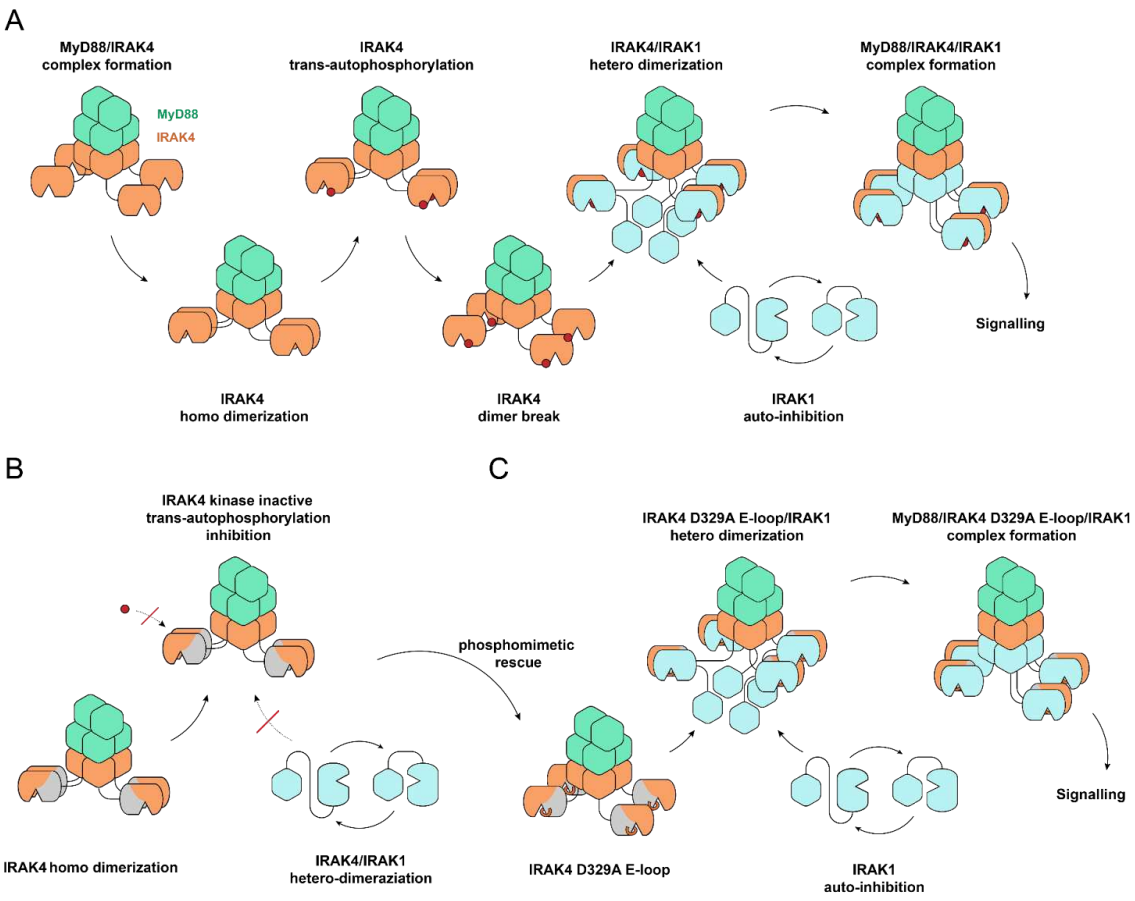


Figure 6. Molecular model for the timeline of Myddosome assembly and maturation.
(A) Conceptual model of IRAK4 kinase activity in Myddosome maturation. After the heterotypic assembly of MyD88 and IRAK4 death domains (DDs), the IRAK4 kinase domains homodimerize and undergo autophosphorylation. This autophosphorylation functions as a molecular switch, enabling the phosphorylated IRAK4 kinase domain to heterodimerize with the IRAK1 kinase domain. Heterodimerization stabilizes IRAK1 in a conformation that permits subsequent incorporation of the IRAK1 DD into the MyD88–IRAK4 DD oligomer.
(B–C) Inhibition of IRAK4 autophosphorylation, either by pharmacological inhibitors or expression of kinase-dead alleles, arrests Myddosome assembly at the MyD88–IRAK4 stage (B). This block can be bypassed by expression of a phosphomimetic IRAK4 mutant (C), which, even in a kinase-inactive context, supports IRAK1 recruitment and incorporation into the Myddosome.

Supplementary Figure 1

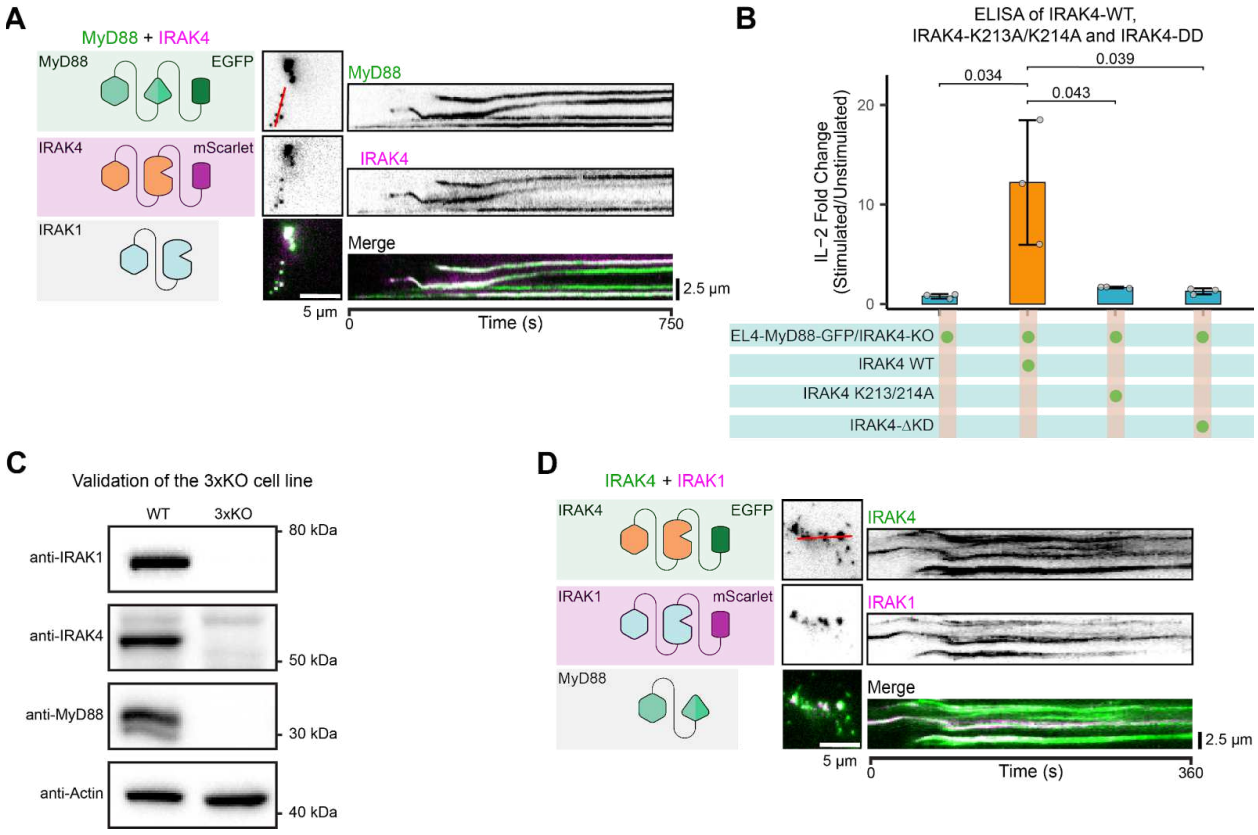


Figure S1. Analysis of IRAK4 mutants and validation of 3xKO cell line.

A) TIRF images of EL4-MyD88-GFP/IRAK4-mScarlet stimulated on IL-1 functionalized SLBs. . Kymographs derived from red line overlaid TIRF images (left panel). Scale bars 5 µm (left panel) and 2.5 µm (right panel).

B) IL-2 release in EL4-MyD88-GFP/IRAK4-KO cells reconstituted with IRAK4-WT-mScarlet, IRAK4-K213/14A-mScarlet and IRAK4-ΔKD-mScarlet. Values shown are the fold change in IL-2 release (n = 3 independent replicates measured per cell line). The bars represent Mean Fold change ± SEM are 0.78 ± 0.22, 12.21 ± 6.25, 1.66 ± 0.08 and 1.28 ± 0.29 for IRAK4-KO, IRAK4-WT-mScarlet, IRAK4-K213A/K214A-mScarlet and IRAK4-ΔKD-mScarlet respectively. One-way Anova was used to compare the replicate means.

C) Western blot validation of a EL4 cell clone that is triple KO for MyD88, IRAK4 and IRAK1.

D) TIRF images of EL4-3xKO cells reconstituted with wild type MyD88, IRAK4-GFP and IRAK1-mScarlet stimulated on IL-1 functionalized SLBs. Kymographs derived from red line overlaid TIRF images (left panel). Scale bars 5 µm (left panel) and 2.5 µm (right panel).

Supplementary Figure 2

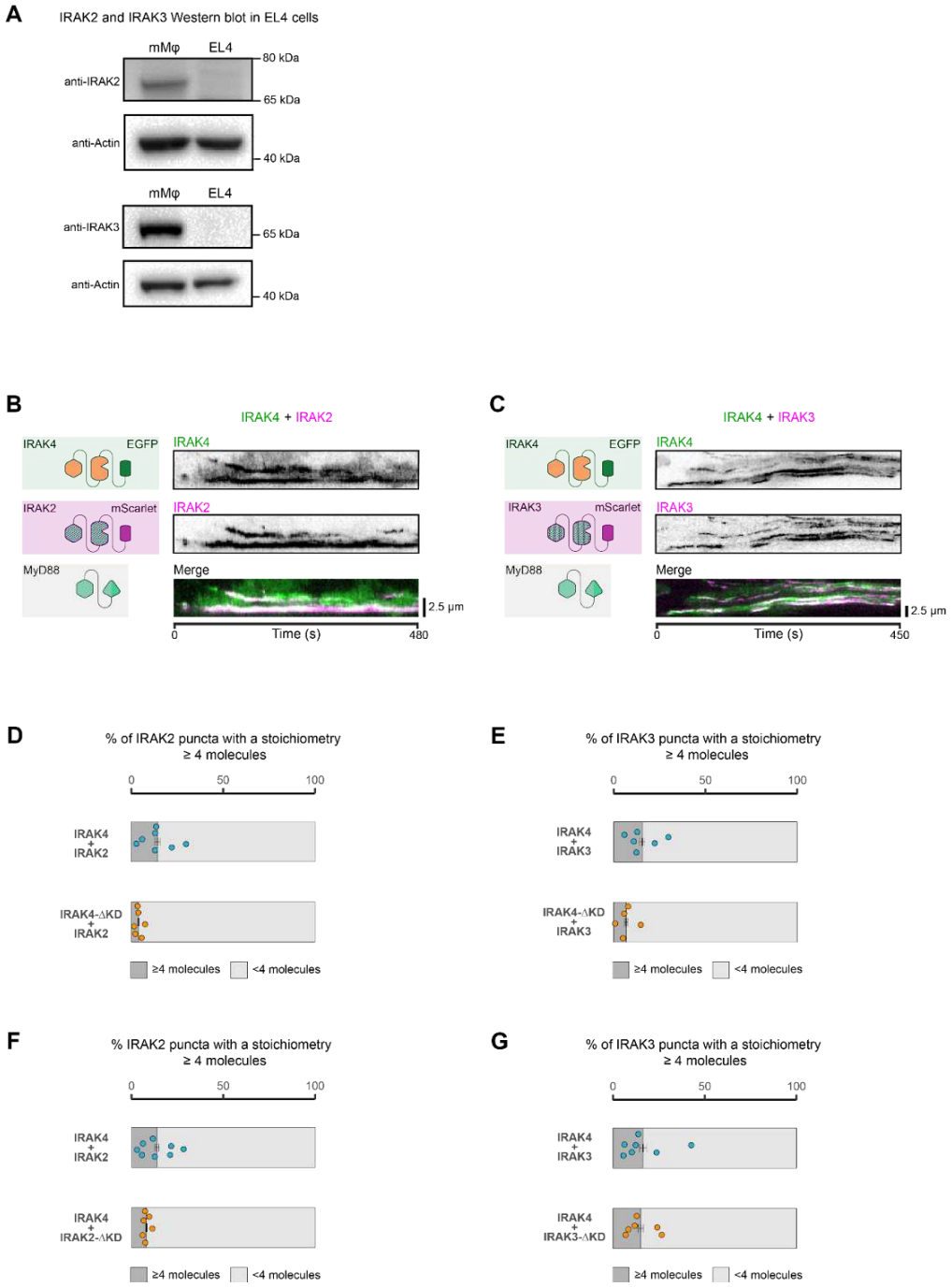


Figure S2: The kinase domain of IRAK4 regulates the recruitment and oligomerization of IRAK2 and IRAK3 at assembling Myddosomes.

A) Western blot analysis of IRAK2 and IRAK3 expression in EL4 cells. Lysates from bone derived mouse macrophages included as a positive control.

B-C) TIRF images and kymograph analysis of EL4-3xKO cells reconstituted with wild type MyD88 IRAK4-GFP and IRAK2-mScarlet (B) or IRAK3-mScarlet (C) stimulated on IL-1

functionalized SLBs. Kymographs derived from red line overlaid TIRF images (left panel). Scale bar, 5 µm (left panels) and 2.5 µm (right panels).

D-E) Percentage of IRAK2 (D) and IRAK3 (E) assemblies recruited to IRAK4 with a stoichiometry greater than or equal to 4 molecules, a stoichiometry consistent with fully assembled myddosomes. Data acquired from EL4-3xKO reconstituted with MyD88, IRAK4-GFP or IRAK4-ΔKD-GFP and IRAK2-mScarlet (D) or IRAK3-mScarlet (E). Mean percentages of stable IRAK2/ IRAK3 sizes ± SEM were 9.94 ± 0.98, 2.18 ± 0.19, 11.7 ± 1.06, 3.93 ± 0.59 for IRAK4-FL + IRAK2, IRAK4-ΔKD + IRAK2, IRAK4 + IRAK3, IRAK4-ΔKD + IRAK3 respectively. Data points superimposed on the bar plots show the mean of individual experimental replicates (n = 7, 6, 6 and 6 independent experimental replicates for cells expressing IRAK4 + IRAK2, IRAK4-ΔKD + IRAK2, IRAK4 + IRAK3, IRAK4-ΔKD + IRAK3 respectively).

F-G) Percentage of IRAK2/IRAK3 assemblies with a stoichiometry greater than or equal to 4 molecules recruited to IRAK4. Data acquired from EL4-3xKO reconstituted with MyD88, IRAK4-GFP and IRAK2-mScarlet or IRAK2-ΔKD-mScarlet (F) and IRAK3-mScarlet or IRAK3-ΔKD-mScarlet (G). Mean percentages of stable IRAK2/ IRAK3 sizes ± SEM were 10.7 ± 1.18, 4.64 ± 0.44, 11.1 ± 0.77, 14.6 ± 1.34 for IRAK4 + IRAK2, IRAK4 + IRAK2-ΔKD, IRAK4 + IRAK3, IRAK4 + IRAK3-ΔKD respectively. Data points superimposed on the bar plots show the mean of individual experimental replicates (n = 8, 6, 7 and 6 independent experimental replicates for cells expressing IRAK4 + IRAK2, IRAK4 + IRAK2-ΔKD, IRAK4 + IRAK3, IRAK4 + IRAK3-ΔKD respectively).

Supplementary Figure 3

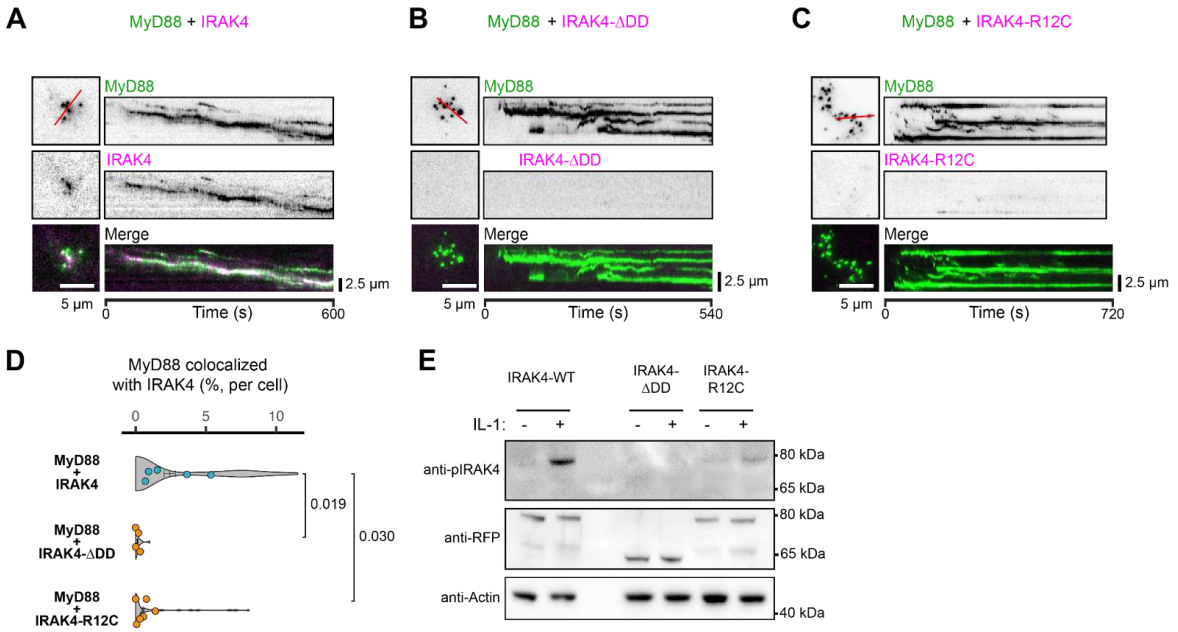


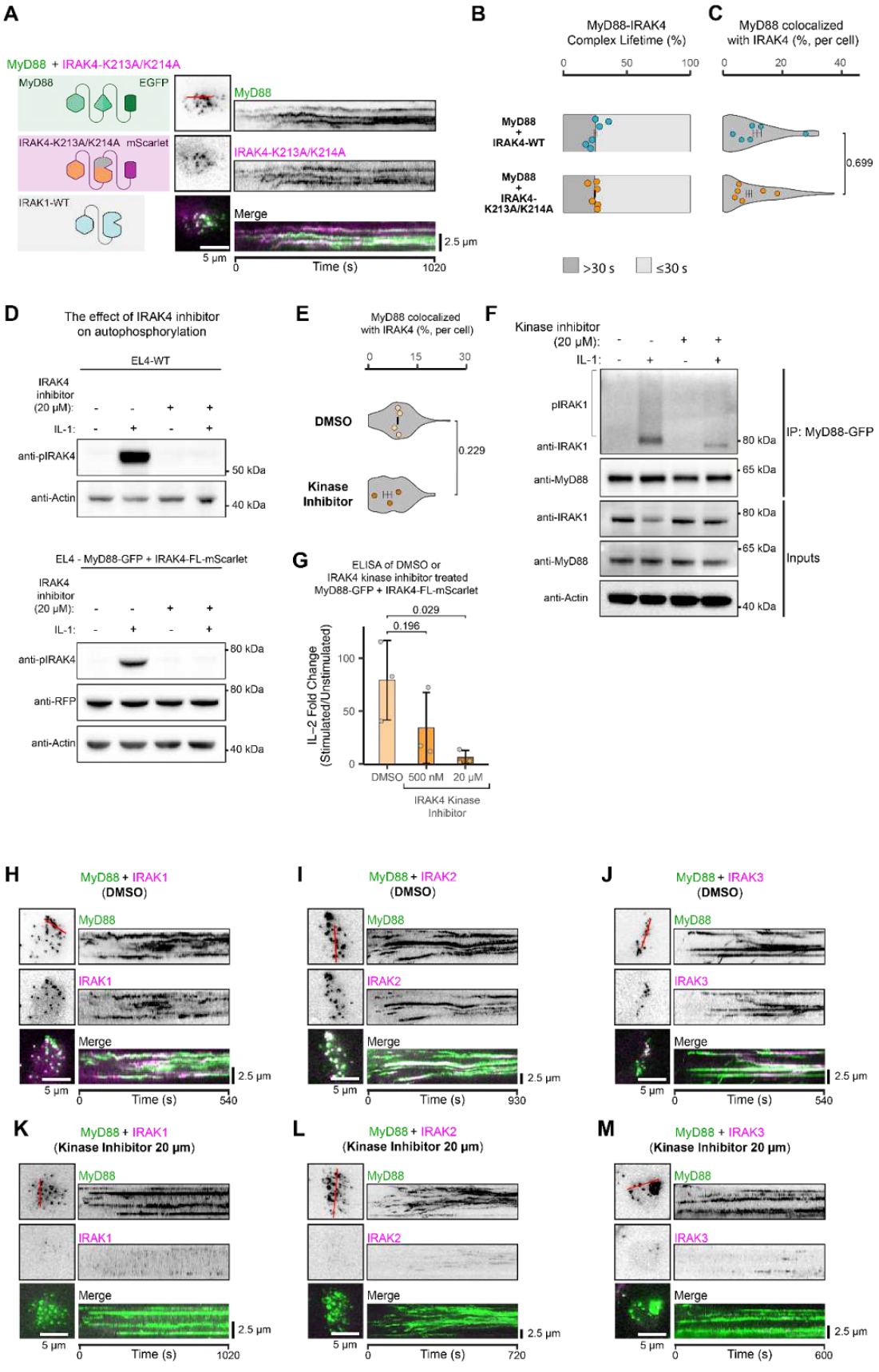
Figure S3. IRAK4 requires a functional DD for co-assembly with MyD88 and autophosphorylation

A-C) IRAK4 requires a functional DD to be recruited to MyD88. TIRF images and kymograph analysis (derived from red line) of EL4-MyD88-GFP/IRAK4-KO reconstituted with IRAK4-WT-mScarlet (A), IRAK4-IRAK4-ΔDD-mScarlet (B) and IRAK4-R12C-mScarlet (C). Scale bar, 5 µm (left panels). Scale bar, 2.5 µm (right panels).

D) The proportion of all MyD88 tracks that stably recruit (≥ 30) IRAK4 in EL4-MyD88-GFP/IRAK4-KO reconstituted with IRAK4-WT-mScarlet, IRAK4-ΔDD-mScarlet and IRAK4-R12C-mScarlet. Mean percentages of stable recruitment ± SEM were 2.42 ± 0.40, 0.13 ± 0.04 and 0.52 ± 0.09 for IRAK4-WT-mScarlet (n = 5), IRAK4-ΔDD-mScarlet. (n = 4) and IRAK4-R12C-mScarlet (n = 6) respectively.

E) IRAK4 autophosphorylation requires a functional DD that can co-assemble with MyD88. Western blot validation of pIRAK4 in EL4-MyD88-GFP/IRAK4-KO reconstituted with IRAK4-WT-mScarlet, IRAK4-ΔDD-mScarlet and IRAK4-R12C-mScarlet.

Supplementary Figure 4



1127

Figure S4: Analysis of IRAK4 kinase-inactive mutants and pharmacological inhibition

A) Time-series TIRF images and fluorescence-intensity time series showing the formation and coassembly of MyD88-GFP and IRAK4-mScarlet puncta from cells treated with DMSO (left panel) . Scale bar, 1 μm.

B) Proportion of MyD88:IRAK4-FL (top) and MyD88:IRAK4-K213A/K214A-mScarlet (bottom) colocalized puncta with lifetimes less than or greater than 30s. The dots superimposed on the bar plots represent the mean proportion of each replicate.

C) The percentage of total MyD88 puncta stably colocalized with IRAK4-FL versus RAK4-K213A/K214A (25.07 ± 1.05 vs. 24.68 ± 0.53 for IRAK4-FL-mScarlet (n = 6) and IRAK4-K213A/K214A-mScarlet (n = 6) respectively). Wilcoxon Ranked sum test was used to compare the replicate means.

D) Western blot analysis of IRAK4 autophosphorylation (pIRAK4) production after IL-1β stimulation showing that IRAK4 kinase inhibitor blocks pIRAK4. Western blot analysis performed in EL4-WT (upper blot) and EL4-MyD88-GFP/IRAK4-FL-mScarlet (lower blot) cell lysates. Cells were treated with 20 μM of IRAK4 kinase inhibitor or DMSO, for 4 hours, before being stimulated with 1 ng/ml of IL-1β for 30 mins.

E) Proportion of MyD88:IRAK4-FL colocalized puncta with lifetimes less than or greater than 30s in cells treated with DMSO (top) or IRAK4 kinase inhibitor (bottom). The dots superimposed on the bar plots represent the mean proportion of each replicate. Mean percentages of stable recruitment ± SEM were 9.00 ± 0.179 and 5.92 ± 1.24 for DMSO (n = 4) and Kinase Inhibitor (n = 3) treated cells respectively. One-way Anova was used to compare the replicate means.

F) Myddosomes were immunoprecipitated from EL4-MyD88-GFP cell lysates treated without or with IRAK4 kinase inhibitor (20 μM) and analyzed by western blot. Treatment with the IRAK4 kinase inhibitor reduced co-assembly and the post-translational modification of IRAK1 within Myddosomes.

G) Dose dependent decrease of cytokine release in response to IRAK4 Kinase Inhibitor (500 nM and 20 μM). IL-2 release was measured by ELISA 24 h after IL-1β stimulation in EL4-MyD88-GFP/IRAK4-FL-mScarlet cells. Values shown are the fold change in IL-2 release (n = 3 independent replicates measured per cell line). Mean Fold change ± SEM are 79.24 ± 37.64, 34.08 ± 33.63 and 6.07 ± 6.68 for cells treated with DMSO, and 500 nM or 20 μM of IRAK4 Kinase Inhibitor respectively.

H-M) IRAK4 Kinase Inhibition reduces recruitment of IRAK1, IRAK2 and IRAK3. TIRF images and kymograph analysis (derived from red line) of MyD88-GFP/IRAK1-FL-mScarlet (H and K), EL4-MyD88-GFP/IRAK1-KO reconstituted with IRAK2-mScarlet (I and M) or IRAK3-mScarlet (J and M). Cells are treated with DMSO (H-J) or IRAK4 Kinase Inhibitor (20 μM, K-M). Scale bar, 5 μm (left panels). Scale bar 5 μm (left panels) and 2.5 μm (right panels).

Supplementary Figure 5

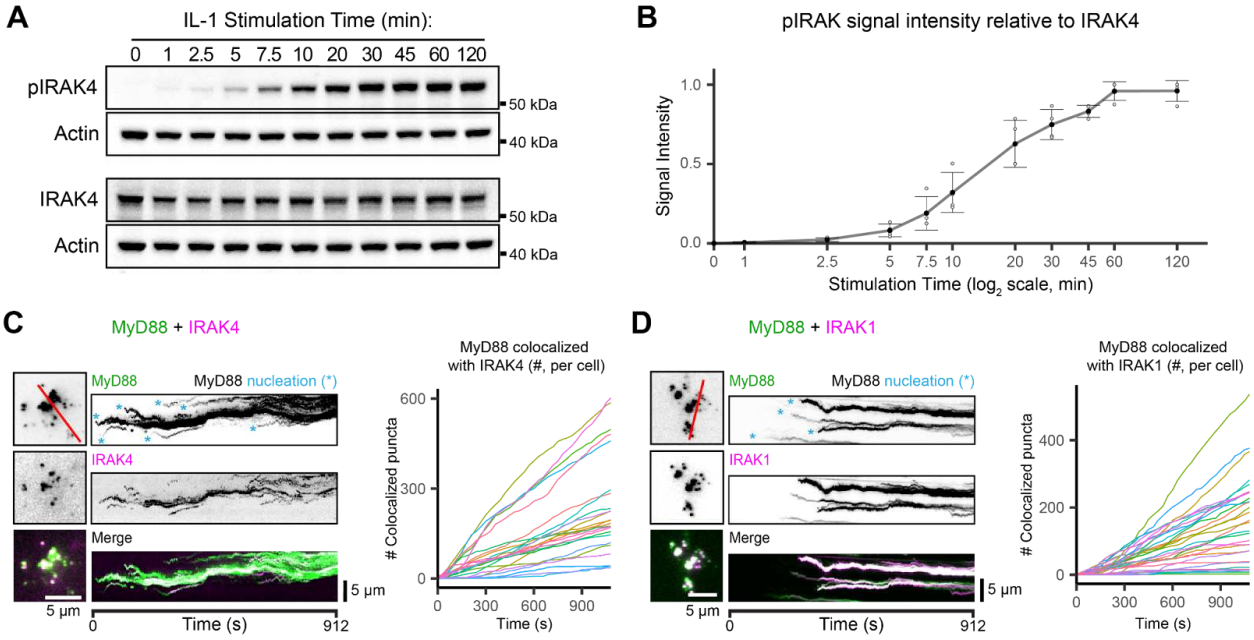


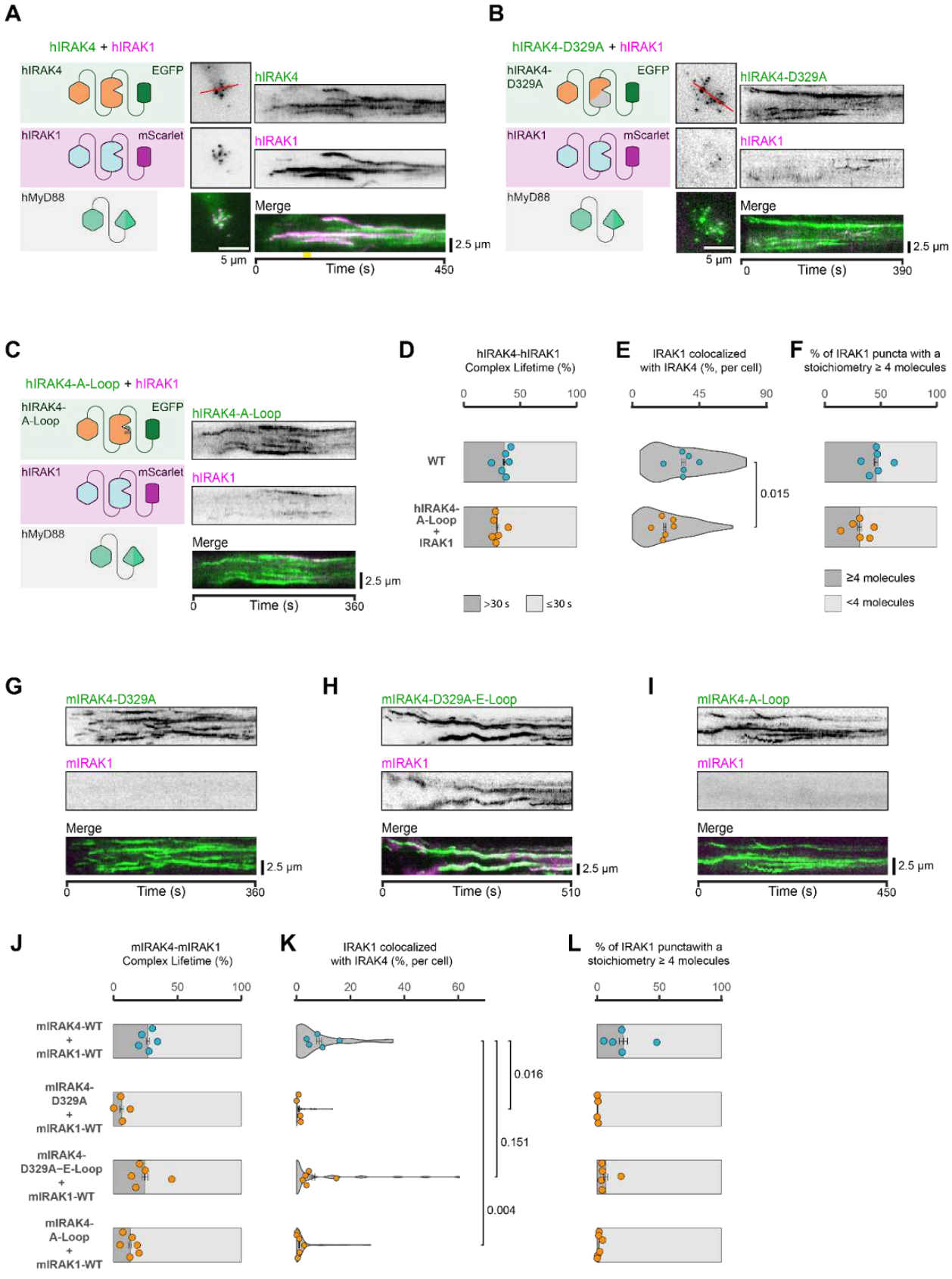
Figure S5. Time course analysis of IRAK4 autophosphorylation and Myddosome assembly

A) Time course Western blot analysis of pIRAK4 levels in EL4 cells after IL-1 stimulation (1 ng/ml). Lysates were separately probed for antibodies specific for pIRAK4 (Thr-345/Ser-346) and total IRAK4. Actin detection was used as a loading control and to normalize the band intensity.

B) Time course quantification of the pIRAK4 signal intensity relative to total IRAK4 signal intensity from the Western blots shown in (C). Each black colored data point is the average relative pIRAK level derived from n=4 experimental replicates (see Appendex_A). Smaller data points are the relative pIRAK signal intensity of individual replicates.

C-D) Nucleation of MyD88 and formation of myddosomes are asynchronous. (Left panels) TIRF images and kymograph analysis (derived from red line) of MyD88-GFP/IRAK4-mScarlet (A) and MyD88-GFP/IRAK1-mScarlet (B). Scale bar, 5 µm. The blue asterisks on the MyD88-GFP kymograph highlight the nucleation of Myddosome complexes. (Right panel) Formation of MyD88-GFP:IRAK4-mScarlet (A) and MyD88-GFP:IRAK1-mScarlet (B) assemblies over time for individual cells. Each color represents one of 24 (A) or 31 cells (B). t = 0 is defined as the time point when the first MyD88 puncta is observed in each cell.

Supplementary Figure 6



1186

Figure S6: Analysis of human and mouse kinase inactive and activation loop IRAK4 mutants

A-C) TIRF images and kymograph analysis of EL4-3xKO cells reconstituted with hMyD88, hIRAK1-mScarlet, and hIRAK4-GFP variants (WT, kinase dead [D329A], and alanine activation loop mutants [T343A/T345A/S346A]) are shown. The kymograph was taken from the red line overlaying the MyD88-GFP image in each panel. Scale bar: 5 μm (left panels), 2.5 μm (right panels).

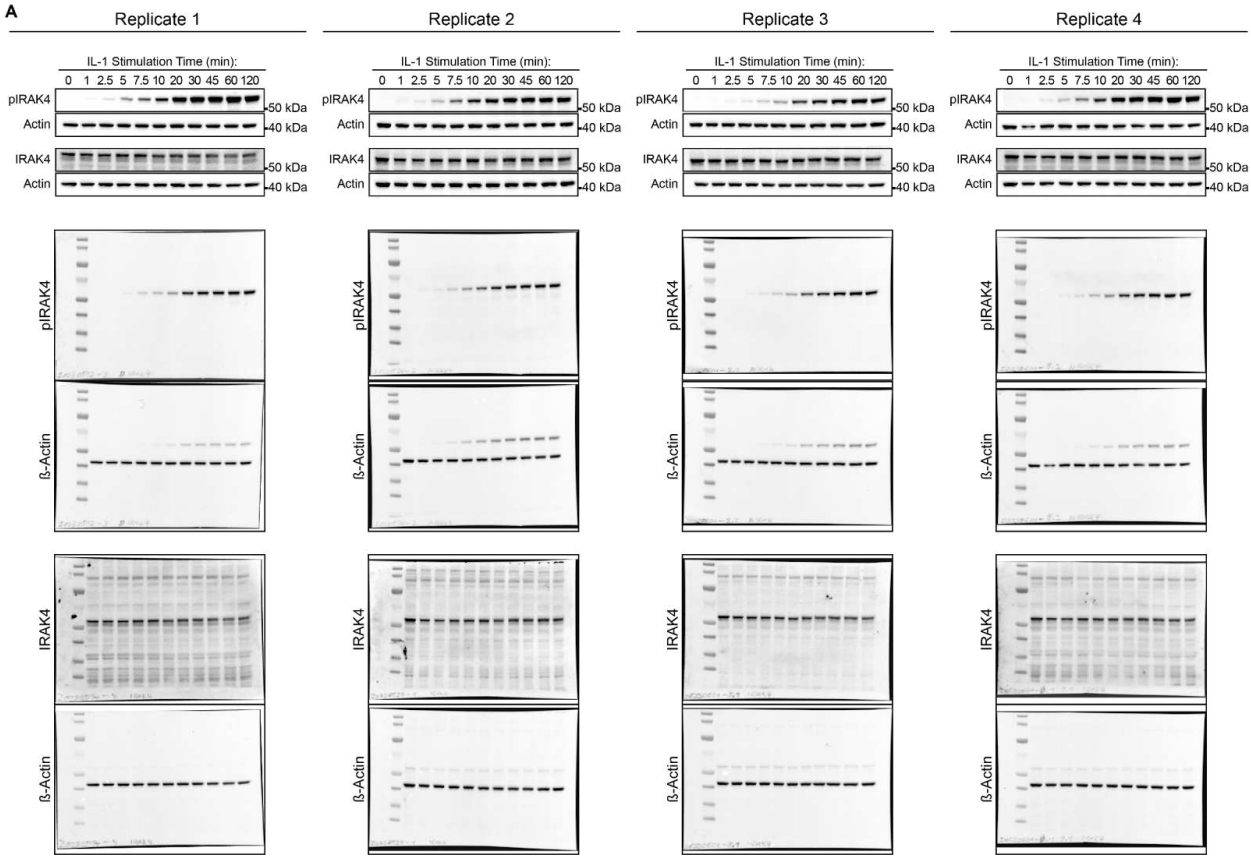
D) Proportion of IRAK4-IRAK1 colocalized puncta with lifetimes ≤30 s or >30 s for IRAK4-WT versus IRAK4-A-loop mutant paired with IRAK1-WT. Data points represent replicate means.

E) Percentage of total IRAK4 puncta stably colocalized with IRAK1-WT for IRAK4-WT versus IRAK4-A-loop mutant. Violin plots show single-cell distributions with replicate means superimposed.

F) Percentage of IRAK1-WT assemblies recruited to IRAK4-WT versus IRAK4-A-loop mutant with a stoichiometry greater than or equal to 4 molecules, a stoichiometry consistent with fully assembled myddosomes.

G-L) Analysis of kinase-inactive and E/A-loop mutants of mouse IRAK4 shows that the E-loop phosphomimetic mutation can restore IRAK1 recruitment and incorporation into Myddosomes. G-H) Kymograph analysis of EL4-3xKO cells reconstituted with mMyD88, mIRAK1-mScarlet, and mIRAK4-GFP variants (WT, kinase-dead [D329A], and alanine activation loop mutants [T343A/T345A/S346A]). Scale bar: 2.5 μm (right panels). J) Proportion of mouse IRAK4-IRAK1 colocalized puncta with lifetimes ≤30 s or >30 s for IRAK4-WT versus IRAK4-A-loop mutant paired with IRAK1-WT. Data points represent replicate means. K) Percentage of total mouse IRAK4 puncta stably colocalized with IRAK1-WT for IRAK4-WT versus IRAK4-A-loop mutant. Violin plots show single-cell distributions with replicate means superimposed. L) Percentage of mouse IRAK1-WT assemblies recruited to IRAK4-WT versus IRAK4-A-loop mutant with a stoichiometry greater than or equal to 4 molecules, a stoichiometry consistent with fully assembled Myddosomes.

Data represent n = 4 to 6 independent replicates for each allelic pairing, with 9-28 cells per replicate. Statistical significance was assessed using the Wilcoxon rank-sum test in panel E and K.



Appendix. Western blot replicates of the time course analysis of pIRAK4 production after IL-1 stimulation. The full length blot is shown below the cropped blot. Replicate 3 is shown in Fig. 1E. The analysis of each replicate was used to generate the time course of pIRAK4 production in Fig. 1F.

Table 1. Protein sequences of IRAK1/2/3/4 mScarlet/mEGFP fusion constructs

Death Domain (DD), Kinase Domain (KD), GGS linker, mScarlet-i ORF, mEGFP point mutations underlined

Mouse IRAK4 Wild Type mScarlet
MNKPLTPSTYIRNLNVGILRKLSDFIDPQEGWKKLAVAIKKPSGDDRYNQFHIRRFEALLQTGK SPTCELLFDWGTTNCTVGDLVDLLVQIELFAPATLLLPDAVPQTVKSLPPREAATVAQTHGPC QEKDRTSVMPMPKLEHSCEPPDSSSPDNRSVESSDTRFHSFSFHELKSITNNFDEQPASAG GNRMGEGGFGVVYKGCVNNTIVAVKKLGAMVEISTEELKQQFDQEIKVMATCQHENLVELLG FSSDSDNLCLVYAYMPNGSLLDRLSCLDGTPPLSWHTRCKVAQGTANGIRFLHENHHIHRDIK SANILLDRDFTAKISDFGLARASARLAQTVMTSRIVGTTAYMAPEALRGEITPKSDIYSFGVVLL ELITGLAAVDENREPQLLLDIKEEIEDEEKTIEDYTDEKMSDADPASVEAMYSAASQCLHEKKN RRPDIAKVQQLLQEMSAGGSGGSGGSVSKGEAVIKEFMRFKVHMEGSMNGHEFEIEGEGE GRPYEGTQTAKLKVTKGGPLPFSWDILSPQFMYGSRAFIKHPADIPDYYKQSFPEGFKWERV MNFEDGGAVTVTQDTSLEDGTLIYKVKLRGTNFPPDGPVMQKKTMGWEASTERLYPEDGVL KGDIKMALRLKDGGRYLADFKTTYKAKKPVQMPGAYNVDRKLDITSHNEDYTVVEQYERSEG RHSTGGMDELYK
Mouse IRAK4 Wild Type mEGFP
MNKPLTPSTYIRNLNVGILRKLSDFIDPQEGWKKLAVAIKKPSGDDRYNQFHIRRFEALLQTGK SPTCELLFDWGTTNCTVGDLVDLLVQIELFAPATLLLPDAVPQTVKSLPPREAATVAQTHGPC QEKDRTSVMPMPKLEHSCEPPDSSSPDNRSVESSDTRFHSFSFHELKSITNNFDEQPASAG GNRMGEGGFGVVYKGCVNNTIVAVKKLGAMVEISTEELKQQFDQEIKVMATCQHENLVELLG FSSDSDNLCLVYAYMPNGSLLDRLSCLDGTPPLSWHTRCKVAQGTANGIRFLHENHHIHRDIK SANILLDRDFTAKISDFGLARASARLAQTVMTSRIVGTTAYMAPEALRGEITPKSDIYSFGVVLL ELITGLAAVDENREPQLLLDIKEEIEDEEKTIEDYTDEKMSDADPASVEAMYSAASQCLHEKKN RRPDIAKVQQLLQEMSAGGSGGSGGSDPPVATMVSKGEELFTGVVPILVELDGDVNGHKFS VSGEGEGDATYGKLTLKFICTTGKLPVPWPTLVTTLTYGVQCFSRYPDHMKQHDFFKSAMPE GYVQERTIFFKDDGNYKTRAEVKFEGDTLVNRIELKGIDFKEDGNILGHKLEYNYNSHNVYIM ADKQKNGIKVNFKIRHNIEDGSVQLADHYQQNTPIGDGPVLLPDNHYLSTQSKLSKDPNEKR DHMVLLEFVTAAGITLGMDELYK
Mouse IRAK4 Kinase Dead (K213/214A) mScarlet
MNKPLTPSTYIRNLNVGILRKLSDFIDPQEGWKKLAVAIKKPSGDDRYNQFHIRRFEALLQTGK SPTCELLFDWGTTNCTVGDLVDLLVQIELFAPATLLLPDAVPQTVKSLPPREAATVAQTHGPC QEKDRTSVMPMPKLEHSCEPPDSSSPDNRSVESSDTRFHSFSFHELKSITNNFDEQPASAG GNRMGEGGFGVVYKGCVNNTIVAVAALGAMVEISTEELKQQFDQEIKVMATCQHENLVELLG FSSDSDNLCLVYAYMPNGSLLDRLSCLDGTPPLSWHTRCKVAQGTANGIRFLHENHHIHRDIK SANILLDRDFTAKISDFGLARASARLAQTVMTSRIVGTTAYMAPEALRGEITPKSDIYSFGVVLL ELITGLAAVDENREPQLLLDIKEEIEDEEKTIEDYTDEKMSDADPASVEAMYSAASQCLHEKKN RRPDIAKVQQLLQEMSAGGSGGSGGSVSKGEAVIKEFMRFKVHMEGSMNGHEFEIEGEGE GRPYEGTQTAKLKVTKGGPLPFSWDILSPQFMYGSRAFIKHPADIPDYYKQSFPEGFKWERV MNFEDGGAVTVTQDTSLEDGTLIYKVKLRGTNFPPDGPVMQKKTMGWEASTERLYPEDGVL KGDIKMALRLKDGGRYLADFKTTYKAKKPVQMPGAYNVDRKLDITSHNEDYTVVEQYERSEG RHSTGGMDELYK
Mouse IRAK4 Kinase Dead (K213/214A) mEGFP

MNKPLTPSTYIRNLNVGILRKLSDFIDPQEGWKKLAVAIKKPSGDDRYNQFHIRRFEALLQTGK
SPTCELLFDWGTTNCTVGDLVDLLVQIELFAPATLLLPDAVPQTVKSLPPREAATVAQTHGPC
QEKDRTSVMPMPKLEHSCEPPDSSSPDNRSVESSDTRFHSFSFHELKSITNNFDEQPASAG
GNRMGEGGFGVVYKGCVNNTIVAVAALGAMVEISTEELKQQFDQEIKVMATCQHENLVELLG
FSSDSDNLCLVYAYMPNGSLLDRLSCLDGTPPLSWHTRCKVAQGTANGIRFLHENHHIHRDIK
SANILLDRDFTAKISDFGLARASARLAQTVMTSRIVGTTAYMAPEALRGEITPKSDIYSFGVVLL
ELITGLAAVDENREPQLLLDIKEEIEDEEKTIEDYTDEKMSDADPASVEAMYSAASQCLHEKKN
RRPDIAKVQQLLQEMSAGGSGGSGGSDPPVATMVSKGEELFTGVVPILVELDGDVNGHKFS
VSGEGEGDATYGKLTLKFICTTGKLPVPWPTLVTTLTYGVQCFSRYPDHMKQHDFFKSAMPE
GYVQERTIFFKDDGNYKTRAEVKFEGDTLVNRIELKGIDFKEDGNILGHKLEYNYNSHNVYIM
ADKQKNGIKVNFKIRHNIEDGSVQLADHYQQNTPIGDGPVLLPDNHYLSTQSKLSKDPNEKR
DHMVLLEFVTAAGITLGMDELYK

Mouse IRAK4-ΔKD-mScarlet

MNKPLTPSTYIRNLNVGILRKLSDFIDPQEGWKKLAVAIKKPSGDDRYNQFHIRRFEALLQTGK
SPTCELLFDWGTTNCTVGDLVDLLVQIELFAPATLLLPDAGGSGGSNRRPDIAKVQQLLQEMS
AGGSGGSGGSVSKGEAVIKEFMRFKVHMEGSMNGHEFEIEGEGEGRPYEGTQTAKLKVTK
GGPLPFSWDILSPQFMYGSRAFIKHPADIPDYYKQSFPEGFKWERVMNFEDGGAVTVTQDT
SLEDGTLIYKVKLRGTNFPPDGPVMQKKTMGWEASTERLYPEDGVLKGDIKMALRLKDGGR
YLADFKTTYKAKKPVQMPGAYNVDRKLDITSHNEDYTVVEQYERSEGRHSTGGMDELYK

Mouse IRAK4-ΔKD-mEGFP

MNKPLTPSTYIRNLNVGILRKLSDFIDPQEGWKKLAVAIKKPSGDDRYNQFHIRRFEALLQTGK
SPTCELLFDWGTTNCTVGDLVDLLVQIELFAPATLLLPDAGGSGGSNRRPDIAKVQQLLQEMS
AGGSGGSGGSDPPVATMVSKGEELFTGVVPILVELDGDVNGHKFSVSGEGEGDATYGKLTL
KFICTTGKLPVPWPTLVTTLTYGVQCFSRYPDHMKQHDFFKSAMPEGYVQERTIFFKDDGNY
KTRAEVKFEGDTLVNRIELKGIDFKEDGNILGHKLEYNYNSHNVYIMADKQKNGIKVNFKIRHN
IEDGSVQLADHYQQNTPIGDGPVLLPDNHYLSTQSKLSKDPNEKRDHMVLLEFVTAAGITLG
MDELYK

Mouse IRAK4 (R12C) mScarlet

MNKPLTPSTYICNLNVGILRKLSDFIDPQEGWKKLAVAIKKPSGDDRYNQFHIRRFEALLQTGK
SPTCELLFDWGTTNCTVGDLVDLLVQIELFAPATLLLPDAVPQTVKSLPPREAATVAQTHGPC
QEKDRTSVMPMPKLEHSCEPPDSSSPDNRSVESSDTRFHSFSFHELKSITNNFDEQPASAG
GNRMGEGGFGVVYKGCVNNTIVAVKKLGAMVEISTEELKQQFDQEIKVMATCQHENLVELLG
FSSDSDNLCLVYAYMPNGSLLDRLSCLDGTPPLSWHTRCKVAQGTANGIRFLHENHHIHRDIK
SANILLDRDFTAKISDFGLARASARLAQTVMTSRIVGTTAYMAPEALRGEITPKSDIYSFGVVLL
ELITGLAAVDENREPQLLLDIKEEIEDEEKTIEDYTDEKMSDADPASVEAMYSAASQCLHEKKN
RRPDIAKVQQLLQEMSAGGSGGSGGSVSKGEAVIKEFMRFKVHMEGSMNGHEFEIEGEGE
GRPYEGTQTAKLKVTKGGPLPFSWDILSPQFMYGSRAFIKHPADIPDYYKQSFPEGFKWERV
MNFEDGGAVTVTQDTSLEDGTLIYKVKLRGTNFPPDGPVMQKKTMGWEASTERLYPEDGVL
KGDIKMALRLKDGGRYLADFKTTYKAKKPVQMPGAYNVDRKLDITSHNEDYTVVEQYERSEG
RHSTGGMDELYK

Mouse IRAK4-ΔDD-mScarlet

MFHELKSITNNFDEQPASAGGNRMGEGGFGVVYKGCVNNTIVAVKKLGAMVEISTEELKQQF
DQEIKVMATCQHENLVELLGFSSDSDNLCLVYAYMPNGSLLDRLSCLDGTPPLSWHTRCKVA

QGTANGIRFLHENHHIHRDIKSANILLDRDFTAKISDFGLARASARLAQTVMTSRIVGTTAYMAP
EALRGEITPKSDIYSFGVVLLELITGLAAVDENREPQLLLDIKEEIEDEEKTIEDYTDEKMSDAD
PASVEAMYSAASQCLHEKKNRRPDIAKVQQLLQEMSAGGSGGSGGSVSKGEAVIKEFMRFK
VHMEGSMNGHEFEIEGEGEGRPYEGTQTAKLKVTKGGPLPFSWDILSPQFMYGSRAFIKHP
ADIPDYYKQSFPEGFKWERVMNFEDGGAVTVTQDTSLEDGTLIYKVKLRGTNFPPDGPVMQ
KKTMGWEASTERLYPEDGVLKGDIKMALRLKDGGRYLADFKTTYKAKKPVQMPGAYNVDRK
LDITSHNEDYTVVEQYERSEGRHSTGGMDELYK

Mouse IRAK4-D329A-mEGFP

MNKPLTPSTYIRNLNVGILRKLSDFIDPQEGWKKLAVAIKKPSGDDRYNQFHIRRFEALLQTGK
SPTCELLFDWGTTNCTVGDLVDLLVQIELFAPATLLLPDAVPQTVKSLPPREAATVAQTHGPC
QEKDRTSVMPMPKLEHSCEPPDSSSPDNRSVESSDTRFHSFSFHELKSITNNFDEQPASAG
GNRMGEGGFGVVYKGCVNNTIVAVKKLGAMVEISTEELKQQFDQEIKVMATCQHENLVELLG
FSSDSDNLCLVYAYMPNGSLLDRLSCLDGTPPLSWHTRCKVAQGTANGIRFLHENHHIHRDIK
SANILLDRDFTAKISAFGLARASARLAQTVMTSRIVGTTAYMAPEALRGEITPKSDIYSFGVVLL
ELITGLAAVDENREPQLLLDIKEEIEDEEKTIEDYTDEKMSDADPASVEAMYSAASQCLHEKKN
RRPDIAKVQQLLQEMSAGGSGGSGGSDPPVATMVSKGEELFTGVVPILVELDGDVNGHKFS
VSGEGEGDATYGKLTLKFICTTGKLPVPWPTLVTTLTYGVQCFSRYPDHMKQHDFFKSAMPE
GYVQERTIFFKDDGNYKTRAEVKFEGDTLVNRIELKGIDFKEDGNILGHKLEYNYNSHNVYIM
ADKQKNGIKVNFKIRHNIEDGSVQLADHYQQNTPIGDGPVLLPDNHYLSTQSKLSKDPNEKR
DHMVLLEFVTAAGITLGMDELYK

Mouse IRAK4-D329A-E-loop-mEGFP

MNKPLTPSTYIRNLNVGILRKLSDFIDPQEGWKKLAVAIKKPSGDDRYNQFHIRRFEALLQTGK
SPTCELLFDWGTTNCTVGDLVDLLVQIELFAPATLLLPDAVPQTVKSLPPREAATVAQTHGPC
QEKDRTSVMPMPKLEHSCEPPDSSSPDNRSVESSDTRFHSFSFHELKSITNNFDEQPASAG
GNRMGEGGFGVVYKGCVNNTIVAVKKLGAMVEISTEELKQQFDQEIKVMATCQHENLVELLG
FSSDSDNLCLVYAYMPNGSLLDRLSCLDGTPPLSWHTRCKVAQGTANGIRFLHENHHIHRDIK
SANILLDRDFTAKISAFGLARASARLAQEVMEERIVGTTAYMAPEALRGEITPKSDIYSFGVVLL
ELITGLAAVDENREPQLLLDIKEEIEDEEKTIEDYTDEKMSDADPASVEAMYSAASQCLHEKKN
RRPDIAKVQQLLQEMSASSGSGGSGGSGGSDPPVATMVSKGEELFTGVVPILVELDGDVNG
HKFSVSGEGEGDATYGKLTLKFICTTGKLPVPWPTLVTTLTYGVQCFSRYPDHMKQHDFFKS
AMPEGYVQERTIFFKDDGNYKTRAEVKFEGDTLVNRIELKGIDFKEDGNILGHKLEYNYNSHN
VYIMADKQKNGIKVNFKIRHNIEDGSVQLADHYQQNTPIGDGPVLLPDNHYLSTQSKLSKDPN
EKRDHMVLLEFVTAAGITLGMDELYK

Mouse IRAK4-A-loop-mEGFP

MNKPLTPSTYIRNLNVGILRKLSDFIDPQEGWKKLAVAIKKPSGDDRYNQFHIRRFEALLQTGK
SPTCELLFDWGTTNCTVGDLVDLLVQIELFAPATLLLPDAVPQTVKSLPPREAATVAQTHGPC
QEKDRTSVMPMPKLEHSCEPPDSSSPDNRSVESSDTRFHSFSFHELKSITNNFDEQPASAG
GNRMGEGGFGVVYKGCVNNTIVAVKKLGAMVEISTEELKQQFDQEIKVMATCQHENLVELLG
FSSDSDNLCLVYAYMPNGSLLDRLSCLDGTPPLSWHTRCKVAQGTANGIRFLHENHHIHRDIK
SANILLDRDFTAKISDFGLARASARLAQAVMAARIVGTTAYMAPEALRGEITPKSDIYSFGVVLL
ELITGLAAVDENREPQLLLDIKEEIEDEEKTIEDYTDEKMSDADPASVEAMYSAASQCLHEKKN
RRPDIAKVQQLLQEMSAGGSGGSGGSDPPVATMVSKGEELFTGVVPILVELDGDVNGHKFS
VSGEGEGDATYGKLTLKFICTTGKLPVPWPTLVTTLTYGVQCFSRYPDHMKQHDFFKSAMPE
GYVQERTIFFKDDGNYKTRAEVKFEGDTLVNRIELKGIDFKEDGNILGHKLEYNYNSHNVYIM

ADKQKNGIKVNFKIRHNIEDGSVQLADHYQQNTPIGDGPVLLPDNHYLSTQSKLSKDPNEKR
DHMVLLEFVTAAGITLGMDELYK

Mouse IRAK1-mScarlet

MAGGPGPGEPVVPGAQHFLYEVPPWVMCRFYKVMDALEPADWCQFAALIVRDQTELRLCE
RSEQRTASVLWPWINRNARVADLVHILTHLQLLRARDIITAWHPPAPVVPPSTAAPRPSSISAG
SEAGDWSPRKLQSSASTFLSPAFPGSQTHSESELLQVPLPVSLGPPLPSSAPSSTKSSPESP
VSGLQRAHPSPFCWPFCEISQGTCNFSEELRIGEGGFGCVYRAVMRNTTYAVKRLKEEADLE
WTMVKQSFLTEVEQLSRFRHPNIVDFAGYCAESGLYCLVYGFLPNGSLEDQLHLQTQACSPL
SWPQRLDILLGTARAIQFLHQDSPSLIHGDIKSSNVLLDERLMPKLGDFGLARFSRFAGAKAS
QSSTVARTSTVRGTLAYLPEEYIKTGRLAVDTDTFSFGVVILETLAGQRAVRTQGAKTKYLKDL
IEDEAEEAGVTLKSTQPTLWVGVATDAWAAPIAAQIYKKHLDSRPGPCPPQLGLALAQLACCC
MHRRAKKRPPMTQVYKRLEGLQAGPPWELEVAGHGSPSPQENSYMSTTGSAQSGDEPWQ
PLVVTTRAPAQAAQQLQRSPNQPVESDESVPGLSATLHSWHLTPGSHPSPASFREASCTQG
GTTRESSVRSSPGFQPTTMEGSPTGSSSLLSSEPPQIIINPARQKMVQKLALYEEGVLDSLQL
LSSGFFPGLDLEPEKSQGPEESDEFQSGSGGSGGSGGSGGSVSKGEAVIKEFMRFKVHMEGSM
NGHEFEIEGEGEGRPYEGTQTAKLKVTKGGPLPFSWDILSPQFMYGSRAFIKHPADIPDYYK
QSFPEGFKWERVMNFEDGGAVTVTQDTSLEDGTLIYKVKLRGTNFPPDGPVMQKKTMGWE
ASTERLYPEDGVLKGDIKMALRLKDGGRYLADFKTTYKAKKPVQMPGAYNVDRKLDITSHNE
DYTVVEQYERSEGRHSTGGMDELYK

Mouse IRAK1-ΔKD-mScarlet

MAGGPGPGEPVVPGAQHFLYEVPPWVMCRFYKVMDALEPADWCQFAALIVRDQTELRLCE
RSEQRTASVLWPWINRNARVADLVHILTHLQLLRARDIITAWHPPAPVVSGSGGSGGSGGSVS
KGEAVIKEFMRFKVHMEGSMNGHEFEIEGEGEGRPYEGTQTAKLKVTKGGPLPFSWDILSP
QFMYGSRAFIKHPADIPDYYKQSFPEGFKWERVMNFEDGGAVTVTQDTSLEDGTLIYKVKLR
GTNFPPDGPVMQKKTMGWEASTERLYPEDGVLKGDIKMALRLKDGGRYLADFKTTYKAKKP
VQMPGAYNVDRKLDITSHNEDYTVVEQYERSEGRHSTGGMDELYK

Mouse IRAK1-ΔDD-mScarlet

MAWHPPAPVVPPSTAAPRPSSISAGSEAGDWSPRKLQSSASTFLSPAFPGSQTHSESELLQ
VPLPVSLGPPLPSSAPSSTKSSPESPVSGLQRAHPSPFCWPFCEISQGTCNFSEELRIGEGG
FGCVYRAVMRNTTYAVKRLKEEADLEWTMVKQSFLTEVEQLSRFRHPNIVDFAGYCAESGLY
CLVYGFLPNGSLEDQLHLQTQACSPLSWPQRLDILLGTARAIQFLHQDSPSLIHGDIKSSNVLL
DERLMPKLGDFGLARFSRFAGAKASQSSTVARTSTVRGTLAYLPEEYIKTGRLAVDTDTFSFG
VVILETLAGQRAVRTQGAKTKYLKDLIEDEAEEAGVTLKSTQPTLWVGVATDAWAAPIAAQIYK
KHLDSRPGPCPPQLGLALAQLACCCMHRRAKKRPPMTQVYKRLEGLQAGPPWELEVAGHG
SPSPQENSYMSTTGSAQSGDEPWQPLVVTTRAPAQAAQQLQRSPNQPVESDESVPGLSAT
LHSWHLTPGSHPSPASFREASCTQGGTTRESSVRSSPGFQPTTMEGSPTGSSSLLSSEPPQ
IIINPARQKMVQKLALYEEGVLDSLQLLSSGFFPGLDLEPEKSQGPEESDEFQSGSGGSGGS
GGSVSKGEAVIKEFMRFKVHMEGSMNGHEFEIEGEGEGRPYEGTQTAKLKVTKGGPLPFSW
DILSPQFMYGSRAFIKHPADIPDYYKQSFPEGFKWERVMNFEDGGAVTVTQDTSLEDGTLIYK
VKLRGTNFPPDGPVMQKKTMGWEASTERLYPEDGVLKGDIKMALRLKDGGRYLADFKTTYK
AKKPVQMPGAYNVDRKLDITSHNEDYTVVEQYERSEGRHSTGGMDELYK

Mouse IRAK2-mScarlet

MACYIYQLPSWVLDDLCRNIDTLSEWDWMQFASYVITDLTQLRKIKSMERVQGVSITRELLW

WWSMRQATVQQLVDLLCHLELYRAAQIVLSWKPVPESTSPLPAFPEAVKPGAVATSRRNLKD
EQEKVRPVKPRSLLDTGPIMAGAQRQRPCEMDAPCSLKTDAPDSPQSKYCSTSTSAPKQER
LLGLPGDRLFWSEADVVQATEDFDQSHRISEGTFADIYQGQRNGVAFAFKKLREVAGSSPGS
MDRFLQAEMQLCLRCCHANVLPLLGFCTGRQFHSLIYPYMANGSLHDRLWAQGNSDMLPW
PQRASICSGLLLAVEHLHSLDIIHSNVKSANVLLDQHLNPKLAHPVAHPHPDNKKTKYTVMRT
HLFQASAAYLPEHFIRVGQLTKQVDIFSCGIVLAEVLTGIPAMDKDRSPVYLKDLLLSEIPNSTS
SVCSRKTSMGKAVVKEICQRHVEKRAGLLPEACEEAWATAVSVCLRRRNASVEEARVSLAG
VEEQLRGQLSLPWSRVSEATGSSSNTPEETDDVDNSSLSVPSLVMMASCPGAASSPLFTGH
GAAQPSTSGRQEADSSSEACTGPQTPQNATETSWKIEINEAKRRLMENIVLYKEERLDSSEL
FGPSGSGGSGGSGGSVSKGEAVIKEFMRFKVHMEGSMNGHEFEIEGEGEGRPYEGTQTAK
LKVTKGGPLPFSWDILSPQFMYGSRAFIKHPADIPDYYKQSFPEGFKWERVMNFEDGGAVTV
TQDTSLEDGTLIYKVKLRGTNFPPDGPVMQKKTMGWEASTERLYPEDGVLKGDIKMALRLKD
GGRYLADFKTTYKAKKPVQMPGAYNVDRKLDITSHNEDYTVVEQYERSEGRHSTGGMDELY
K

Mouse IRAK2-ΔKD-mScarlet

MACYIYQLPSWVLDDLCRNIDTLSEWDWMQFASYVITDLTQLRKIKSMERVQGVSITRELLW
WWSMRQATVQQLVDLLCHLELYRAAQIVLSWKPVPESTSPLPAFPEAVGSGGSGGSGGSVS
KGEAVIKEFMRFKVHMEGSMNGHEFEIEGEGEGRPYEGTQTAKLKVTKGGPLPFSWDILSP
QFMYGSRAFIKHPADIPDYYKQSFPEGFKWERVMNFEDGGAVTVTQDTSLEDGTLIYKVKLR
GTNFPPDGPVMQKKTMGWEASTERLYPEDGVLKGDIKMALRLKDGGRYLADFKTTYKAKKP
VQMPGAYNVDRKLDITSHNEDYTVVEQYERSEGRHSTGGMDELYK

Mouse IRAK2-ΔDD-mScarlet

MPVPESTSPLPAFPEAVKPGAVATSRRNLKDEQEKVRPVKPRSLLDTGPIMAGAQRQRPCE
MDAPCSLKTDAPDSPQSKYCSTSTSAPKQERLLGLPGDRLFWSEADVVQATEDFDQSHRIS
EGTFADIYQGQRNGVAFAFKKLREVAGSSPGSMDRFLQAEMQLCLRCCHANVLPLLGFCTG
RQFHSLIYPYMANGSLHDRLWAQGNSDMLPWPQRASICSGLLLAVEHLHSLDIIHSNVKSAN
VLLDQHLNPKLAHPVAHPHPDNKKTKYTVMRTHLFQASAAYLPEHFIRVGQLTKQVDIFSCGI
VLAEVLTGIPAMDKDRSPVYLKDLLLSEIPNSTSSVCSRKTSMGKAVVKEICQRHVEKRAGLL
PEACEEAWATAVSVCLRRRNASVEEARVSLAGVEEQLRGQLSLPWSRVSEATGSSSNTPEE
TDDVDNSSLSVPSLVMMASCPGAASSPLFTGHGAAQPSTSGRQEADSSSEACTGPQTPQN
ATETSWKIEINEAKRRLMENIVLYKEERLDSSELFGPSGSGGSGGSGGSVSKGEAVIKEFMRF
KVHMEGSMNGHEFEIEGEGEGRPYEGTQTAKLKVTKGGPLPFSWDILSPQFMYGSRAFIKH
PADIPDYYKQSFPEGFKWERVMNFEDGGAVTVTQDTSLEDGTLIYKVKLRGTNFPPDGPVM
QKKTMGWEASTERLYPEDGVLKGDIKMALRLKDGGRYLADFKTTYKAKKPVQMPGAYNVDR
KLDITSHNEDYTVVEQYERSEGRHSTGGMDELYK

Mouse IRAK3-mScarlet

MAGRCGARGALSPQLLLFDLPPALLGELCGILDSCDGPLGWRGLAERLSNSWLDVRHIEKYV
NQGKSGTRELLWSWAQKNKTIGDLLEVLQDMGHQRAIHLIINYGVSWTPSVQTHHELPFPSF
PPEVKHACRENDPGPLEPANVTVDNVLVPEHNEKGTLQKTPISFQSILEGTKHFHKDFLIGEG
EIFEVYRVDIRNQAYAVKLFKQEKKMQLKKHWKRFLSELEVLLLFRHPHILELAAYFTETEKLCL
VYPYMSNGTLFDRLQCTNGTTPLSWHVRISVLIGIAKAIQYLHNTQPCAVICGNVSSANILLDD
QLQPKLTDFAAAHFRPNLEQQSSTINMTGGGRKHLWYMPEEYIRQGRLSVKTDVYSFGIVIM
EVLTGCKVVLDDPKHVQLRDLLMELMEKRGLDSCLSFLDRKIPPCPRNFSAKLFSLAGRCVAT
KAKLRPTMDEVLSSLESTQPSLYFAEDPPTSLKSFRCPSPLFLDNVPSIPVEDDENQNNHSVP

PKEVLGTDRVTQKTPFECSQSEVTFLGLDRNRGNRGSEADCNVPSSSHEECWSPELVAPSQ
DLSPTVISLGSSWEVPGHSYGSKPMEKRCSSGLFCSEHEQSKKQGSGGSGGSGGSVSKGE
AVIKEFMRFKVHMEGSMNGHEFEIEGEGEGRPYEGTQTAKLKVTKGGPLPFSWDILSPQFM
YGSRAFIKHPADIPDYYKQSFPEGFKWERVMNFEDGGAVTVTQDTSLEDGTLIYKVKLRGTN
FPPDGPVMQKKTMGWEASTERLYPEDGVLKGDIKMALRLKDGGRYLADFKTTYKAKKPVQM
PGAYNVDRKLDITSHNEDYTVVEQYERSEGRHSTGGMDELYK

Mouse IRAK3-ΔDD-mScarlet

MNYGVSWTPSVQTHHELPFPSFPPEVKHACRENDPGPLEPANVTVDNVLVPEHNEKGTLQK
TPISFQSILEGTKHFHKDFLIGEGEIFEVYRVDIRNQAYAVKLFKQEKKMQLKKHWKRFLSELE
VLLLFRHPHILELAAYFTETEKLCLVYPYMSNGTLFDRLQCTNGTTPLSWHVRISVLIGIAKAIQ
YLHNTQPCAVICGNVSSANILLDDQLQPKLTDFAAAHFRPNLEQQSSTINMTGGGRKHLWYM
PEEYIRQGRLSVKTDVYSFGIVIMEVLTGCKVVLDDPKHVQLRDLLMELMEKRGLDSCLSFLD
RKIPPCPRNFSAKLFSLAGRCVATKAKLRPTMDEVLSSLESTQPSLYFAEDPPTSLKSFRCPS
PLFLDNVPSIPVEDDENQNNHSVPPKEVLGTDRVTQKTPFECSQSEVTFLGLDRNRGNRGS
EADCNVPSSSHEECWSPELVAPSQDLSPTVISLGSSWEVPGHSYGSKPMEKRCSSGLFCSE
HEQSKKQGSGGSGGSGGSVSKGEAVIKEFMRFKVHMEGSMNGHEFEIEGEGEGRPYEGT
QTAKLKVTKGGPLPFSWDILSPQFMYGSRAFIKHPADIPDYYKQSFPEGFKWERVMNFEDGG
AVTVTQDTSLEDGTLIYKVKLRGTNFPPDGPVMQKKTMGWEASTERLYPEDGVLKGDIKMAL
RLKDGGRYLADFKTTYKAKKPVQMPGAYNVDRKLDITSHNEDYTVVEQYERSEGRHSTGGM
DELYK

Human IRAK4 Wild Type-mEGFP

MNKPITPSTYVRCLNVGLIRKLSDFIDPQEGWKKLAVAIKKPSGDDRYNQFHIRRFEALLQTGK
SPTSELLFDWGTTNCTVGDLVDLLIQNEFFAPASLLLPDAVPKTANTLPSKEAITVQQKQMPFC
DKDRTLMTPVQNLEQSYMPPDSSSPENKSLEVSDTRFHSFSFYELKNVTNNFDERPISVGG
NKMGEGGFGVVYKGYVNNTTVAVKKLAAMVDITTEELKQQFDQEIKVMAKCQHENLVELLGF
SSDGDDLCLVYVYMPNGSLLDRLSCLDGTPPLSWHMRCKIAQGAANGINFLHENHHIHRDIK
SANILLDEAFTAKISDFGLARASEKFAQTVMTSRIVGTTAYMAPEALRGEITPKSDIYSFGVVLL
EIITGLPAVDEHREPQLLLDIKEEIEDEEKTIEDYIDKKMNDADSTSVEAMYSVASQCLHEKKNK
RPDIKKVQQLLQEMTASSGSGGSGGSGGSDPPVATMVSKGEELFTGVVPILVELDGDVNGH
KFSVSGEGEGDATYGKLTLKFICTTGKLPVPWPTLVTTLTYGVQCFSRYPDHMKQHDFFKSA
MPEGYVQERTIFFKDDGNYKTRAEVKFEGDTLVNRIELKGIDFKEDGNILGHKLEYNYNSHNV
YIMADKQKNGIKVNFKIRHNIEDGSVQLADHYQQNTPIGDGPVLLPDNHYLSTQSKLSKDPNE
KRDHMVLLEFVTAAGITLGMDELYK

Human IRAK4-<u>D329A</u>-mEGFP

MNKPITPSTYVRCLNVGLIRKLSDFIDPQEGWKKLAVAIKKPSGDDRYNQFHIRRFEALLQTGK
SPTSELLFDWGTTNCTVGDLVDLLIQNEFFAPASLLLPDAVPKTANTLPSKEAITVQQKQMPFC
DKDRTLMTPVQNLEQSYMPPDSSSPENKSLEVSDTRFHSFSFYELKNVTNNFDERPISVGG
NKMGEGGFGVVYKGYVNNTTVAVKKLAAMVDITTEELKQQFDQEIKVMAKCQHENLVELLGF
SSDGDDLCLVYVYMPNGSLLDRLSCLDGTPPLSWHMRCKIAQGAANGINFLHENHHIHRDIK
SANILLDEAFTAKIS<u>A</u>FGLARASEKFAQTVMTSRIVGTTAYMAPEALRGEITPKSDIYSFGVVLL
EIITGLPAVDEHREPQLLLDIKEEIEDEEKTIEDYIDKKMNDADSTSVEAMYSVASQCLHEKKNK
RPDIKKVQQLLQEMTASSGSGGSGGSGGSDPPVATMVSKGEELFTGVVPILVELDGDVNGH
KFSVSGEGEGDATYGKLTLKFICTTGKLPVPWPTLVTTLTYGVQCFSRYPDHMKQHDFFKSA
MPEGYVQERTIFFKDDGNYKTRAEVKFEGDTLVNRIELKGIDFKEDGNILGHKLEYNYNSHNV

YIMADKQKNGIKVNFKIRHNIEDGSVQLADHYQQNTPIGDGPVLLPDNHYLSTQSKLSKDPNE
KRDHMVLLEFVTAAGITLGMDELYK

Human IRAK4-D329A-E-loop-mEGFP

MNKPITPSTYVRCLNVGLIRKLSDFIDPQEGWKKLAVAIKKPSGDDRYNQFHIRRFEALLQTGK
SPTSELLFDWGTTNCTVGDLVDLLIQNEFFAPASLLLPDAVPKTANTLPSKEAITVQQKQMPFC
DKDRTLMTPVQNLEQSYMPPDSSSPENKSLEVSDTRFHSFSFYELKNVTNNFDERPISVGG
NKMGEGGFGVVYKGYVNNTTVAVKKLAAMVDITTEELKQQFDQEIKVMAKCQHENLVELLGF
SSDGDDLCLVYVYMPNGSLLDRLSCLDGTPPLSWHMRCKIAQGAANGINFLHENHHIHRDIK
SANILLDEAFTAKISAFGLARASEKFAQEVMEERIVGTTAYMAPEALRGEITPKSDIYSFGVVLL
EIITGLPAVDEHREPQLLLDIKEEIEDEEKTIEDYIDKKMNDADSTSVEAMYSVASQCLHEKKNK
RPDIKKVQQLLQEMTASSGSGGSGGSGGSDPPVATMVSKGEELFTGVVPILVELDGDVNGH
KFSVSGEGEGDATYGKLTLKFICTTGKLPVPWPTLVTTLTYGVQCFSRYPDHMKQHDFFKSA
MPEGYVQERTIFFKDDGNYKTRAEVKFEGDTLVNRIELKGIDFKEDGNILGHKLEYNYNSHNV
YIMADKQKNGIKVNFKIRHNIEDGSVQLADHYQQNTPIGDGPVLLPDNHYLSTQSKLSKDPNE
KRDHMVLLEFVTAAGITLGMDELYK

Human IRAK4-A-loop-mEGFP

MNKPITPSTYVRCLNVGLIRKLSDFIDPQEGWKKLAVAIKKPSGDDRYNQFHIRRFEALLQTGK
SPTSELLFDWGTTNCTVGDLVDLLIQNEFFAPASLLLPDAVPKTANTLPSKEAITVQQKQMPFC
DKDRTLMTPVQNLEQSYMPPDSSSPENKSLEVSDTRFHSFSFYELKNVTNNFDERPISVGG
NKMGEGGFGVVYKGYVNNTTVAVKKLAAMVDITTEELKQQFDQEIKVMAKCQHENLVELLGF
SSDGDDLCLVYVYMPNGSLLDRLSCLDGTPPLSWHMRCKIAQGAANGINFLHENHHIHRDIK
SANILLDEAFTAKISDFGLARASEKFAQAVMAARIVGTTAYMAPEALRGEITPKSDIYSFGVVLL
EIITGLPAVDEHREPQLLLDIKEEIEDEEKTIEDYIDKKMNDADSTSVEAMYSVASQCLHEKKNK
RPDIKKVQQLLQEMTASSGSGGSGGSGGSDPPVATMVSKGEELFTGVVPILVELDGDVNGH
KFSVSGEGEGDATYGKLTLKFICTTGKLPVPWPTLVTTLTYGVQCFSRYPDHMKQHDFFKSA
MPEGYVQERTIFFKDDGNYKTRAEVKFEGDTLVNRIELKGIDFKEDGNILGHKLEYNYNSHNV
YIMADKQKNGIKVNFKIRHNIEDGSVQLADHYQQNTPIGDGPVLLPDNHYLSTQSKLSKDPNE
KRDHMVLLEFVTAAGITLGMDELYK

Human IRAK1 Wild Type-mScarlet

MAGGPGPGEPAAPGAQHFLYEVPPWVMCRFYKVMDALEPADWCQFAALIVRDQTELRLCE
RSGQRTASVLWPWINRNARVADLVHILTHLQLLRARDIITAWHPPAPLPSPGTTAPRPSSIPAPA
EAEAWSPRKLPSSASTFLSPAFPGSQTHSGPELGLVPSPASLWPPPPSPAPSSTKPGPESSV
SLLQGARPFPFCWPLCEISRGTHNFSEELKIGEGGFGCVYRAVMRNTVYAVKRLKENADLEW
TAVKQSFLTEVEQLSRFRHPNIVDFAGYCAQNGFYCLVYGFLPNGSLEDRLHCQTQACPPLS
WPQRLDILLGTARAIQFLHQDSPSLIHGDIKSSNVLLDERLTPKLGDFGLARFSRFAGSSPSQS
SMVARTQTVRGTLAYLPEEYIKTGRLAVDTDTFSFGVVVLETLAGQRAVKTHGARTKYLKDLV
EEEAEEAGVALRSTQSTLQAGLAADAWAAPIAMQIYKKHLDPRPGPCPPELGLGLGQLACCC
LHRRAKRRPPMTQVYERLEKLQAVVAGVPGHSEAASCIPPSPQENSYVSSTGRAHSGAAPW
QPLAAPSGASAQAAEQLQRGPNQPVESDESLGGLSAALRSWHLTPSCPLDPAPLREAGCPQ
GDTAGESSWGSGPGSRPTAVEGLALGSSASSSSEPPQIIINPARQKMVQKLALYEDGALDSL
QLLSSSSLPGLGLEQDRQGPEESDEFQSSGSGGSGGSGGSVSKGEAVIKEFMRFKVHMEG
SMNGHEFEIEGEGEGRPYEGTQTAKLKVTKGGPLPFSWDILSPQFMYGSRAFIKHPADIPDY
YKQSFPEGFKWERVMNFEDGGAVTVTQDTSLEDGTLIYKVKLRGTNFPPDGPVMQKKTMG
WEASTERLYPEDGVLKGDIKMALRLKDGGRYLADFKTTYKAKKPVQMPGAYNVDRKLDITSH

NEDYTVVEQYERSEGRHSTGGMDELYK

1232

1233

1234

References:

1. Kagan, J.C., Magupalli, V.G., and Wu, H. (2014). SMOCs: supramolecular organizing centres that control innate immunity. Nat. Rev. Immunol. *14*, 821–826.

2. Wu, H. (2013). Higher-Order Assemblies in a New Paradigm of Signal Transduction. Cell *153*, 287–292.

3. Ferrao, R., and Wu, H. (2012). Helical assembly in the death domain (DD) superfamily. Curr. Opin. Struct. Biol. *22*, 241–247.

4. Wu, E.J., Kandalkar, A.T., Ehrmann, J.F., Tong, A.B., Zhang, J., Cong, Q., and Wu, H. (2025). A structural atlas of death domain fold proteins reveals their versatile roles in biology and function. Proc. Natl. Acad. Sci. U. S. A. *122*, e2426986122.

5. Motshwene, P.G., Moncrieffe, M.C., Grossmann, J.G., Kao, C., Ayaluru, M., Sandercock, A.M., Robinson, C.V., Latz, E., and Gay, N.J. (2009). An oligomeric signaling platform formed by the Toll-like receptor signal transducers MyD88 and IRAK-4. J. Biol. Chem. *284*, 25404–25411.

6. Lin, S.-C., Lo, Y.-C., and Wu, H. (2010). Helical assembly in the MyD88-IRAK4-IRAK2 complex in TLR/IL-1R signalling. Nature *465*, 885–890.

7. Moncrieffe, M.C., Bollschweiler, D., Li, B., Penczek, P.A., Hopkins, L., Bryant, C.E., Klenerman, D., and Gay, N.J. (2020). MyD88 death-domain oligomerization determines Myddosome architecture: Implications for toll-like receptor signaling. Structure *28*, 281–289.e3.

8. Ye, H., Arron, J.R., Lamothe, B., Cirilli, M., Kobayashi, T., Shevde, N.K., Segal, D., Dzivenu, O.K., Vologodskaia, M., Yim, M., et al. (2002). Distinct molecular mechanism for initiating TRAF6 signalling. Nature *418*, 443–447.

9. Flannery, S., and Bowie, A.G. (2010). The interleukin-1 receptor-associated kinases: critical regulators of innate immune signalling. Biochem. Pharmacol. *80*, 1981–1991.

10. Kawagoe, T., Sato, S., Jung, A., Yamamoto, M., Matsui, K., Kato, H., Uematsu, S., Takeuchi, O., and Akira, S. (2007). Essential role of IRAK-4 protein and its kinase activity in Toll-like receptor-mediated immune responses but not in TCR signaling. J. Exp. Med. *204*, 1013–1024.

11. Deliz-Aguirre, R., Cao, F., Gerpott, F.H.U., Auevechanichkul, N., Chupanova, M., Mun, Y., Ziska, E., and Taylor, M.J. (2021). MyD88 oligomer size functions as a physical threshold to trigger IL1R Myddosome signaling. J. Cell Biol. *220*. https://doi.org/10.1083/jcb.202012071.

12. Cushing, L., Stochaj, W., Siegel, M., Czerwinski, R., Dower, K., Wright, Q., Hirschfield, M., Casanova, J.-L., Picard, C., Puel, A., et al. (2014). Interleukin 1/Toll-like receptor-induced autophosphorylation activates interleukin 1 receptor-associated kinase 4 and controls cytokine induction in a cell type-specific manner. J. Biol. Chem. *289*, 10865–10875.

13. De, S., Karim, F., Kiessu, E., Cushing, L., Lin, L.-L., Ghandil, P., Hoarau, C., Casanova, J.-L., Puel, A., and Rao, V.R. (2018). Mechanism of dysfunction of human variants of the IRAK4 kinase and a role for its kinase activity in interleukin-1 receptor signaling. J. Biol. Chem. *293*, 15208–15220.

14. Ferrao, R., Zhou, H., Shan, Y., Liu, Q., Li, Q., Shaw, D.E., Li, X., and Wu, H. (2014). IRAK4 dimerization and trans-autophosphorylation are induced by Myddosome assembly. Mol. Cell *55*, 891–903.

15. Abramson, J., Adler, J., Dunger, J., Evans, R., Green, T., Pritzel, A., Ronneberger, O., Willmore, L., Ballard, A.J., Bambrick, J., et al. (2024). Accurate structure prediction of biomolecular interactions with AlphaFold 3. Nature *630*, 493–500.

16. Kawagoe, T., Sato, S., Matsushita, K., Kato, H., Matsui, K., Kumagai, Y., Saitoh, T., Kawai, T., Takeuchi, O., and Akira, S. (2008). Sequential control of Toll-like receptor-dependent responses by IRAK1 and IRAK2. Nat. Immunol. *9*, 684–691.

17. Kobayashi, K., Hernandez, L.D., Galán, J.E., Janeway, C.A., Jr, Medzhitov, R., and Flavell, R.A. (2002). IRAK-M is a negative regulator of Toll-like receptor signaling. Cell *110*, 191–202.

18. Murphy, J.M., Zhang, Q., Young, S.N., Reese, M.L., Bailey, F.P., Eyers, P.A., Ungureanu, D., Hammaren, H., Silvennoinen, O., Varghese, L.N., et al. (2014). A robust methodology to subclassify pseudokinases based on their nucleotide-binding properties. Biochem. J *457*, 323–334.

19. Lange, S.M., Nelen, M.I., Cohen, P., and Kulathu, Y. (2021). Dimeric Structure of the Pseudokinase IRAK3 Suggests an Allosteric Mechanism for Negative Regulation. Structure *29*, 238–251.e4.

20. Cheng, H., Addona, T., Keshishian, H., Dahlstrand, E., Lu, C., Dorsch, M., Li, Z., Wang, A., Ocain, T.D., Li, P., et al. (2007). Regulation of IRAK-4 kinase activity via autophosphorylation within its activation loop. Biochem. Biophys. Res. Commun. *352*, 609–616.

21. Li, S., Strelow, A., Fontana, E.J., and Wesche, H. (2002). IRAK-4: a novel member of the IRAK family with the properties of an IRAK-kinase. Proc. Natl. Acad. Sci. U. S. A. *99*, 5567–5572.

22. Dossang, A.C.G., Motshwene, P.G., Yang, Y., Symmons, M.F., Bryant, C.E., Borman, S., George, J., Weber, A.N.R., and Gay, N.J. (2016). The N-terminal loop of IRAK-4 death domain regulates ordered assembly of the Myddosome signalling scaffold. Sci. Rep. *6*, 37267.

23. Yamamoto, T., Tsutsumi, N., Tochio, H., Ohnishi, H., Kubota, K., Kato, Z., Shirakawa, M., and Kondo, N. (2014). Functional assessment of the mutational effects of human IRAK4 and MyD88 genes. Mol. Immunol. *58*, 66–76.

24. Lee, K.L., Ambler, C.M., Anderson, D.R., Boscoe, B.P., Bree, A.G., Brodfuehrer, J.I., Chang, J.S., Choi, C., Chung, S., Curran, K.J., et al. (2017). Discovery of Clinical Candidate 1-{[(2S,3S,4S)-3-Ethyl-4-fluoro-5-oxopyrrolidin-2-yl]methoxy}-7-methoxyisoquinoline-6-carb oxamide (PF-06650833), a Potent, Selective Inhibitor of Interleukin-1 Receptor Associated Kinase 4 (IRAK4), by Fragment-Based Drug Design. J. Med. Chem. *60*, 5521–5542.

25. Kuglstatter, A., Villaseñor, A.G., Shaw, D., Lee, S.W., Tsing, S., Niu, L., Song, K.W., Barnett, J.W., and Browner, M.F. (2007). Cutting Edge: IL-1 Receptor-Associated Kinase 4 Structures Reveal Novel Features and Multiple Conformations. The Journal of Immunology

178, 2641–2645.

26. Wang, Z., Liu, J., Sudom, A., Ayres, M., Li, S., Wesche, H., Powers, J.P., and Walker, N.P.C. (2006). Crystal structures of IRAK-4 kinase in complex with inhibitors: a serine/threonine kinase with tyrosine as a gatekeeper. Structure *14*, 1835–1844.

27. Wang, L., Qiao, Q., Ferrao, R., Shen, C., Hatcher, J.M., Buhrlage, S.J., Gray, N.S., and Wu, H. (2017). Crystal structure of human IRAK1. Proc. Natl. Acad. Sci. U. S. A. *114*, 13507–13512.

28. De Nardo, D., Balka, K.R., Cardona Gloria, Y., Rao, V.R., Latz, E., and Masters, S.L. (2018). Interleukin-1 receptor-associated kinase 4 (IRAK4) plays a dual role in myddosome formation and Toll-like receptor signaling. J. Biol. Chem. *293*, 15195–15207.

29. Lye, E., Mirtsos, C., Suzuki, N., Suzuki, S., and Yeh, W.-C. (2004). The role of interleukin 1 receptor-associated kinase-4 (IRAK-4) kinase activity in IRAK-4-mediated signaling. J. Biol. Chem. *279*, 40653–40658.

30. Prehoda, K.E., Scott, J.A., Mullins, R.D., and Lim, W.A. (2000). Integration of multiple signals through cooperative regulation of the N-WASP-Arp2/3 complex. Science *290*, 801–806.

31. Shen, B., and Manley, J.L. (2002). Pelle kinase is activated by autophosphorylation during Toll signaling in Drosophila. Development *129*, 1925–1933.

32. Li, J., McQuade, T., Siemer, A.B., Napetschnig, J., Moriwaki, K., Hsiao, Y.-S., Damko, E., Moquin, D., Walz, T., McDermott, A., et al. (2012). The RIP1/RIP3 necrosome forms a functional amyloid signaling complex required for programmed necrosis. Cell *150*, 339–350.

33. Cho, Y.S., Challa, S., Moquin, D., Genga, R., Ray, T.D., Guildford, M., and Chan, F.K.-M. (2009). Phosphorylation-driven assembly of the RIP1-RIP3 complex regulates programmed necrosis and virus-induced inflammation. Cell *137*, 1112–1123.

34. Park, Y.-H., Jeong, M.S., and Jang, S.B. (2014). Death domain complex of the TNFR-1, TRADD, and RIP1 proteins for death-inducing signaling. Biochem. Biophys. Res. Commun. *443*, 1155–1161.

35. Vollmer, S., Strickson, S., Zhang, T., Gray, N., Lee, K.L., Rao, V.R., and Cohen, P. (2017). The mechanism of activation of IRAK1 and IRAK4 by interleukin-1 and Toll-like receptor agonists. Biochem. J *474*, 2027–2038.

36. Lichtenstein, M.A., Cao, F., Lobnow, F., Dirvanskyte, P., Weyhenmeyer, D., Kulesza, A., Ziska, E., Halfmann, R., and Taylor, M.J. (2025). Bottom-up reconstruction of functional death fold signalosomes reveals a requirement for polymer stability and avidity. Science *388*, 415–422.

37. Gibson, D.G., Young, L., Chuang, R.-Y., Venter, J.C., Hutchison, C.A., and Smith, H.O. (2009). Enzymatic assembly of DNA molecules up to several hundred kilobases. Nat. Methods *6*, 343–345.

38. Bieniossek, C., Richmond, T.J., and Berger, I. (2008). MultiBac: multigene baculovirus-based eukaryotic protein complex production. Curr. Protoc. Protein Sci.

Chapter 5, Unit 5.20.

39. Lange, S.M., and Kulathu, Y. (2022). Purification, crystallization and drug screening of the IRAK pseudokinases. Methods Enzymol. *667*, 101–121.

40. Cao, F., and Taylor, M.J. (2023). Visualization of Myddosome Assembly in Live Cells. Methods Mol. Biol. *2654*, 231–250.

41. Cao, F., Deliz-Aguirre, R., Gerpott, F.H.U., Ziska, E., and Taylor, M.J. (2023). Myddosome clustering in IL-1 receptor signaling regulates the formation of an NF-kB activating signalosome. EMBO Rep. *n/a*, e57233.

Supplementary Files

This is a list of supplementary files associated with this preprint. Click to download.

- SupplementaryMovie1IRAK4WTIRAK1WTvsIRAK4DelKDIRAK1WT1.mp4
- SupplementaryMovie2IRAK4WTIRAK1WTvsIRAK4WTIRAK1DelKD1.mp4
- SupplementaryMovie3IRAK4DelKDIRAK2WTandIRAK4DelKDIRAK3WT.mp4
- SupplementaryMovie4IRAK4WTIRAK2DelKDandIRAK4WTIRAK3DelKD.mp4
- SupplementaryMovie5.mp4
- SupplementaryMovie6.mp4
- SupplementaryMovie7.mp4